INSTITUTO POTOSINO DE INVESTIGACIÓN CIENTÍFICA Y TECNOLÓGICA, A.C.

POSGRADO EN CIENCIAS APLICADAS

Reactive and harmonic compensation in power electronic systems using adaptive control

Tesis que presenta

Andrés Alejandro Valdez Fernández

Para obtener el grado de

Doctor en Ciencias Aplicadas

En la opción de

Control y Sistemas Dinámicos

Director de la Tesis:

Dr. Gerardo Escobar Valderrama

San Luis Potosí, S.L.P., septiembre de 2009

Constancia de aprobación de la tesis

La tesis **Reactive and harmonic compensation in power electronic systems using adaptive control** presentada para obtener el Grado de Doctor en Ciencias Aplicadas en la opción Control y Sistemas Dinámicos fue elaborada por **Andrés Alejandro Valdez** y aprobada el **dd de mm de aaaa** por los suscritos, designados por el Colegio de Profesores de la División de Matem´aticas Aplicadas del Instituto Potosino de Investigación Científica y Tecnológica, A.C.

_____

Dr. Gerardo Escobar Valderrama
(Director de la tesis)

_____

Dr. Dr. Jaime Eugenio Arau Roffiel
(Sinodal)

_____

Dr. Víctor Manuel Cárdenas Galindo
(Sinodal)

_____

Dr. David Antonio Lizárraga Navarro
(Sinodal)

_____

Dr. Juan Gonzalo Barajas Ramírez
(Sinodal)

Créditos Institucionales

Esta tesis fue elaborada en la División de Matemáticas Aplicadas del Instituto Potosino de Investigación Científica y Tecnológica, A.C., bajo la dirección del Dr. Gerardo Escobar Valderrama.

Durante la realización del trabajo el autor recibió una beca académica del Consejo Nacional de Ciencia y Tecnología (No. de registro 180050) y del Instituto Potosino de Investigación Científica y Tecnológica, A. C.

Parte de esta tesis fue elaborada en el Laboratoire des Signaux et Systèmes (LSS) del École Supérieure d' Electricité (SUPÉLEC) bajo la supervición del Dr. Romeo Ortega.

IPICYT

Instituto Potosino de Investigación Científica y Tecnológica, A.C.

Acta de Examen de Grado

El Secretario Académico del Instituto Potosino de Investigación Científica y Tecnológica, A.C., certifica que en el Acta 008 del Libro Primero de Actas de Exámenes de Grado del Programa de Doctorado en Ciencias Aplicadas en la opción de Control y Sistemas Dinámicos está asentado lo siguiente:

En la ciudad de San Luis Potosí a los 17 días del mes de septiembre del año 2009, se reunió a las 10:00 horas en las instalaciones del Instituto Potosino de Investigación Científica y Tecnológica, A.C., el Jurado integrado por:

Dr. Víctor Manuel Cárdenas Galindo	**Presidente**	**UASLP**
Dr. David Antonio Lizárraga Navarro	**Secretario**	**IPICYT**

a fin de efectuar el examen, que para obtener el Grado de:

DOCTOR EN CIENCIAS APLICADAS
EN LA OPCIÓN DE CONTROL Y SISTEMAS DINÁMICOS

sustentó el C.

Andrés Alejandro Valdez Fernández

sobre la Tesis intitulada:

Reactive and harmonic compensation in power electronic systems using adaptive control

que se desarrolló bajo la dirección de

Dr. Gerardo Escobar Valderrama

El Jurado, después de deliberar, determinó

APROBARLO

Dándose por terminado el acto a las 13:00 horas, procediendo a la firma del Acta los integrantes del Jurado. Dando fe el Secretario Académico del Instituto.

A petición del interesado y para los fines que al mismo convengan, se extiende el presente documento en la ciudad de San Luis Potosí, S.L.P., México, a los 17 días del mes de septiembre de 2009.

Dr. Marcial Bonilla Marín
Secretario Académico

Mtra. Ivonne Lizette Cuevas Vélez
Jefa del Departamento de Asuntos Escolares

INSTITUTO POTOSINO DE INVESTIGACIÓN CIENTÍFICA Y TECNOLÓGICA, A.C.
IPICYT
SECRETARIA ACADEMICA

CONTENTS

RESUMEN

En este trabajo de tesis se proponen tres controladores basados en modelo matemático de tres sistemas electrónicos de potencia. Los modelos analizados consideran el caso general de voltaje de fuente y corriente de carga distorsionados y desbalanceados. Los controladores propuestos incluyen leyes adaptables para compensar incertidumbres paramétricas de los sistemas. A continuación se describen brevemente los casos analizados.

Un primer controlador es propuesto para un filtro activo paralelo, el cual es utilizado para compensar potencia reactiva y distorsión armónica de corriente en un sistema de potencia monofásico. El controlador propuesto considera los efectos negativos que causan la interacción entre las impedancias de la carga y de la línea que pueden causar problemas de inestabilidad. Especial atención es puesta en el lazo de control de corriente, debido a que es precisamente en este lazo donde se generan los problemas de inestabilidad. Así, la solución propuesta consiste en remplazar el típico término de amortiguamiento del lazo de corriente por un compensador de adelanto con una ganancia ajustada adaptivamente. Esta modificación relaja las condiciones de estabilidad cuando las impedancias de la carga y de la línea no son despreciables. En particular, el esquema de control fue probado para un escenario crítico en donde la carga es compuesta por un capacitor conectado en paralelo con la carga. Resultados numéricos ilustran los beneficios de la solución propuesta.

Un segundo controlador es propuesto para un filtro de potencia híbrido, el cual es utilizado para reducir la distorsión armónica de la corriente en un sistema de potencia trifásico. El filtro de potencia híbrido bajo estudio está compuesto por un filtro activo conectado entre el capacitor y el inductor de un filtro pasivo. El objetivo de esta topología es reducir el rango de corriente en la fuente inversora de voltaje (VSI) del filtro activo. El diseño del controlador es separado en dos etapas, una primera etapa de regulación que considera la componente fundamental de la dinámica del sistema y una segunda etapa para la compensación de armónicos que considera únicamente la componente armónica de la dinámica del sistema. En la etapa

de regulación se desarrolla una ley de control sobre la corriente de la fuente, de tal manera que se pueda extraer potencia activa de la fuente hacia el filtro activo, la cual es necesaria para mantener la carga del capacitor del lado de corriente directa. La etapa de compensación de armónicos inyecta la corriente necesaria a la red para compensar la distorsión armónica presente en la línea. En esta sección se presentan resultados experimentales para evaluar la solución propuesta.

El tercer controlador se propone con el objetivo de regular las potencias activa y reactiva instantáneas de un rectificador trifásico. El análisis es realizado considerando las dinḿicas de las secuencias positiva y negativa del voltaje de línea, esto permite una descripción más completa del modelo matemático utilizado para el diseño del controlador. Se muestra además que el caso balanceado es un caso particular del esquema propuesto. Se presentan resultados experimentales para ilustrar los beneficios de la solución propuesta.

ABSTRACT

In this thesis work three model-based controllers are proposed for power electronics systems considering the general case of distorted and unbalanced source voltage and load currents. These controllers incorporate an adaptation mechanism to cope with system uncertainties.

The first controller is proposed for an active filter to compensate reactive power and current harmonic distortion in a single-phase system. The proposed controller considers the deleterious effects caused by the interaction between load and line impedances, which may lead to instabilities when the controller is enabled. The rationale behind the solution consists in the introduction of a lead compensator with a gain that is adjusted by adaptation, which replaces the conventional proportional term. This modification improves the stability conditions when the load and source impedances are non-negligible. In particular, the scheme provides a solution in the critical scenario, when the load is composed by a capacitor connected in parallel to a distorted current source. Special attention is given to the current control loop because it is precisely in this loop where the instability problems are generated. Realistic numerical results are provided to illustrate the benefits of the proposed solution.

The second controller is designed for a hybrid power filter to reduce the current harmonic distortion in a three-phase power system. The hybrid power filter topology considered is composed of an active filter connected to the grid by means of an inductor-capacitor (LC) passive filter. The aim of this topology is to reduce the current rating handled by the active filter voltage source inverter (VSI). The controller design is split in two stages, a regulation stage considering the fundamental component of the system dynamics, and a harmonics compensation stage considering the harmonic component of the system dynamics. In the regulation stage a current control is established to force the active filter current to extract only active power from the source, which is used to maintain the DC-link capacitor charged to a certain level. The load reactive current compensation is left to the passive filter mainly. The harmonic compensation stage forces the injection of current to the mains to compensate

the harmonic distortion appearing in the line due to the distorting load. Experimental results are provided to assess the proposed solution.

The third controller is aimed to control the instantaneous active and reactive power of a pulse width modulation (PWM) rectifier in the unbalanced case, and is referred as direct power control (DPC). The source voltage is considered in terms of both sequences, positive and negative, which allows a more complete description of the model. It is shown that regulation of instantaneous powers is possible at the expenses of deformation of the line current. Also, it is shown that the balanced case can be recovered from the proposed controller by simply neglecting the source voltage negative sequence, and thus, the balanced case is a special case of the proposed scheme. It is clear, however, that the use of the balanced DPC controller in an unbalanced situation may produce a quite deteriorated performance. Experimental tests are provided to illustrate the merits of the proposed solution.

NOTATION

Frequent Acronyms

AC	alternating current
ADC	analog-to-digital converter
ADP	analogical digital port
BPF	band pass filter
CE	chip enable
DC	direct current
DSP	digital signal processor
IGBT	isolated gate bipolar transistor
KCL	Kirchhoff's current law
KVL	Kirchhoff's voltage law
LC	inductor-capacitor
LPF	low pass filter
LTI	linear time invariant
OPWM	optimum pulse width modulation
PWM	pulse width modulation
SPWM	sine pulse width modulation
RMS	root mean square
THD	total harmonic distortion
UPS	uninterruptible power supplies
VSI	voltage source inverter

Most common mathematical symbols

$\mathbb{R}$	field of real numbers
$\mathbb{R}^n$	linear space of ordered n-tuples in $\mathbb{R}$.

$\stackrel{\triangle}{=}$	"defined as"
$(\cdot)^T$	transpose operator
$(\cdot)^{-1}$	inverse operator
t	time, $t \in \mathbb{R}_+$
$\frac{d}{dt}, \dot{(\cdot)}$	differentiation operator
$(\cdot)_k^p$,	k-th harmonic coefficients for the positive sequence representation
$(\cdot)_k^n$	k-th harmonic coefficients for the negative sequence representation
$\mathcal{J}$	the skew symmetric matrix $\begin{bmatrix} 0 & -1 \\ 1 & 0 \end{bmatrix}$
$e^{(\cdot)}$	(natural, matrix) exponential function
$e^{\mathcal{J}(\cdot)}$	the 2×2 rotation matrix $\begin{bmatrix} \cos(\cdot) & -\sin(\cdot) \\ \sin(\cdot) & \cos(\cdot) \end{bmatrix}$
$\hat{(\cdot)}$	estimate of $(\cdot)$
$\tilde{(\cdot)}$	error between a quantity and its reference $(\cdot) - (\cdot)_d$, $\hat{(\cdot)} - (\cdot)$
$(\cdot)^*$	desired external references

Frequently used variables

$\delta_i \in \{0, 1\}$	:	switching sequence $\forall\, i \in \{1, 2, 3\}$
$\nu_i \in [0, 1]$	:	duty cycle $\forall\, i \in \{1, 2, 3\}$
$u_i \in [-1, 1]$	:	control signal $\forall\, i \in \{1, 2, 3\}$
L		inductance
C		capacitance
E		voltage source
α, β		weights for i_C and i_0, resp.
i_{Li}		inductor currents, $\forall\, i \in \{1, 2, 3\}$
i_{Ci}		capacitor currents, $\forall\, i \in \{1, 2, 3\}$
i_{0i}		load current, $\forall\, i \in \{1, 2, 3\}$
i_{mi}		combined current, $\forall\, i \in \{1, 2, 3\}$
$R_1,\ R_2$		control parameters
w_0		fundamental frequency

LIST OF FIGURES

1. INTRODUCTION

NONLINEAR loads, such as uninterruptible power systems, diodes and thyristor-based rectifiers, among others, introduce reactive and harmonic distortion into the electric grid. As a consequence, direct negative effects arise such as low power factor (PF), deterioration of devices connected to the point of common coupling (PCC), overheating of transformers, etc. The growing importance of nonlinear loads and the need for highly efficient systems have motivated to the power electronics community to find different forms to mitigate reactive and harmonic distortion. One traditional solution to mitigate harmonic problems is the use of passive filters due to their low cost and high efficiency. However, their harmonic compensation performance may be affected by the source impedance performance, and moreover, they may present resonances with the loads. Another effective solution is the use of shunt active filters. These systems have the ability to compensate reactive power, harmonic distortion and current unbalance. Nevertheless, their cost is relatively higher than passive filter cost. A solution that alleviates this issue is the use of hybrid power filters. These systems have emerged as a combination between passive and active filters to benefit from the advantages of both. It is clear that the use of active front end rectifiers avoids the production of low order harmonics, and thus it can also be considered as a solution to achieve current harmonic reduction. These solutions are referred as PFCs and are used in applications, where the energy flow can be reversed during the operation. These systems, under an appropriated control scheme, offer significant advantages such as low harmonic distortion in the line current and a PF close to unity and regulation of the dc link voltage, in contrast to conventional uncontrolled rectifiers.

The present thesis work is aimed to obtain adaptive control laws for three conceptually different power electronics systems involving reactive and harmonic compensation. The

proposed approaches are based on the mathematical model of the systems considering the general case of distorted and unbalance source voltage and load currents. Thus, the structural characteristics of the studied systems can be exploited for a better control design. Specifically, the solutions are established on a frequency domain description of the periodic disturbances including both symmetric components (the negative and positive sequence), which allows the treatment under unbalanced operation. The proposed control schemes incorporate adaptive algorithms to guarantee robustness of the proposed controller against system uncertainties. It is shown that after transformations, the proposed controllers get a simple and practical form including damping terms to guarantee stability, and selective harmonic compensators, such as resonant regulators, to achieve harmonic compensation. The proposed controllers belong to the family of the proportional-resonant (PR) controllers, which is a widely accepted solution. The idea behind this approach consists in compensating each harmonic under concern by the corresponding resonant filter tuned at that harmonic precisely [1], [2] [1]. Either numerical or experimental results are provided to assess the performance of each studied system in close loop with the proposed control solutions. The experimental results have been carried out in 1.5 kVA three-phase prototypes.

In this Chapter, concepts such as nonlinear loads, reactive and harmonic distortion, and the negative effects of the connection of nonlinear loads to the grid are described. Besides, a brief survey on the different approaches involving the compensation of reactive and harmonic distortion, including passive, active and hybrid filters, as well as PWM rectifier topologies, is given in order to introduce the topologies studied in this thesis work. The outline of the dissertation is given at the end of this chapter.

1.1 Nonlinear loads

Many domestic and industrial loads are composed of electronic devices with a nonlinear behavior. These nonlinear loads draw non-sinusoidal currents and their connection to the electric grid produces the introduction of reactive and harmonic distortion. Common examples of nonlinear loads are the energy conversion equipments such as uncontrolled bridge

[1] This type of controllers have besides appeared under different names in the power electronics literature: resonant regulator [3], stationary-frame generalized integrator [4] and multi-resonant controller [5]. In fact, they are all in agreement with the internal model principle [6]

rectifiers, switched-mode power supplies, electronic fluorescent lamp ballasts, dc arc furnaces, flexible ac transmission components, and adjustable speed drives, among others.

The uncontrolled rectifier, which involves the use of a diode bridge with a capacitive filter, is perhaps the nonlinear system most commonly found in industrial, domestic and office electronic equipments. This system causes a considerable current distortion. The preference of these topologies is justified mainly on their low cost, reliability and robustness. For instance, it is well known that a single-phase rectifiers generates harmonics at odd multiples of the fundamental frequency. Figure 1.1 shows (from top to bottom) the source voltage and source current of a single-phase rectifier, and the frequency spectrum of the source current. From the figure, it can be observed that the single-phase rectifier generates a non-sinusoidal current containing odd harmonics. On the other hand, it has been observed that three-phase three-wire rectifiers generate harmonic multiples of $6n \pm 1$ (for $n = 0, 1, 2, ...$) of the fundamental frequency, without triplet harmonics (multiples of 3). Figure 1.2 shows (middle graphic) a nonlinear current generated by a three-phase rectifier and (third plot) its frequency spectrum. Notice that the current is a non-sinusoidal signal containing harmonic multiples of $6n \pm 1$. Thus, it can be stated that this type of non controlled rectifiers (nonlinear loads) produces a low power factor and generates a considerable amount of harmonic distortion in the line current [7]. To overcome such issues, new rectifier topologies have emerged [8]-[10]. Among the different topologies, it is perhaps the PWM regenerative rectifier the one that has received most attention [11]. This topology is described in the section 1.5 and a controller for that topology is proposed in the Part III of this thesis.

The principal consequence of the connection of nonlinear loads is a low PF, which may cause possible penalties to customers, mainly in industry. Besides, other negative effects arise in the power systems connected to the grid. Some of the most typical negative effects are listed next:

- ◇ *Overheating of transformers.* Modern electronic devices (nonlinear loads) connected to distribution transformers produce current harmonic distortion. This induces a high-frequency magnetic flux in the magnetic core of the transformer, which results in high losses and overheating of the transformers. To overcome this problem, it is common to oversize transformers, increasing their cost.

- ◇ *Overheating of capacitors for power factor correction*. A resonance effect may arise

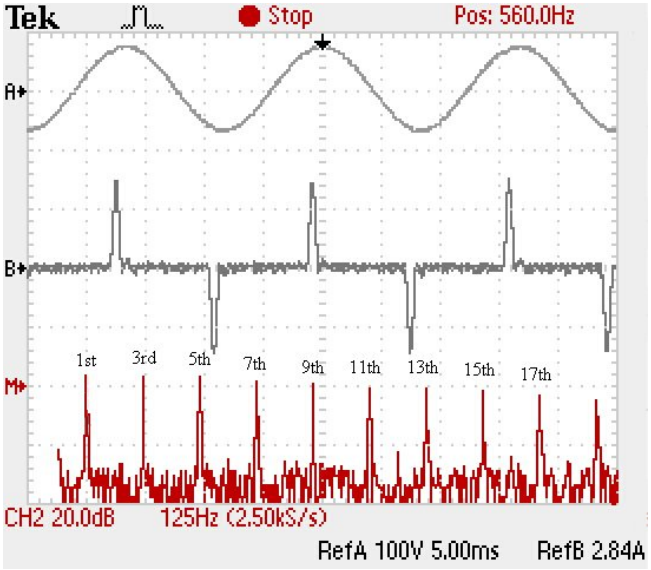

Fig. 1.1: **(from top to bottom)** source current, a single-phase nonlinear load generated by an uncontrolled H-bridge rectifier, and frequency spectrum of the nonlinear load.

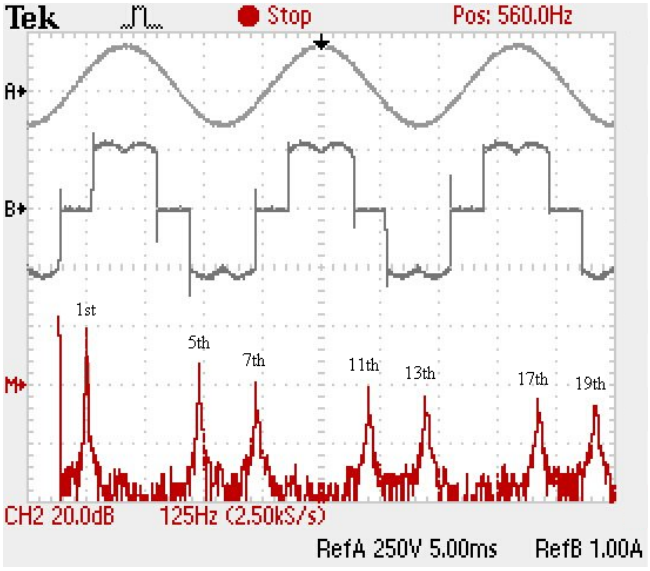

Fig. 1.2: **(from top to bottom)** source current, a three-phase nonlinear load generated by an uncontrolled rectifier, and frequency spectrum of the nonlinear load.

if the combination of the line impedance and the impedance of capacitors for power factor correction create a resonant peak at the same frequency of a harmonic current generated by the nonlinear load. As a consequence, an overcurrent arises, which may overheat or even damage the bank of capacitors.

- ◇ *Voltage wave form distortion*. In weak grids, nonlinear loads may cause voltage waveform distortion that can interfere with the performance of other electronic devices connected to the grid.

- ◇ *Voltage flicker*. If the frequency spectrum generated by nonlinear loads have harmonic components below the fundamental frequency, particularly in the frequency range of 8 to 30 Hz, then a flicker effect may arise in lighting equipment.

Nowadays, the harmonic distortion in electric distribution systems is increasingly growing due to the widespread use of nonlinear industrial and domestic loads. A simple example can illustrate the aforementioned problem: a “single” low-power diode rectifier, commonly used in most electronic devices, injects a negligible amount of harmonic current compared with the total system current. However, multiple low-power diode rectifiers connected in parallel can produce a significant amount of harmonics into the electric grid. In other words, the accumulation of many nonlinear loads of small power have the potential to increase the harmonic distortion in an electrical distribution system to reach unacceptable high levels. The growing importance of nonlinear loads and the need for highly efficient and reliable systems have motivated the power electronics community to find different approaches to mitigate reactive and harmonic distortion. In the following sections some of the most common systems to compensate harmonic and reactive power are described.

1.2 Passive filters

A traditional solution to reduce the harmonic problem and consequently to improve the power factor is the use of passive filters. These filters are exclusively built with passive components such as inductors and capacitors. In this thesis work, two systems containing passive filters are analyzed. The first studied system includes a power-factor correction capacitor, while the second system incorporates a shunt passive filter. They are both described in more detail next.

1.2.1 Power-factor correction capacitor

Power-factor correction by means of capacitors is a widely used technique in industry. The methodology consists in the parallel connection of capacitors banks to the distorting nonlinear load. PFC capacitors work as reactive current generators, and reduce the total current drawn from the distribution system. By keeping the reactive current down, the overall plant power factor is improved. These filters have been used extensively because they offer intrinsic advantages such as: cost reduction, power losses reduction in transformer and distribution equipment, extending the life of distribution equipment, stabilization of voltage levels, and increasing of systems capacity.

A common problem that occurs when PFC capacitors are used in a distribution system is the creation of a resonance peak due to the combination of the bank of capacitors and the line impedance mainly inductive. As a consequence, the system may "resonate" if the harmonic contents of the load current has a component at the resonance frequency. A simple solution to avoid this issue consists in increasing the size of the bank of capacitors when a resonance phenomenon is detected. However, resizing the bank of capacitors to move the resonance point may impact other operational aspects (over/under correction, voltage rise, etc.).

Another effective solution consists in the addition of a reactor in series with the PFC capacitor to generate a LC filter, which is connected in parallel with the nonlinear load. This filter moves the system resonance peak out of the load current harmonic component under concern. This LC filter is typically known as shunt passive filter and is described below.

1.2.2 Shunt passive filter

Figure 1.3 shows a nonlinear load and a bank of shunt passive filters (SPFs) connected to the electric grid. This SPF is one of the most popular passive topologies. It consists in tuned inductor-capacitor (LC) filters connected in parallel to the distorting nonlinear load. The objective of this SPF is to eliminate selected harmonics from the distorted current generated by the nonlinear load. Each LC filter is tuned at a given frequency to offer a relatively low impedance path for that specific harmonic component of the load current. Thus, these harmonic currents do not flow back to the utility grid but are sink by the LC filter. Notice that, a SPF should be included for each harmonic component to be compensated of the distorted

current caused by the nonlinear load.

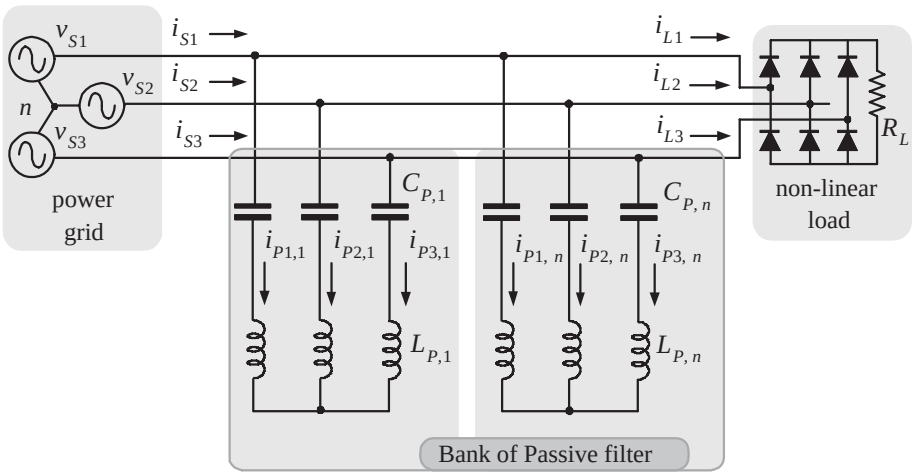

Fig. 1.3: Nonlinear load with a bank of shunt passive filters.

This type of filters have been used traditionally in the industry power systems due to their intrinsic advantages, which are listed below.

- ◇ Low cost and high reliability.
- ◇ They can be used in applications involving large current or voltage levels.
- ◇ Little noise compared to circuits using active filters. They produce only thermal noise due to the resistance associated to the passive elements.

However, they present the following disadvantages:

- ◇ For the design of the passive filter, it is necessary to know the grid impedance, which depends directly on the system configuration and strongly affects the filtering characteristics.
- ◇ Parallel resonance between the grid impedance and the passive filter impedance causes amplification of high harmonic voltage on the point of common connection (PCC) at specific frequencies.

- ◇ They are very sensitive to the component value tolerances and the variability in the value of the same ones throughout the time.
- ◇ Their performance is decreased if the nonlinear load is not constant.

Summarizing, passive filters have been extensively used with proven efficacy. Nevertheless, they present several disadvantages, and nowadays they may be insufficient due to the daily growing of connected nonlinear loads. In contrast, shunt active filters arise to cope with these disadvantages, and as an effective solution for harmonic and reactive power compensation [12], even under current unbalanced operation [13]. These systems are described in the following section.

1.3 Shunt active filters

Shunt active filters (SAFs), in contrast to SPFs, can track and compensate (*in real time*) changes in the current harmonic content of a selected nonlinear load. They are built with passive components and power semiconductor devices, such as, insulated gate bipolar transistors (IGBT), metal-oxide-semiconductor field-effect transistors (MOSFETs) and others. These power devices are considered medium-power, high-speed switching devices. This allows compensation of current harmonics in medium-voltage applications, as the switching frequency can be relatively high.

Basically, a SAF works by continuously detecting the current harmonic components and by injecting them with opposite phase, so they can be eliminated from the load current. In other words, SAFs act to eliminate the reactive power and harmonic currents produced by non-linear loads from the grid by injecting the necessary current to guarantee a purely sinusoidal current observed by the grid, which is in phase with the voltage signal at the PCC, thus guaranteeing a power factor close to one.

Figure 1.4 shows a basic configuration of a SAF connected to the grid. It consists mainly of a controller, a modulation scheme, and a voltage- or current-source PWM inverter (voltage-source inverters (VSI), which are typically used in commercial operation [14]). The main functions of the controller is to accurately detect harmonics *in real time* and reinject them with an opposite phase shift, and to keep the DC link voltage in a constant value under

different operating conditions. The generated control signals are the duty ratios serving as references for a modulation scheme, which can generate the switching signals to control the power devices of the PWM inverter. Thus, it is possible to use these systems to compensate low-order harmonics and comply with harmonic standards such as the IEEE 519.

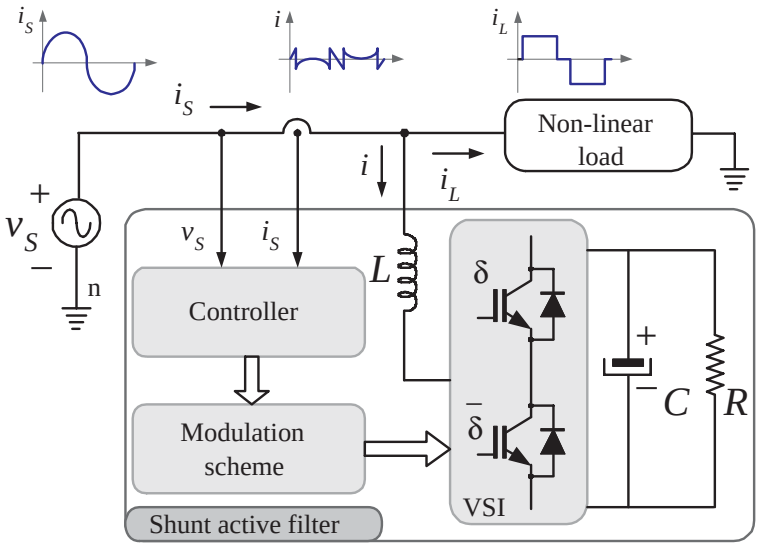

Fig. 1.4: Basic configuration of a shunt active filter.

Obviously, the current harmonic compensation of a SAF strongly depends on the selected control scheme. Different control schemes for these systems have been reported in the literature [5], [15]-[19]. The control schemes proposed in [16]-[18] are designed using instantaneous active and reactive power theory (p-q Theory [19]). Most applications of SAFs are intended to compensate for the load current harmonics. Conventional techniques [15] used for active power filters seem to reduce the achievable performance mainly due to the limited control bandwidth, delays in digital implementation, and interaction with load and line dynamics [20]. To overcome these limitations, in [13] is presented an adaptive control based on the ideas of passivity theory [21] for reactive power, unbalance and selective harmonic compensation using a D-Statcom. This approach is based on the measurements of line currents, and ensures precise compensation for some harmonics, regardless of the limited switching frequency. Moreover, the authors follow an approach that ensures, for any compensated frequency, that the line currents are proportional to the line voltages, so that the same apparent resistance is observed in all phases and at all compensated frequencies,

for any unbalanced and distorted supply and load conditions.

The solution proposed in [13] is studied in Part I of this thesis considering a dynamic load and the line impedance. In particular, the case studied here considers an inductance plus a resistor as the line impedance, and a PFC capacitor as load impedance. This is a critical benchmark that has received a lot of attention in the last few years [22]-[25]. As the models used for the control design (in [13] and other works [3]-[5]) do not consider the dynamics of these impedances, then direct application of an active filter under a controller that considers only a proportional term in the current loop may produce oscillations or instability of the system [24]. In this thesis it is shown that, this situation gets worst in the case that a harmonic compensation mechanism (for instance, band pass filters (BPFs)) is also included. Then, a controller is proposed to guarantees the compensation of reactive power and harmonic distortion in spite of the presence of these impedances. The rationale behind the solution consists in replacing the proportional term used in the current loop of earlier proposed controllers ([3]-[5], [13]) by a lead compensator. It is analytically shown that, after this modification, the stability conditions are considerably improved. In addition, it is proposed the use of an adaptation mechanism to estimate the associated gain of the lead compensator. The last has the additional advantage of enhancing the robustness against parameter variations. Finally, to show the benefits of the proposed solution, numerical results using PSCAD 4.0 are provided, which were carried out in a 3 kVA using a single-phase full-bridge shunt active filter. This result has been recently reported in an international journal [26].

In general, SAFs consisting of VSI have been studied and put into practical because they have demonstrated to be a effective mechanism to alleviate the effects of the injection of highly distorted currents. At the same time, they have the skill to overcome the above mentioned disadvantages in passive filters. However, they have the following two inherent drawbacks:

- ◇ It is difficult to construct active filters for a large-rated current source
- ◇ In higher power applications, the switching frequency is considerably reduced.
- ◇ The initial and running costs are high compared with those of passive filters.

To try to alleviate the issues observed in shunt passive and active filters, hybrid power filters have been developed, which are described in the following section.

1.4 Hybrid Power Filters

Hibrid power filters [27]-[31] have emerged as a combination between passive and active filters to benefit from the advantages of both schemes. When regarding the power capacity and cost issues, HPF arise as a promising choice for the future [32].

One interesting HPF proposed in [27] combines the use of a SPF and a small rated series active filter. In this approach, the function of the series active filter is not to compensate for the harmonic voltages directly as in a basic series active filter, but to enhance the SPF characteristics by providing harmonic isolation. That is, the active filter provides high resistance for the harmonic frequencies and zero resistance for the fundamental frequency. Thus, the authors achieve the so-called ”active impedance”. Besides, the above mentioned series and parallel resonances in the SPF, which are caused by the inductive source impedance, can be eliminated by inserting the series active filter (see [19], [27] and [33] for details).

Another alternative to built a hybrid filter is presented in [29]. In this approach, the small-rated active filter is connected in series with the passive filter. The composed hybrid filter is connected in parallel to the nonlinear load that produces harmonics. In this case, the passive filter suppresses the harmonic currents, whereas the active filter improves the filtering characteristics of the passive filter. As a result, the proposed system solves the main issues found in passive filters. Besides, the active filter is much smaller in rating than a conventional active filter. One problem of this topology is that, due to the series connection between the active and passive filters, all reactive power drained by the passive filter circulates through the switching devices of the VSI. To alleviate this issue another HPF topology is proposed in [30]. In this topology, the active filter is connected between the inductor and the capacitor of the passive filter. Therefore, the reactive current that circulates through the inverter is in direct relation to the ratio of the used inductances. Thus, the current rate handled by the active filter is smaller than the topology reported in [29]. A controller for the topology proposed in [30], which considers only the balanced case, has been presented in [34]. The authors follow the idea of splitting the controller design in two stages, as in [29]. First, a regulation stage considering the fundamental component of the system dynamics, and, second, a harmonics compensation stage considering the harmonic component of the system dynamics.

A model-based controller for the topology proposed in [30] is presented in Part II of this thesis. The proposed solution reduces the current harmonic distortion in a three-phase power

system in the general case of unbalanced and distorted source voltages and load currents. The controller design is split in two stages as well, a regulation stage considering the fundamental component of the system dynamics, and a harmonics compensation stage considering the harmonic component of the system dynamics. In the regulation stage a current control is established to force the active filter current to only extract active power from the source, which is used to maintain the DC-link capacitor charged to a certain level. Therefore, the load reactive current compensation is mainly left to the passive filter. The harmonic compensation stage forces the injection of current to the mains to compensate the harmonic distortion appearing in the line due to the distorting load. The final proposed controller incorporates adaptive estimators to cope with the system uncertainties. Experimental results, which have been carried out in a 1.5 kVA three-phase HPF prototype, are provided to illustrate the benefits of proposed solution. This result has been recently reported in a international conference [35].

1.5 PWM regenerative rectifiers

Another conceptually different solution for harmonic reduction is the use of active rectifier topologies. These topologies are known as PFC, which can be regenerative and non-regenerative, also referred as two or four quadrants rectifiers. The non-regenerative PFCs like Vienna and boost [8] rectifiers are appropriated for applications where power is only transmitted from the source to the DC-side load.

PWM regenerative rectifiers [9], [10] are some of the most studied topologies capable of power regeneration. These topologies are of particular interest in applications, such as locomotives and downhill conveyors, where energy flow should be reversed during the operation. In this case, the line-side rectifier must be able to regenerate energy back to the power supply. Recently, these rectifiers are widely used as high-performance grid interface in power systems like renewable energy generation [36]. These rectifiers can be classified as voltage-source rectifiers (VSRs) and current-source rectifiers (CSRs) for single- and three-phase operation. In Part III of this thesis work a regenerative three-phase PWM VSR is studied. The controlled PWM rectifier has the advantages of, for instance, a bidirectional power flow, a low harmonic distortion in the line current, a power factor close to unity, a regulation of the DC-link voltage despite of disturbances in line voltage and load, among

others [10], [11]. Clearly, the performance of this converter largely depends of the applied control strategy. Different control schemes to exploit the advantages of PWM rectifiers have emerged in the last few years [10], [11], [36]-[48]. Within the different controllers for active PWM rectifiers two families can be identified, those controlling the instantaneous line current [10], [11], [37], [38] and those controlling the instantaneous active and reactive powers [39]-[48].

The classical control scheme for a controlled single-phase PWM rectifier in bridge connection [37] consists in a voltage regulation loop and a current tracking loop. Typically, a proportional-integrative (PI) controller is used in the regulation loop, which maintains the DC-link voltage at a desired constant value by means of controlling the input power. The input current reference is built as the product of the calculated power multiplied by the source voltage. In the current loop, the source current is forced to be a purely sinusoidal signal with the same phase as the source voltage, and, as consequence, the input power factor is improved. This same control scheme applies for a single-phase PWM rectifier in half-bridge connection. In this case, given that the half-bridge topology has a branch of two capacitors on the DC-side, an additional control loop should be included to balance the capacitor voltages. Typically, a proportional term associated to the difference of the capacitor voltages, is used as controller to achieve the balance [38]. On other hand, three-phase VSRs are controlled in two different ways: as a current-controlled PWM rectifier or as a voltage-controlled PWM rectifier. The first method controls the input current, while the second controls the magnitude and phase of a voltage reference (see [10] for details).

The power-based techniques for PWM rectifiers are of special interest whenever it is necessary to guarantee direct and effective regulation of both instantaneous powers towards presumably constant references. This motivates the name of direct power control (DPC) [39]-[48] for strategies based on this concept. DPC is a fairly simple and efficient control strategy that achieves good dynamical performance and a power factor close to one [40]. The idea behind DPC consists in expressing the model in terms of the instantaneous (active and reactive) powers, instead of currents, and then realize the inner control loop based on these new variables [16]. As in most controllers for PWM rectifiers, DPC also requires an outer loop with the purpose of computing the reference for the inner loop, in this case the active power reference. This reference is usually obtained by means of a PI that guarantees regulation of the DC-link capacitor voltage. According to the way the switching sequence

is obtained, the inner loop in DPC can be performed following two approaches: (i) using a look up table [39], [40], [42]; and (ii) using a PWM to generate the switching sequence [44], [45].

Most controllers following the DPC approach assume that the source voltage is balanced (see [47] and [48]), which is a situation rarely found in practice. In Part III of this thesis work, an adaptive DPC controller is proposed, which directly controls the instantaneous active and reactive power of a three-phase three-wire PWM regenerative VSR under unbalanced operation of the source voltage. Thus, instrumental for the proposed controller is to express the source voltage in terms of both symmetric sequences, positive and negative, which allows a more complete description of the model. The proposed controller incorporates an adaptation mechanism to cope with the system uncertainties. It is shown that regulation of instantaneous powers is possible at the expenses of deformation of the line current. Moreover, it is shown that the balanced case can be recovered by simply neglecting the source voltage negative sequence and thus it is a special case of the proposed scheme. Clearly, the use of the balanced case DPC controller, i.e., neglecting the negative sequence, in unbalanced voltage operation may produce a quite deteriorated performance. Experimental tests have been carried out in a 1.5 kVA three-phase PWM rectifier prototype to illustrate the merits of the proposed solution. This result has been recently reported in a international conference [49].

1.6 Outline of the dissertation

The contents of the present dissertation has been divided into three parts. Each part contains an introduction, three chapters and particular conclusions. In particular, the following three power electronics systems for harmonic and reactive power compensation have been studied:

◇ **Part I**. A single phase shunt active filter connected to a more realistic distribution system. The investigation is described in Chapters 2-5. In Chapter 2, it is shown that a proportional resonant (PR) controller [13] may lead to instabilities when the line and load impedances are considered. In Chapter 3, a controller is proposed to compensate reactive power and current harmonic distortion in a single phase system, i.e., to guarantee a power factor close to unity. The proposed controller considers the deleterious effects caused by the interaction between load and line impedances. The rationale behind the solution consists

in the introduction of a lead compensator with a gain that is adjusted online by adaptation, which replaces the conventional proportional term. This modification improves the stability conditions when the load and source impedances are non-negligible. In Chapter 4, realistic numerical results are presented to illustrate the benefits of the proposed solution.

◇ **Part II**. A HPF is studied. In this case, the active filter is connected between the inductor and capacitor of a LC passive filter. A model-based controller is proposed for this topology, which reduces the current harmonic distortion in a three-phase power system in the general case of unbalanced and distorted source voltages and load currents. The investigation is described in Chapters 5-7. In Chapter 5, the system configuration of the studied HPF is explained, the mathematical model is obtained, and the control objective is stated. Chapter 6 focuses on the controller design. This is split in two stages, a regulation stage considering the fundamental component of the system dynamics, and a harmonics compensation stage considering the harmonic component of the system dynamics. The regulation stage guarantees that the DC-link capacitor achieves a certain voltage reference level. The harmonic compensation stage forces the injection of current to compensate the harmonic distortion appearing in the line. In both stages, adaptive estimators are included to cope with the system uncertainties. Experimental results carried out in a 1.5 kVA three-phase HPF prototype are presented in Chapter 7 to assess the performance of the proposed solution.

◇ **Part III**. A three-phase three-wire regenerative PWM rectifier. In this part, a model based controller is proposed that directly controls the instantaneous active and reactive power of the PWM rectifier in the unbalanced case. This study is described in the Chapters 8-10. In Chapter 8, the problem formulation is established. In particular, the system description, the voltage source description in the unbalanced case, the transformation to instantaneous powers and the control objectives are stated. In Chapter 9, the controller design is described. It is shown that regulation of instantaneous powers is possible at the expenses of deformation of the line current. It is shown that the balanced case can be recovered by simply neglecting the source voltage negative sequence, and thus it is a special case of the proposed scheme. In Chapter 10, experimental tests are obtained to illustrate the merits of the proposed solution, which have been carried out in a 1.5 kVA three-phase PWM rectifier prototype.

Part I

AN ADAPTIVE CONTROLLER FOR THE SHUNT ACTIVE FILTER CONSIDERING A DYNAMIC LOAD AND THE LINE IMPEDANCE

INTRODUCTION

MANY domestic and industrial loads are of nonlinear nature, that is, they are composed of electronic devices with a nonlinear behavior, which introduce harmonic distortion into the electric grid, and thus they are also referred to as distorting loads. Direct consequences are a low power factor, deterioration of devices connected to the net, overheating of transformers and interferences to the nearby customers, among others. The shunt active filters arise as an effective solution for the compensation of reactive power, harmonic distortion and current unbalance due to distorting loads. Different control solutions for active filters have appeared in [1], [13]-[20]. Usually, the models used for the control design do not consider the dynamics of the load nor the line impedances, then it is expected that direct application of an active filter under this controller may produce oscillations and an instability scenario is prone to happen [24]. It has been observed that this issue is particularly worsened when the active filter intends to compensate higher order harmonics [22]. As a consequence of the unmodeled dynamics a resonance effect arises, which is produced by the interaction between a predominantly capacitive load,[2] the line impedance and the connection of the shunt active filter. This phenomenon may induce instability and frequent firing of protections, damaging the bank of capacitors and the line isolation. It is clear that the accelerated growth of harmonic distortion sources worsen these problems. Some works have explained the instability mechanism when the aforementioned impedances are considered. In [22]-[25] the authors explain the instability mechanism that arises when a dynamical load is connected to the electric grid. Then, it is shown that the conventional strategies, using the load and line current detection method, may cause to an unstable operation. In [24] the authors show that current detection methods may become unstable when a capacitor is connected in parallel

[2] It is common in practice to use capacitors or passive filters to correct the power factor in industry.

to the load. In [22] and [25] the authors present a voltage detection method that somehow alleviates this issue. On the other hand, a solution commonly used in practice consists in introducing an inductor in series to the load, with the idea of making the equivalent load predominantly inductive [52]. However, this solution, although effective in most cases, may turn out to be expensive.

This Part of the thesis proposes a controller to guarantee the compensation of harmonic distortion in spite of the presence of impedances in the line and load. In particular, the case studied considers an inductance plus a resistor as the line impedance and a capacitor as the load impedance, which is a critical situation that has received much attention in the last few years [22]-[25]. The idea behind this solution consists in replacing the proportional term used in the current loop of recently proposed controllers [3]-[5], [13] by a lead compensator. It is analytically shown that, after this modification, the stability conditions are improved. Then, it is proposed to use an adaptation mechanism to estimate the associated gain of the lead compensator to enhance the robustness against parameter variations. Finally, to show the benefits of the proposed controller, numerical results using PSCAD 4.0 are included, which were carried out in a 3 kVA using a single-phase full-bridge shunt active filter.

2. PROBLEM FORMULATION

2.1 A conventional controller for the shunt Active Filter

Figure 2.1 shows the topology of a shunt active filter, which is designed to compensate reactive power and harmonic distortion in a distribution system. This topology is composed of a VSI connected to the line via an inductor L. A distorting nonlinear load is connected to the voltage source v_S producing a distorting current i_L, which is considered as a disturbance. Traditionally, for control design purposes, it is assumed that the load current is static, in the sense that it can be considered as a simple distorted current source without any associated impedance. It is also assumed that the impedances associated to voltage source and transmission line are both negligible. A capacitor C is connected on the DC-side of the VSI.

The system dynamics of the shunt active filter shown in Figure 2.1 (where the impedances of line and load have been omitted) are described by

$$L\frac{di}{dt} = v_S - e \tag{2.1}$$

$$v_C C\frac{dv_C}{dt} = ei - \frac{v_C^2}{R} \tag{2.2}$$

$$i_S = i + i_L \tag{2.3}$$

where i_S and i represent line and injected currents, respectively, v_C is the capacitor voltage on the DC-side; $e \stackrel{\triangle}{=} uv_C$ is the injected voltage representing the actual control input, with u the duty ratio of a PWM generated switching sequence δ of a relatively high frequency. This is referred in the power electronics literature as the average model [53]. For security

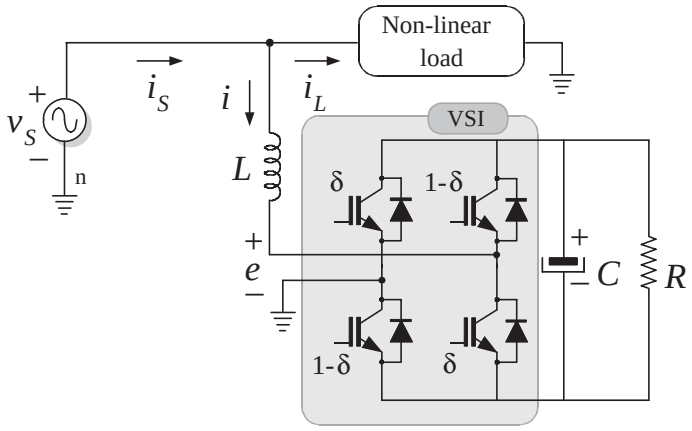

Fig. 2.1: Single-phase full-bridge shunt active filter connected to an ideal distribution system.

purposes, it is usual, in common active filters, to connect a large resistor to discharge the capacitor whenever the system is turned off. This resistor, together with switching and other losses are lumped in the model as an unknown constant resistive element R.

To facilitate the control design, it is common in practice to assume that the current dynamics (2.1) responds much faster than the dynamics involving the capacitor (2.2), and thus, they can be decoupled invoking time scale separation. This assumption allows one to split the control design in two loops, namely, *current inner loop* and *voltage outer loop*. Based on this idea, and following the *energy shaping plus damping injection* technique of the passivity-based control approach, a solution was presented in [13], which is briefly revisited below as it will serve as the basis for the proposed controller.

Current inner loop. The control objective of this control loop consists in injecting the necessary current so that the currents i_S is forced to be proportional to the source line voltage v_S. The proportionality constant, denoted as g, represents an equivalent conductance observed at the point of common connection. In other words, the objective consists in driving $\tilde{i}_S = i_S - i_S^*$ to zero, where

$$i_S^* = g v_S \tag{2.4}$$

where g is determined by the voltage regulation loop, as will be shown later.

The solution for this tracking objective consists in the construction of a control signal e that cancels v_S, adds a damping term to reinforce the stability, and introduces a bank of resonant filters tuned at the harmonics under compensation. The expression of such a current

tracking loop is given by

$$e = v_S + k_1 \tilde{i}_S + \sum_{k \in \mathcal{H}} \frac{2\gamma_k s}{s^2 + k^2 \omega_0^2} \tilde{i}_S \tag{2.5}$$

where s denotes the Laplace complex variable, k_1 and γ_k, with $k \in \mathcal{H}$, are positive control design parameters and $\mathcal{H} = \{1, 3, 5, ...\}$ represents the set of harmonics indexes considered for compensation; in this case the odd harmonics[1]. Notice that the resonant filters are tuned at the k-th harmonic component, i.e., $k\omega_0$.

In [13] the authors show that controller (2.5), in closed loop with system (2.1)-(2.3), guarantees that $\tilde{i}_S$ goes to zero asympotically, as far as there are enough resonant filters to compensate each harmonic component of the disturbances, and under the assumption of nonlinear static disturbances. This type of controllers have been reported in the power electronics literature under different names: resonant regulator [3], stationary frame generalized integrator [4], multi-resonant controller [5] and others. All these controllers are based on the internal model principle [6], [54] and belong to the family of selective compensators.

The infinite gain provided by the resonant filters in the control scheme (2.5) represents a potential source of instability. To alleviate this issue, in this thesis work, and as it is common practice, the resonant filters are replaced by bandpass filters (BPFs) of the form

$$\frac{(k\omega_0 A_k/Q_k)s}{s^2 + (k\omega_0/Q_k)s + k^2\omega_0^2} \quad , \quad k \in \mathcal{H} \tag{2.6}$$

where $A_k > 0$ and $Q_k > 0$ are the desired gain and the quality factor of the k-th BPFs, respectively. In this way, the resonance peaks have a limited gain of value A_k.

Voltage outer loop. To accomplish the regulation objective, the capacitor voltage v_C should be maintained at a constant voltage level V_d. This regulation objective is solved by suitably designing the scalar g, which, as seen in equation (2.4), is used to construct the reference i_S^*. This control loop is formed by a proportional term of limited bandwidth plus an integral term of the form

$$G = \frac{k_i}{s}\tilde{z} + \frac{k_p}{\tau_1 s + 1}\tilde{z} \tag{2.7}$$

$$g = \frac{G}{v_{S,RMS}^2} \tag{2.8}$$

[1] Single phase distorting loads produce mainly odd harmonics of the fundamental frequency.

where $\tilde{z} \triangleq (V_d^2 - v_C^2)/2$; k_p and k_i are the proportional and integral gains, respectively, and $v_{S,RMS}$ is the root mean square (RMS) value of the source voltage v_S. The scale factor $1/v_{S,RMS}^2$ in (2.8) is introduced to avoid numerical errors in the computation of g. In fact, G represents an approximate of the total power delivered by the power supply to the system composed by both active filter and load.

2.2 Stability analysis considering line and load dynamics

Figure 2.2 shows the electric circuit of the shunt active filter connected into a realistic distribution system. In contrast to the previous case, the output impedance of the power supply and the associated impedance of the line, as well as the effect of the associated passive elements on the load side, will be considered now.

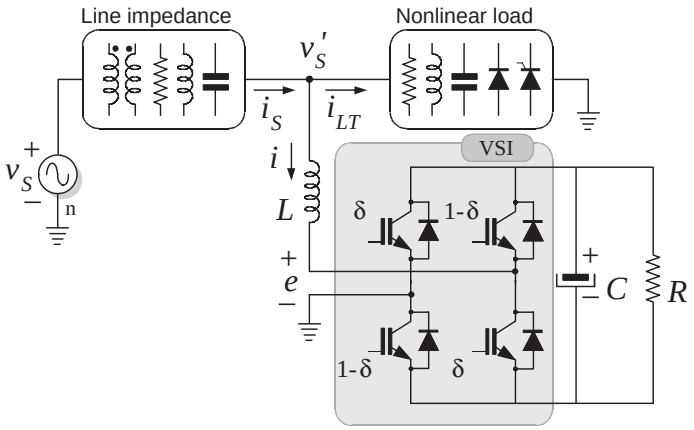

Fig. 2.2: Single phase shunt active filter connected to a "more realistic" distribution system.

Figure 2.3 shows the equivalent circuit of the shunt active filter considering impedances in both the line and the load. In this system, an impedance $Z_S(s)$ is connected in series with the internal voltage v_S. The load is represented by a Norton equivalent circuit, where the static current source i_L represents the purely distorting load and the impedance $Z_L(s)$ models its associated passive components. The active filter is composed of a voltage source e connected in parallel to the overall load by means of an inductor L.

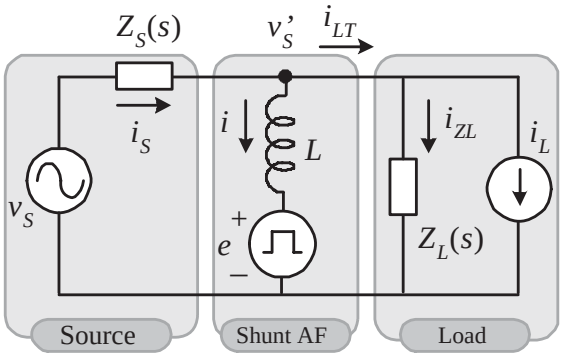

Fig. 2.3: Equivalent circuit of a shunt active filter connected to a "more realistic" distribution system considering load and line impedances.

It is straightforward from the equivalent circuit of Fig. 2.3, that

$$i_S = i + i_{LT} = i + i_{ZL} + i_L \tag{2.9}$$

$$i_{ZL} = \frac{v_S'}{Z_L(s)} = \frac{v_S - i_S Z_S(s)}{Z_L(s)} \tag{2.10}$$

By direct substitution of (2.10) in (2.9), the source current can be calculated as

$$i_S = \frac{Z_L(s)}{Z_S(s) + Z_L(s)} \left(\frac{v_S}{Z_L(s)} + i + i_L \right) \tag{2.11}$$

Notice that, in the ideal case where the line is an ideal conductor, the source impedance is negligible, and the load current is static, then $Z_S(s) = 0$ and $Z_L(s) = \infty$, out of which $i_S = i_L + i$.

The new definition of the source current (2.11) in terms of impedances $Z_S(s)$ and $Z_L(s)$ defines the new current dynamics. Figure 2.4 shows the closed loop diagram of the new expression of the source current dynamics (2.11) with the controller (2.5), and after rearranging the terms. Notice that, in contrast with the ideal case, the gain loop includes an extra transfer function denoted by

$$G_Z(s) = \frac{Z_L(s)\,(1 + gZ_S(s))}{Z_S(s) + Z_L(s)} \tag{2.12}$$

The characteristic polynomial must include now the poles associated to impedances $Z_S(s)$ and $Z_L(s)$. As it will become clear later, some poles risk to be unstable if the original controller scheme is preserved.

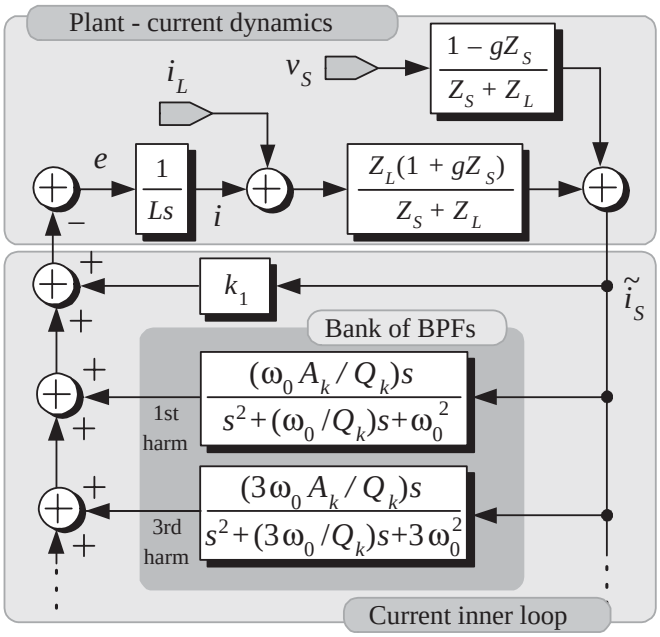

Fig. 2.4: Block diagram of the current loop considering load and line impedances.

A critical case that has been studied lately consists in taking the line impedance as an inductor in series with a resistor, and the load impedance as a capacitor [24], that is, they have the frequency domain representation $Z_S(s) = L_S s + R_S$ and $Z_L(s) = 1/(C_L s)$. In this case, instability problems have been experimentally observed even for arbitrarily small C_L. The transfer function $G_Z(s)$, for this particular case, is given by

$$G_Z(s) = \frac{gL_S s + gR_S + 1}{L_S C_L s^2 + C_L R_S s + 1} \tag{2.13}$$

which adds, in the gain loop, a couple of complex-conjugate poles and a zero[2] located at $\lambda_Z = -(gR_S + 1)/(gL_S)$.

To show in a simpler form the influence of the impedances, consider first the unperturbed system with a proportional damping term only as the controller. This yields the following characteristic polynomial

$$1 + \frac{gL_S s + gR_S + 1}{Ls(L_S C_L s^2 + C_L R_S s + 1)} k_1 = 0 \tag{2.14}$$

In this simplified case the Routh-Hurwitz criterion provides the following necessary and sufficient stability condition $0 < k_1 < R_S L / L_S$, which depends directly on the unknown line

[2] Notice that, for $1 \gg gR_S$, as normal in practice, the zero location is approximately $-1/(gL_S)$.

parameters R_S and L_S. Notice that, for practical values of L, R_S and L_S, the admissible value of k_1 can be considerably limited. Figure 2.5 shows the root locus plot for the characteristic polynomial (2.14). The parameters values used here (and throughout Part 1 of this thesis work) are $L = 5$ mH, $C_L = 82\,\mu$F, $L_S = 2.65$ mH and $R_S = 2.59\,\Omega$. Notice that the poles can have a positive real part only for relatively small values of k_1.

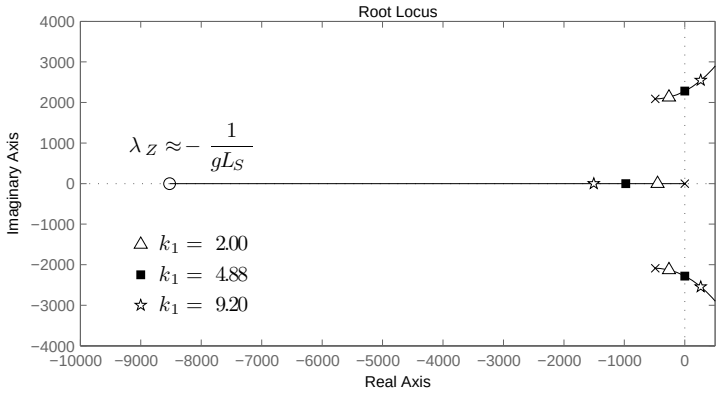

Fig. 2.5: Root locus of the unperturbed system considering load and source impedances, where the controller is a simple damping gain k_1 (without any resonant filter).

On the other hand, it has been observed that this situation gets worst in the case that BPFs (2.6) are also included as part of the controller (2.5). This adverse case is explained by means of Fig. 2.6, which shows the maximum permissible bounds for the damping term k_1, under different controller characteristics. The top (dash-dot) line represents the upper bound of the expression $0 < k_1 < R_S L/L_S$, i.e., when a simple proportional term is used as controller. The other three (solid) lines consider the addition of a k-th BPF under different values of gain A_k. The permissible region to guarantee stability in each case is the area below the lines. A first observation is that, with the introduction of a single k-th resonant filter, there is a limitation of the maximum harmonic to compensate ($k_1 > 0$). Second, it can be observed that as A_k grows, this limitation gets worst. Third, for a given A_k the value of k_1 is considerably reduced if higher (allowed) harmonics are required to compensate. In other words, to preserve stability, gains k_1 and A_k ($k \in \mathcal{H}$) must take considerably reduced values when higher harmonics are required to compensate, and viceversa, if large values for k_1 and A_k are used, then only lower harmonics can be compensated. For instance, consider that a resonant filter is included with a gain $A_k = 60$, then it is not possible to compensate harmonics beyond the 15th. Moreover, if it is required to compensate up to the 9th harmonic,

then gain k_1 should take values lower than 3. Due to the limitation on the highest harmonic to compensate, and the unavoidable reduction of gains k_1 and A_k the performance of the overall system will be considerably deteriorated.

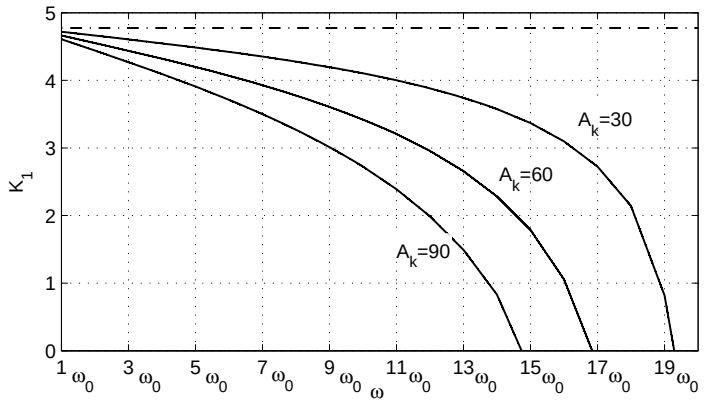

Fig. 2.6: Permissible regions for parameter k_1 under different control conditions: **(-·-)** the controller is composed of k_1 only, **(–)** a band pass filter (BPF) is added at different values of A_k (30, 60, 90).

From the frequency domain viewpoint, the instability problem can be associated to the resonance peak generated by the pair of dominant complex poles of $G_Z(s)$ which are added in the loop gain. Figure 2.7 shows the Bode plot of the closed loop system when several BPFs are included. This plot shows that the resonance peak due to $G_Z(s)$ exhibits a negative phase margin, which explains the instability reported in [24].

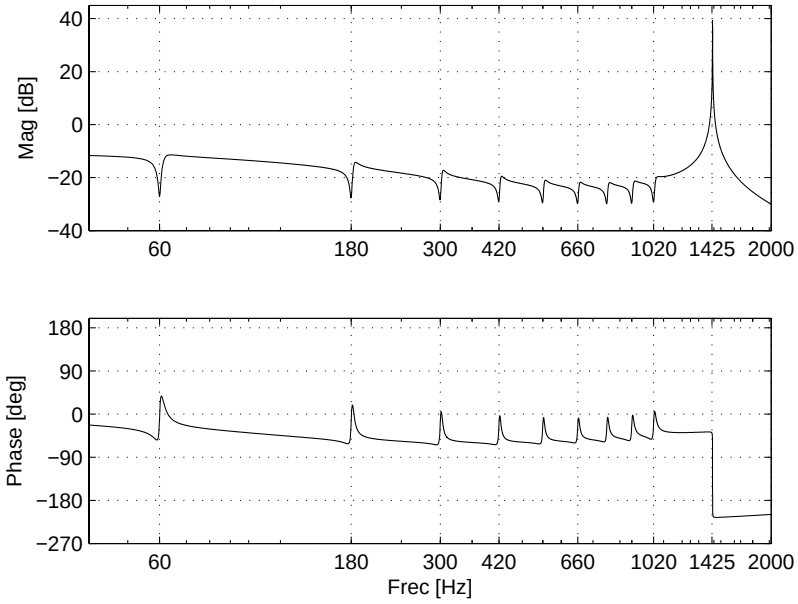

Fig. 2.7: Bode plot of the closed loop system with $A_k = 50$, $Q_k = 40$, $k_1 = 3.5$ and $k = 17$.

3. PROPOSED CONTROLLER

3.1 Lead compensator

To overcome the instability problem induced by the presence of line and load impedances, it is proposed to modify the inner loop (2.5) of the controller. A first proposal consists in adding in the damping term a lead compensator as shown in (3.1)-(3.2). This modified current loop controller includes also a term that cancels v'_S and a bank of BPFs tuned at the harmonics under compensation.

$$e = v'_S + k_1 F(s)\tilde{i}_S + \sum_{k\in\mathcal{H}} \frac{(k\omega_0 A_k/Q_k)s}{s^2 + (k\omega_0/Q_k)s + k^2\omega_0^2}\tilde{i}_S \tag{3.1}$$

$$F(s) = \frac{\tau_z s + 1}{\tau_p s + 1} \tag{3.2}$$

where the compensator $F(s)$ introduces a zero at $-1/\tau_z$ and a pole at $-1/\tau_p$. In this work $F(s)$ is a lead compensator, which is obtained by fixing $\tau_p < \tau_z$.

Figure 3.1 (top) shows the root locus,[1] in terms of k_1, of the unperturbed closed loop system considering controller (3.1)-(3.2) where a single BPF tuned at the 15th harmonic is considered.[2]

[1] To obtain the root locus the following parameters have been used $A_{15} = 50$, $Q_{15} = 40$, $\tau_z = 0.004$ s and $\tau_p = 0.0001$ s.

[2] A BPF tuned at the 15th harmonic is considered here as stability issues arise starting at this harmonic (and for higher order harmonics) in the studied example.

In this case the characteristic polynomial is given by

$$1 + \frac{N(s)}{D(s)} k_1 = 0 \tag{3.3}$$

$$\begin{aligned} N(s) &= (\tau_z s + 1)(gL_S s + gR_S + 1)(s^2 + (15\omega_0/Q_{15})s + 225\omega_0^2) \\ D(s) &= s(\tau_p s + 1)\left[L(L_S C_L s^2 + C_L R_S s + 1)(s^2 + (15\omega_0/Q_{15})s + 225\omega_0^2)\right. \\ &\quad \left. +(gL_S s + gR_S + 1)(15\omega_0 A_{15}/Q_{15})\right] \end{aligned}$$

By fixing $\tau_p \ll \tau_z$, the pole of the lead compensator $F(s)$ is located far to the left of its zero, reducing its influence. Moreover, the pole of $F(s)$ can be placed on one or the other side of the zero located at λ_z, introduced by $G_Z(s)$. However, it has been observed that placing the pole[3] to the left offers a wider range of admissible values for k_1. In this case, the effect of the zero is used to pull the resonant dominant part towards the left of the complex plane, as shown in Fig. 3.1.

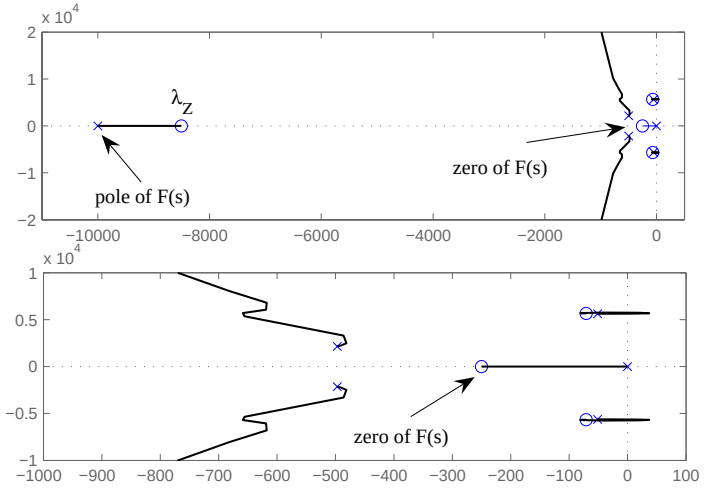

Fig. 3.1: **(top)** Root locus of the loop gain as a function of k_1 considering load and line impedances where the controller is composed of a gain k_1, a lead compensator and a BPF tuned at the 15th harmonic; **(bottom)** a zoom-in of the pole-zero pair produced by the BPF.

Roughly speaking, this simple modification allows, not only a wider range of values for k_1, but also the compensation of higher harmonics. However, it is also observed that part of

[3] It is important to remark that in case of a digital implementation, this pole location is limited by the sampling time.

this root locus falls into the right hand side of the plane for a small range of k_1. This can be observed in Fig. 3.1 (bottom), where a zoom-in to the pole-zero pairs produced by the BPF is shown. This effect is only observed when BPFs of higher order are introduced, which is the case of the BPF tuned at the 15th harmonic considered here.

Notice that the admissible range of k_1 strongly depends on the parameters of the system and BPF. In other words, if these parameters are known, then a suitable gain, say k_1^*, can be fixed to preserve stability of the equilibrium point.

3.2 Adaptive implementation

Since the parameters of the system are usually unknown and possibly time varying, the selection of k_1^* could be incorrect, which might entail poor performance and even instability. To alleviate these issues, the following adaptive estimator for the parameter k_1^* is proposed

$$\phi = F(s)\tilde{i}_S \tag{3.4}$$

$$\dot{\hat{k}}_1 = \mu\phi\tilde{i}_S \tag{3.5}$$

where $\hat{k}_1$ is an estimate of k_1^*, μ is a positive design parameter, ϕ is the so-called regressor, and $F(s)$ is the transfer function of the lead compensator.

The structure of the previous adaptive law, based on [58], is as follows. Let us define the estimation error $\tilde{k}_1 = \hat{k}_1 - k_1^*$. In Fig. 2.4, add the filter $F(s)$, in this case of the form of the lead compensator (3.1), and replace the constant gain k_1 by its estimate $\hat{k}_1$. Then, decompose the estimate $\tilde{k}_1$ into the ideal (unknown) constant gain k_1^* and the parameter error $\tilde{k}_1$, that is $\hat{k}_1 = \tilde{k}_1 + k_1^*$. Then, consider $\tilde{k}_1\phi$ as the error input. Figure 3.2 shows the block diagram considering all these changes, where, for simplicity, the resonant filters have been omitted. Computing the transfer function from the signal $\tilde{k}_1\phi$ to $\tilde{i}_S$ (neglecting the additional inputs due to v_S and i_L) yields

$$\tilde{i}_S = -H(s)[\tilde{k}_1\phi], \quad H(s) = \frac{G_Z(s)}{Ls + k_1^* F(s)G_Z(s)},$$

Replacing the expression above in (3.5), and noting that $\dot{\tilde{k}}_1 = \dot{\hat{k}}_1$, yields

$$\dot{\tilde{k}}_1 = -\mu\phi[H(s)(\tilde{k}_1\phi)]. \tag{3.6}$$

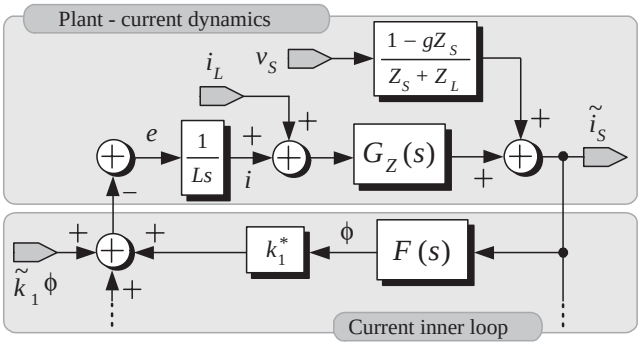

Fig. 3.2: Block diagram of the modified current loop.

This differential equation is ubiquitous in adaptive control and has been studied extensively [56], [57]. To get an idea of the nature of the equation consider an ideal case where $H(s)$ is a simple positive gain, say h, (this is the case when ϕ is "slow" with respect to the bandpass filtering of $H(s)$ and μ is small, so $\hat{k}_1$ changes also slowly). Then, the equation reduces to the non–autonomous linear equation

$$\dot{\tilde{k}}_1 = -\mu h \phi^2(t) \tilde{k}_1,$$

that can be explicitly solved as

$$\tilde{k}_1(t) = \exp^{-\mu h \int_0^t \phi^2(\tau) d\tau} \tilde{k}_1(0).$$

It is clear that the parameter estimation error satisfies $|\tilde{k}_1(t)| \leq |\tilde{k}_1(0)|$ for all $t \geq 0$, showing that the search tends to reduce the estimation error as desired. Under some conditions on $\phi(t)$—namely, that it is not square integrable—it can be also shown that $\tilde{k}_1(t) \to 0$ as $t \to \infty$. The explanation given above can be formalized using averaging analysis and the notion of average positive realness [58] of the transfer function leading to the following proposition. The proof of this preposition 3.2.1 is a consequence of Theorem 3.8 of [58].

Proposition 3.2.1 Consider the dynamical system described by (3.6). Assume

(i) $H(s)$ is a stable transfer function.

(ii) $\phi(t)$ is a nonzero T–periodic integrable function of t.

(iii) The average positive real condition

$$\sum_{i=-\infty}^{i=\infty} \mathcal{R}_e\{H(j\omega_i)\}|c_i|^2 > 0,$$

is satisfied, where c_i are the coefficients of the exponential Fourier series of ϕ and $\omega_i = 2\pi i/T$.

Then there exists $\mu^* > 0$ such that, for all $\mu \in (0, \mu^*)$, $\tilde{k}_1(t)$ converges exponentially to zero. ■

In words, the proposition states that, if

- μ is sufficiently small, i.e., slow adaptation, and
- the energy of the spectrum of ϕ is concentrated on the frequency range when $\mathcal{R}_e H(j\omega) \geq 0$, that is, in the range when the phase shift is smaller that $\pi/2$,

then the overall system will have some suitable stability properties. Notice that, in this analysis, the presence of signals v_S and i_L has been neglected and more attention is given to the adaptation loop.

In practice, disturbances are composed of fundamental and higher order harmonic components whose amplitudes decay in such a way that harmonics above certain order can be neglected [13]. Therefore, $\phi(t)$ is also a periodic signal with similar harmonic contents as the disturbance. In the example under study signal $\phi(t)$ is mainly composed of a fundamental plus odd harmonics up to the 17th harmonic, i.e., $\mathcal{H} \in \{1, 3, ..., 17\}$. In this case, $\mathcal{R}_e\{H(jk\omega_0)\} > 0$ for all $k \in \mathcal{H}$. Figure 3.3 shows the Nyquist plot of $H(s)$ highlighting the points evaluated in $k\omega$ for $k \in \{1, 3, 5, ..., 17\}$ where it is clear that $\mathcal{R}_e\{H(jk\omega_0)\} > 0$. In this case $H(s)$ includes also a bank of resonant filters tuned at harmonics at those frequencies[4].

A block diagram of the overall proposed controller is shown in Fig. 3.5.

[4] By considering more realistic values, for example those used in [19] $L_S = 0.15$ mH and $R_S = 0.008\,\Omega$, the admissible value of k_1 is considerably limited to be $0 < k_1 < 0.27$. In this case, by using the proposed solution, the condition $\mathcal{R}_e\{H(jk\omega_0)\} > 0$ is also fulfilled for all $k \in \mathcal{H}$ as is shown in Figure 3.4.

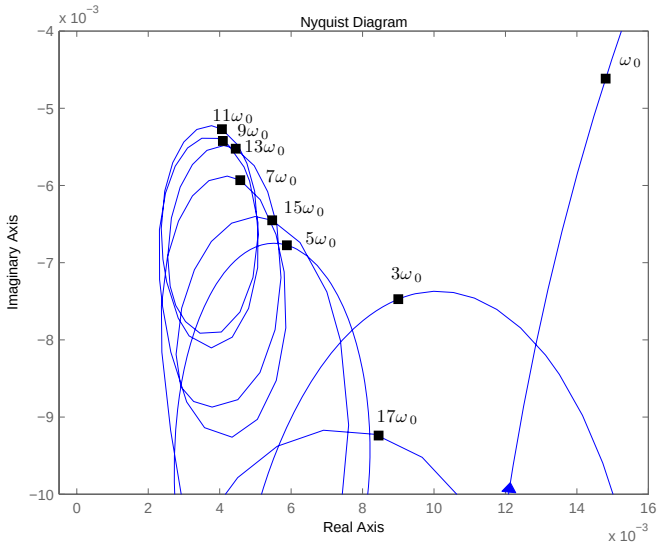

Fig. 3.3: Nyquist plot of $H(s)$ and points in $k\omega$ for $k \in \{1, 3, 5, ..., 17\}$.

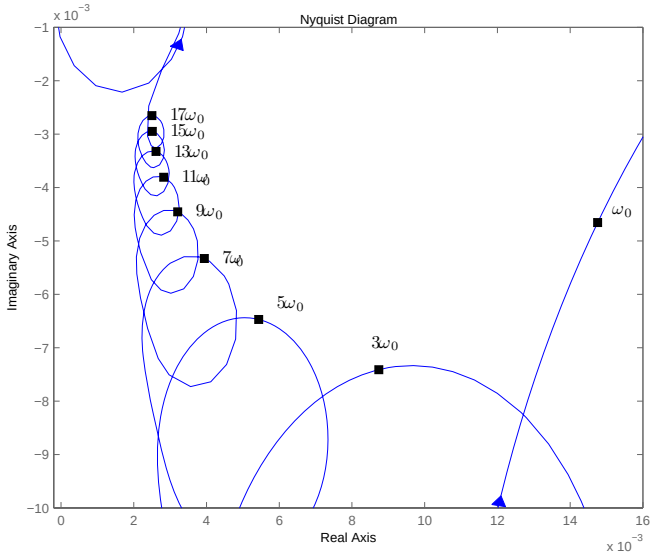

Fig. 3.4: Nyquist plot of $H(s)$ and points in $k\omega$ for $k \in \{1, 3, 5, ..., 17\}$ considering more realistic values.

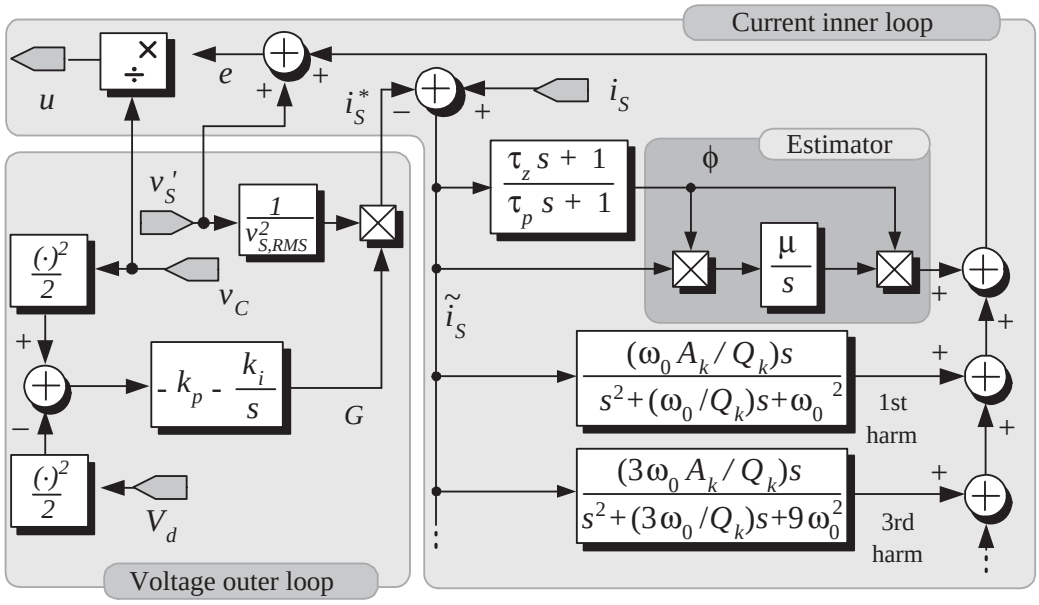

Fig. 3.5: Block diagram of the overall proposed controller.

4. NUMERICAL RESULTS

The proposed controller shown in Fig. 3.5 that uses the estimator of k_1 (3.5) has been tested in the simulation program PSCAD 4.0 with the following parameters: $L = 5$ mH, $C = 2200\,\mu$F, $V_d = 380$ V$_{DC}$, and the switching frequency $f_{sw} = 20$ kHz. A voltage source of $127\,V_{RMS}$ at $f = 60$ Hz is considered with source impedance parameters $L_S = 2.65$ mH and $R_S = 2.59\,\Omega$ (in the previous section used). The load is composed of a single-phase diode rectifier with a capacitor of $10\,\mu$F with an associated load resistance on the DC side. The critical case, connecting a capacitor of $82\,\mu$F in parallel to a distorted current load, has been considered[1]. The design parameters of the proposed controller are selected as follows: $A_k = 50$ and $Q_k = 40\,\forall\, k = \{1, 3, 5, ..., 17\}$, $k_p = 0.4$, $k_i = 0.06$, $\tau_z = 0.004$, $\tau_p = 0.0001$ and $\mu = 0.001$.

Figure 4.1 shows the responses of the system under the basic controller (2.5), after the connection of a capacitor C_L on the load side. This figure shows (from top to bottom) the line voltage v'_S, the compensated line current i_S, the load current i_L and the current i injected by the active filter. Notice that, before the connection of capacitor C_L, the responses have reached the desired equilibrium with a given k_1, in particular, the compensated current i_S is almost sinusoidal and in phase with the line voltage v'_S, thus guaranteeing a power factor close to unity. After the connection of capacitor C_L, the selected k_1 falls outside the admissible region, i. e., resonant dominant poles get a positive real part. As a consequence, a resonance effect is produced causing oscillations that considerably distort all signals. In

[1] It is important to remark that in case of a practical implementation, the power-factor correction capacitor offers the lowest impedance path and the current components associated to the switching frequency flow through this capacitor. This lowest impedance path may be changed by including a damped filter tuned to the switching frequency. A “c type” damped filter may be used for this purpose.

contrast, Fig. 4.2, shows the responses using the proposed controller depicted in Fig. 3.5, after the connection of the capacitor C_L on the load side. As before, this figure shows (from top to bottom) the line voltage v'_S, the compensated line current i_S, the load current i_L and the current i injected by the active filter. It is observed that, after a relatively small transient due to the connection of capacitor C_L, the compensated source current i_S recovers its almost sinusoidal shape with the same phase as the line voltage v'_S.

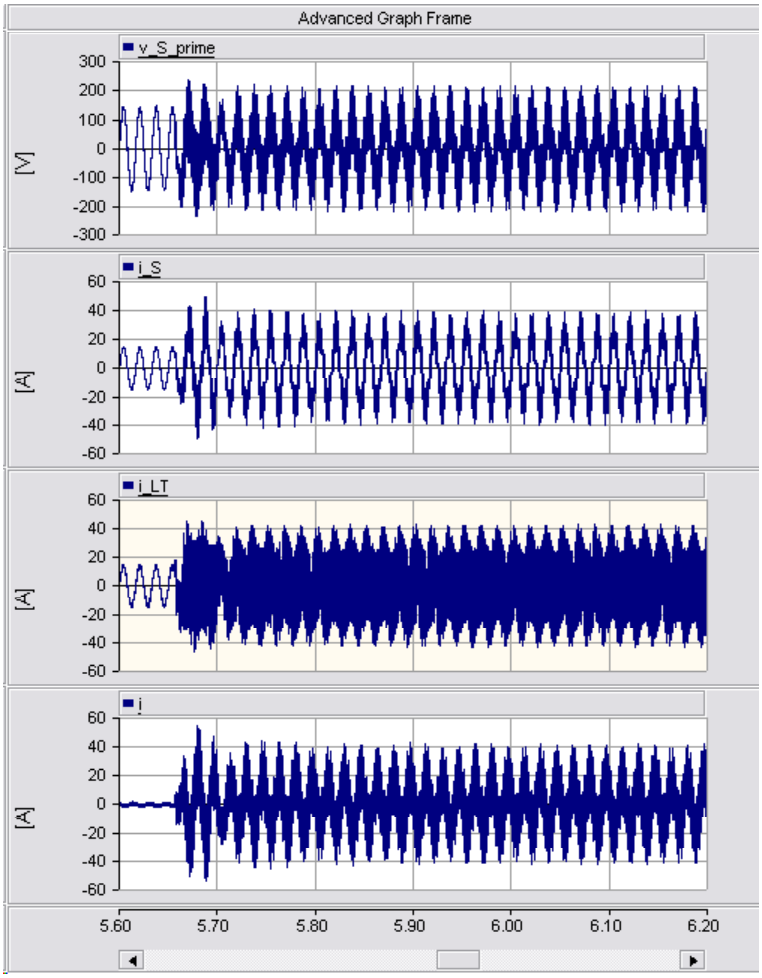

Fig. 4.1: Transient responses under the original compensator (2.5) and (2.7) during the connection of capacitor C_L on the load side of: **(from top to bottom)** line voltage v'_S, compensated line current i_S, load current i_L and active filter current i.

Figure 4.3 shows the transient responses of (top) the equivalent conductance g and (bottom) the capacitor voltage v_C when capacitor C_L is connected on the load side and under the

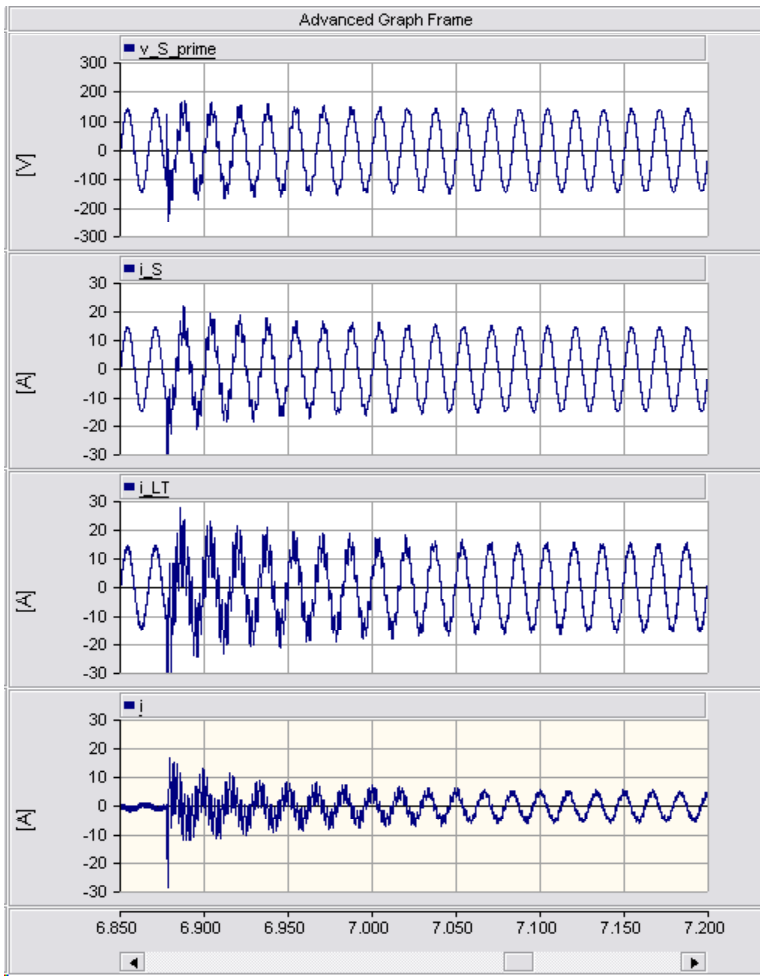

Fig. 4.2: Transient responses under the proposed compensator of Fig. 3.5, when the capacitor C_L is connected on the load side: **(from top to bottom)** line voltage v'_S, line current i_S, load current i_L and active filter current i.

proposed controller. It is observed that, after a relatively small transient, the capacitor voltage is maintained close to the reference $V_d = 280\ \mathrm{V}_{DC}$, while the equivalent conductance g converges towards a certain positive constant value. Figure 4.4 shows the transient responses of (top) the estimate $\hat{k}_1$ and (bottom) the regressor ϕ after the connection of the capacitor C_L on the load side. This figure shows that, after a relatively short transient, the estimate $\hat{k}_1$ asymptotically converges towards a constant, while the regressor ϕ reaches practically zero.

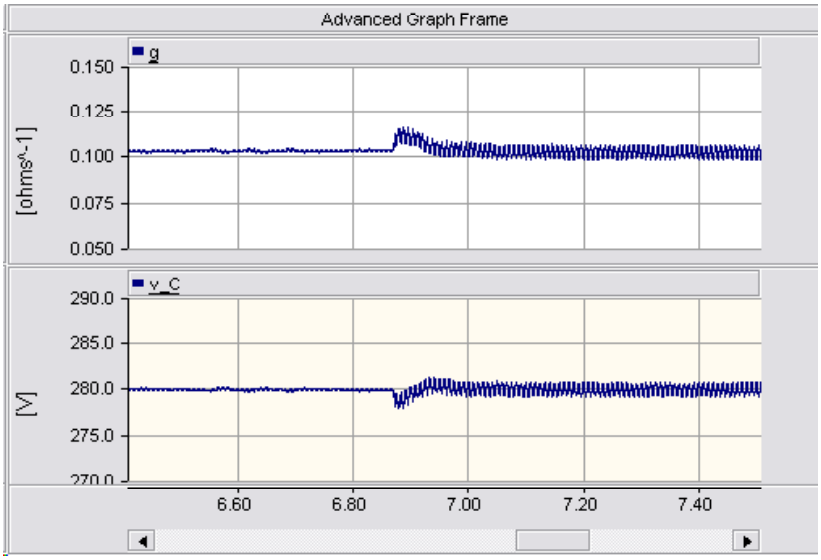

Fig. 4.3: Transient responses under the proposed controller when capacitor C_L is connected on the load side: **(top)** the equivalent conductance g and **(bottom)** the capacitor voltage v_C.

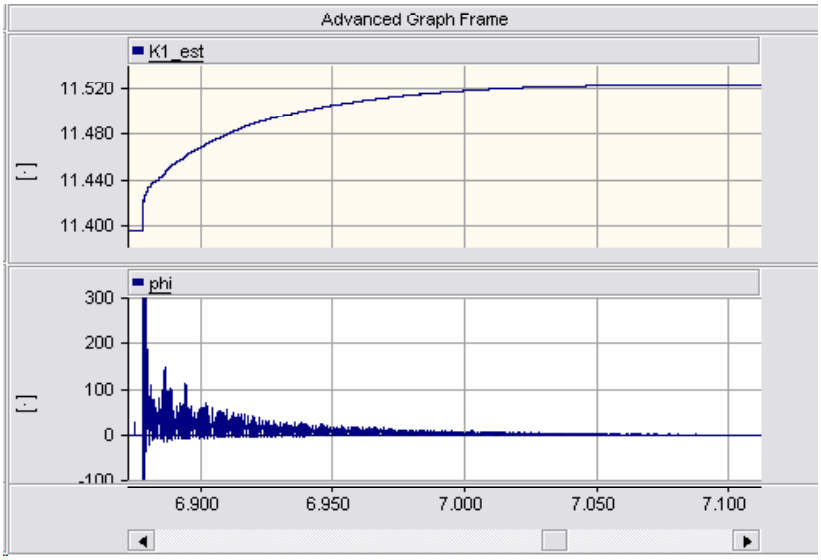

Fig. 4.4: Transient responses under the proposed controller when capacitor C_L is connected on the load side: **(top)** the estimated damping term $\hat{k}_1$ and **(bottom)** the regressor ϕ.

CONCLUSION OF PART I

In this Part, a modification is presented to a well-known controller (PR structure) for an active filter to guarantee compensation of reactive power and current harmonic distortion in spite of the presence of a critical dynamical and distorting load. The critical case, that has been studied here, consisted in the connection of a capacitor in parallel to the original load. This represents a compensation mechanism commonly used in practice for power factor correction, which explains the interest given in the Part I of this work and in previous works. A mathematical model of the overall system has been presented considering the load and source impedances. It was shown that the interaction between the line and load impedances, in this critical case, produces a resonance effect, which induces instability. The proposed solution included an adaptive implementation to enhance the robustness against system parameters uncertainties. Numerical results have been provided to illustrate the benefits of this solution.

In comparison to the previous works [22]-[25], the research developed in this thesis part has the following contributions:

- ◇ It shown that instability problems are worst in the case that BPFs are included in addition to the classical proportional term in the current loop.
- ◇ A pioneering controller is proposed to guarantee the compensation of reactive power and harmonic distortion in spite of the presence of these impedances.
- ◇ The proposed scheme is based, and duly justified, on a new mathematical model of the system that considers the presence of such impedances in the line and load.

- ◇ It is analytically shown, after this modification, that the stability conditions are improved.
- ◇ The proposed solution consists in modifying the classical PR structure. Thus, the proposed solution is easier and more inexpensive than other solutions commonly used in practice, where an inductor is connected in series to the load.

The disadvantages of the proposed solution are the following:

- ◇ An specific case, which considers an inductance plus a resistor as the line impedance and a capacitor as the load impedance, was studied in this thesis part. Although, this is a critical situation that has received much attention in the last few years, is a particular case in practice.
- ◇ The stability conditions of the proposed solution depend directly on the transfer function $H(s)$, which in turn depends on the extra function $G_Z(s)$ that appears in the gain loop when the load and line impedances are considered. Thus, the stability conditions depend, to a large degree, on the form of the load and line impedances.

Part II

A MODEL-BASED CONTROLLER FOR A HYBRID POWER FILTER TO COMPENSATE HARMONIC DISTORTION IN UNBALANCED OPERATION

INTRODUCTION

MANY domestic and industrial loads, such as uninterruptible power systems, diodes and thyristor-based rectifiers are of nonlinear nature, which introduce current harmonic distortion into the electric grid. Passive filters have been used traditionally to mitigate the harmonics due to their low cost and high efficiency. However, they present some disadvantages, for instance, resonances problems may arise with the loads, and the source impedance may affect the harmonic compensation performance. The shunt active filters arise as an effective solution for the compensation of reactive power, harmonic distortion and current unbalance due to nonlinear loads. However, their cost is relatively higher than passive filters. To alleviate this issue different HPF topologies [27]-[31] have emerged as a combination between passive and active filters to benefit from the advantages of both. For instance, in [30] a parallel hybrid power filter configuration has been proposed to force the reactive current to flow through an LC passive filter, and thus, the current rate handled by the active filter is reduced. A controller for this topology considering the balanced case has been presented in [34], the authors follow the idea of splitting the controller design in two stages as in [29]. First, a regulation stage considering the fundamental component of the system dynamics, and, second, a harmonics compensation stage considering the harmonic component of the system dynamics.

In this thesis part, a controller to compensate harmonic distortion in the case of distorted and unbalanced source voltage and load current is proposed. The proposed approach is based on the model of the system, it incorporates damping terms to guarantee stability and resonant regulators to achieve harmonic compensation. An adaptive algorithm, which is based on the ideas of passivity theory (see [21]), is included to cope with the parametric uncertainties. After transformations, this algorithm gets a simple and practical form that includes a bank

of resonant regulators which achieves a selective harmonic compensation. As in [29], the regulation stage is aimed at maintaining the DC-link capacitor in a reference voltage level, thus letting the reactive current be handled by the passive filter, the latter dealing exclusively with the compensation of the harmonic distortion in the line current. Experimental tests have been carried out in a 1.5 kVA three-phase HPF prototype to assess the performance of the proposed controller.

5. PROBLEM FORMULATION

5.1 System description

The electric circuit of the HPF studied in this thesis part is shown in Fig. 5.1. In this topology, the active filter is connected between the inductor and capacitor of an LC passive filter. The aim of this topology is to reduce the current rating handled by the active filter VSI.

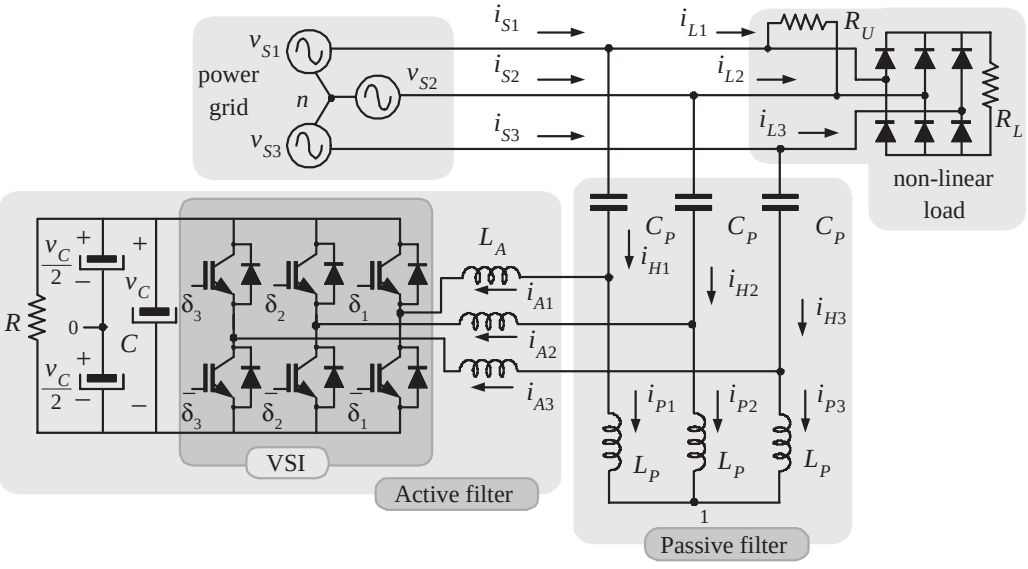

Fig. 5.1: Scheme of a hybrid power filter with the active filter connected between the passive elements.

The mathematical model can be obtained by using Kirchhoff's laws, which yields

$$L_A \frac{d}{dt}\mathbf{i}_{A123} = \mathbf{v}_{S123} - \boldsymbol{\vartheta}_{123} + v_{n0} - \mathbf{v}_{CP123} \tag{5.1}$$

$$L_P \frac{d}{dt}\mathbf{i}_{P123} = \mathbf{v}_{S123} + v_{n1} - \mathbf{v}_{CP123} \tag{5.2}$$

$$C_P \frac{d}{dt}\mathbf{v}_{CP123} = \mathbf{i}_{A123} + \mathbf{i}_{P123} = \mathbf{i}_{H123} \tag{5.3}$$

$$\mathbf{i}_{S123} = \mathbf{i}_{A123} + \mathbf{i}_{P123} + \mathbf{i}_{L123} \tag{5.4}$$

$$C \frac{d}{dt}\left(\frac{v_C^2}{2}\right) = \boldsymbol{\vartheta}_{123}^{\top}\mathbf{i}_{A123} + \frac{v_C}{R} \tag{5.5}$$

$$\boldsymbol{\vartheta}_{123} \triangleq \frac{v_C}{2}\boldsymbol{u}_{123} \tag{5.6}$$

where vectors $\mathbf{v}_{S123}$ and $\mathbf{v}_{CP123}$ represent line and passive filter capacitor voltages, respectively; $\mathbf{i}_{A123}$, $\mathbf{i}_{P123}$, $\mathbf{i}_{H123}$, $\mathbf{i}_{S123}$ and $\mathbf{i}_{L123}$ are the vectors of currents of active filter, passive filter, total hybrid injected, line and load, respectively; each vector of the form $\boldsymbol{x}_{123} = [x_1,\, x_2,\, x_3]^{\top}$; v_C is the DC-link capacitor voltage; C_P and L_P are the capacitor and inductance of the passive filter; L_A is the active filter inductance; C is the DC-link capacitance. Switching and other losses are modeled as an unknown resistor R. It is assumed that the switching sequence $\boldsymbol{\delta}_{123}$ is generated by a PWM scheme at a relatively high frequency. Thus, the *average model* is considered. Hence the duty ratio $\boldsymbol{u}_{123}$, which represents the actual control input, can be used in the place of the switching sequence $\boldsymbol{\delta}_{123}$. The control input $\boldsymbol{u}_{123}$ represents continuous signals taking values in the range $[-1,\, 1]$, which are used later in a modulation algorithm to generate the switching sequence. The load is represented by a diode rectifier with an associated resistance R_L. A resistor R_U is connected between two phases to create the unbalance current condition.

Since three-phase three-wire topology is used, then it can be assumed that the sum of the source voltages is zero. This permits to solve[1] for v_{n0} and v_{n1} from (5.1) and (5.2), as follows

$$v_{n0} = \frac{v_{CP1} + v_{CP2} + v_{CP3} + u_1 + u_2 + u_3}{3} \tag{5.7}$$

$$v_{n1} = \frac{v_{CP1} + v_{CP2} + v_{CP3}}{3} \tag{5.8}$$

where v_{n0} represents the voltage measured from point "0" to "n" and v_{n1} represents the voltage measured from point "n" to "1".

[1] Typically, it is considered that the capacitor voltage on the DC-link can be divided in two values denoted $v_C/2$. The point between the two imaginary capacitors is the point "0".

Substituting (5.7) in (5.1) and (5.8) in (5.2) yields the following expressions

$$
\begin{aligned}
L_A \frac{d}{dt}\mathbf{i}_{A123} &= \mathbf{v}_{S123} - \mathbf{B}\boldsymbol{\vartheta}_{123} - \mathbf{B}\mathbf{v}_{CP123} && (5.9)\\
L_P \frac{d}{dt}\mathbf{i}_{P123} &= \mathbf{v}_{S123} - \mathbf{B}\mathbf{v}_{CP123} && (5.10)\\
C_P \frac{d}{dt}\mathbf{v}_{CP123} &= \mathbf{i}_{A123} + \mathbf{i}_{P123} = \mathbf{i}_{H123} && (5.11)\\
\mathbf{i}_{S123} &= \mathbf{i}_{A123} + \mathbf{i}_{P123} + \mathbf{i}_{L123} && (5.12)\\
C\frac{d}{dt}\left(\frac{v_C^2}{2}\right) &= \boldsymbol{\vartheta}_{123}^{\top}\mathbf{i}_{A123} + \frac{v_C^2}{R} && (5.13)\\
\boldsymbol{\vartheta}_{123} &\triangleq \frac{v_C}{2}\boldsymbol{u}_{123} && (5.14)
\end{aligned}
$$

where the matrix $\mathbf{B}$ is given by

$$
\mathbf{B} = \frac{1}{3}\begin{bmatrix} 2 & -1 & -1 \\ -1 & 2 & -1 \\ -1 & -1 & 2 \end{bmatrix}
$$

The model in terms of the (fixed frame) $\alpha\beta$-coordinates is obtained using the Clarke's transformation (see Appendix A and [19]) given by

$$
\begin{aligned}
\begin{bmatrix} \xi_\alpha \\ \xi_\beta \end{bmatrix} &= \sqrt{\frac{2}{3}}\begin{bmatrix} 1 & -\frac{1}{2} & -\frac{1}{2} \\ 0 & \frac{\sqrt{3}}{2} & -\frac{\sqrt{3}}{2} \end{bmatrix}\begin{bmatrix} \xi_1 \\ \xi_2 \\ \xi_3 \end{bmatrix} && (5.15)\\
\boldsymbol{\xi}_{\alpha\beta} &= \mathbf{T}\boldsymbol{\xi}_{123} && (5.16)
\end{aligned}
$$

for which the properties $\mathbf{T}^{-1} = \mathbf{T}^{\top}$ and $\mathbf{T}^{-1}\mathbf{T}^{\top} = \mathbf{T}^{\top}\mathbf{T}^{-1} = \mathbf{I}$ are valid.

Thus, after the above transformations, the final expression for the model takes the form

$$
\begin{aligned}
L_A \frac{d}{dt}\mathbf{i}_{A\alpha\beta} &= \mathbf{v}_{S\alpha\beta} - \boldsymbol{\vartheta}_{\alpha\beta} - \mathbf{v}_{CP\alpha\beta} && (5.17)\\
L_P \frac{d}{dt}\mathbf{i}_{P\alpha\beta} &= \mathbf{v}_{S\alpha\beta} - \mathbf{v}_{CP\alpha\beta} && (5.18)\\
C_P \frac{d}{dt}\mathbf{v}_{CP\alpha\beta} &= \mathbf{i}_{A\alpha\beta} + \mathbf{i}_{P\alpha\beta} = \mathbf{i}_{H\alpha\beta} && (5.19)\\
\mathbf{i}_{S\alpha\beta} &= \mathbf{i}_{A\alpha\beta} + \mathbf{i}_{P\alpha\beta} + \mathbf{i}_{L\alpha\beta} && (5.20)\\
C\frac{d}{dt}\left(\frac{v_C^2}{2}\right) &= \boldsymbol{\vartheta}_{\alpha\beta}^{\top}\mathbf{i}_{A\alpha\beta} + \frac{v_C^2}{R} && (5.21)\\
\boldsymbol{\vartheta}_{\alpha\beta} &\triangleq \frac{v_C}{2}\boldsymbol{u}_{\alpha\beta} && (5.22)
\end{aligned}
$$

Figure 5.2 shows the equivalent circuit in $\alpha\beta$-coordinates. In this case, the static current generator i_L represents the purely distorting load. The active filter is composed of a voltage source $\boldsymbol{\vartheta}_{\alpha\beta}$ connected by means of an inductor L_A, between the capacitor C_L and the inductor L_P of the passive filter. In contrast with the original circuit shown in Fig. 5.1, the control input $\boldsymbol{\vartheta}_{\alpha\beta}$ has a common reference point. Notice that a similar equivalent circuit is obtained for either α or β-coordinates.

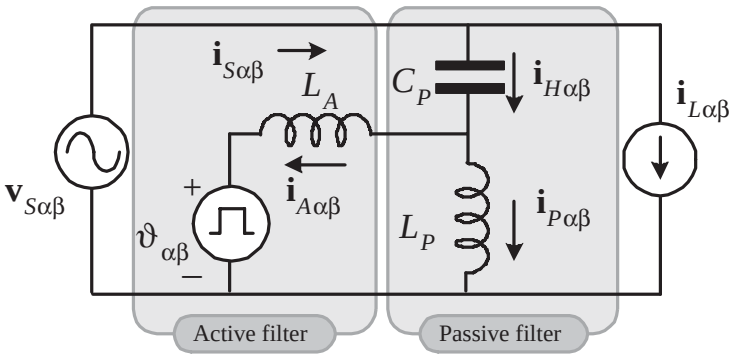

Fig. 5.2: Equivalent circuit of the studied hybrid power filter connected to a distribution system.

5.2 Control objectives and main assumptions

The control design will be divided in two stages. First, a *regulation stage* considering the fundamental component of the system dynamics, whose state variables are indicated by the subscript f. This regulation stage includes the *tracking* and a *regulation loops*. Second, a *harmonic compensation stage* considering the harmonic component of the system dynamics, whose states variables are denoted by the subscript h. The *control objectives* for each stage are stated as follows:

A. The tracking objective consists in designing a controller to force the fundamental component of the active filter currents $\mathbf{i}_{Af\alpha\beta}$ to follow a reference signal proportional to the source fundamental voltage $\mathbf{v}_{Sf\alpha\beta}$. Thus, active power is extracted from the source to accomplish of the following *regulation objective*. This tracking objective is stated as follows

$$\mathbf{i}_{Af\alpha\beta} \rightarrow \mathbf{i}^{*}_{Af\alpha\beta} = g\mathbf{v}_{Sf\alpha\beta} = G\mathbf{v}_{Sf\alpha\beta}/v^{2}_{S,RMS}$$

where g represents the apparent conductance, which is proportional to the scalar $G = gv_{S,RMS}^2$ to be defined in the *voltage regulation loop*, and $1/v_{S,RMS}^2$ is a scale factor introduced to avoid numerical errors, with $v_{S,RMS}$ the root mean square (RMS) value of the source voltage $\mathbf{v}_S$.

B. The regulation objective consists in regulating the capacitor voltage v_C towards a constant reference V_d. This guaranties that enough energy is stored in the capacitor to accomplish the following *harmonic compensation objective*. This objective can be expressed as

$$v_C \rightarrow V_d$$

C. The harmonic compensation objective consists in injecting the required current to the grid, so that the harmonic component of the line currents $\mathbf{i}_{Sh}$ are forced to zero, that is, the active filter should be able to inject the necessary current to cancel the harmonic distortion produced by the load. This objective can be expressed as follows

$$\mathbf{i}_{Sh\alpha\beta} \rightarrow 0$$

To facilitate the controller design, the following *assumptions* are considered:

A1. Parameters of the HPF L_A, L_P, C_P, and C are all assumed to be unknown constants.

A2. Signal $\boldsymbol{u}_{\alpha\beta}$, representing the actual control, is a continuous signal proportional to the duty ratio $\boldsymbol{d}_{\alpha\beta}$ of a sine pulse width modulation (SPWM) switching sequence $\boldsymbol{\delta}_{\alpha\beta}$ at a relatively high frequency. Thus, the switching sequence $\boldsymbol{\delta}_{\alpha\beta}$ can be replaced by the vector of corresponding duty ratio $\boldsymbol{d}_{\alpha\beta}$, which is afterwards replaced by the vector $\boldsymbol{u}_{\alpha\beta}$.

A3. The fundamental frequency ω_0 is considered as an unknown constant.

A4. It is assumed that the source voltage $\mathbf{v}_{S\alpha\beta}$ and the load current $\mathbf{i}_{L\alpha\beta}$ are unbalanced periodic signals that contain odd harmonics of the known fundamental frequency denoted by ω_0, therefore, they include both positive and negative sequences of the fundamental component.

A5. It is considered that the unbalance periodical signals can be split in two components, fundamental components and higher harmonics components, that is, they can be represented as sums of harmonic components as follows. From now on, the subscripts $\alpha\beta$

are omitted to facilitate the notation.

$$\begin{aligned}
\mathbf{v}_S &= \mathbf{v}_{Sf} + \mathbf{v}_{Sh} \\
&= \mathbf{v}^p_{Sf} + \mathbf{v}^n_{Sf} + \mathbf{v}^p_{Sh} + \mathbf{v}^n_{Sh} \\
&= \mathbf{e}^{\boldsymbol{J}\omega_0 t}\mathbf{V}^p_{S,f} + \mathbf{e}^{-\boldsymbol{J}\omega_0 t}\mathbf{V}^n_{S,f} \\
&+ \sum_{k\in\mathcal{H}} \mathbf{e}^{\boldsymbol{J}k\omega_0 t}\mathbf{V}^p_{S,k} + \sum_{k\in\mathcal{H}} \mathbf{e}^{-\boldsymbol{J}k\omega_0 t}\mathbf{V}^n_{Ss,k} \qquad (5.23) \\
\mathbf{i}_L &= \mathbf{i}_{Lf} + \mathbf{i}_{Lh} \\
&= \mathbf{i}^p_{Lf} + \mathbf{i}^n_{Lf} + \mathbf{i}^p_{Lh} + \mathbf{i}^n_{Lh} \\
&= \mathbf{e}^{\boldsymbol{J}\omega_0 t}\mathbf{I}^p_{L,f} + \mathbf{e}^{-\boldsymbol{J}\omega_0 t}\mathbf{I}^n_{L,f} \\
&+ \sum_{k\in\mathcal{H}} \mathbf{e}^{\boldsymbol{J}k\omega_0 t}\mathbf{I}^p_{L,k} + \sum_{k\in\mathcal{H}} \mathbf{e}^{-\boldsymbol{J}k\omega_0 t}\mathbf{I}^n_{L,k} \qquad (5.24)
\end{aligned}$$

where $\mathbf{v}_{Sf} = \mathbf{v}^p_{Sf} + \mathbf{v}^n_{Sf}$ and $\mathbf{i}_{Lf} = \mathbf{i}^p_{Lf} + \mathbf{i}^n_{Lf}$ with $\mathbf{v}^p_{Sf}$, $\mathbf{v}^n_{Sf}$, $\mathbf{i}^p_{Lf}$ and $\mathbf{i}^n_{Lf}$ representing the positive and negative sequence components of fundamental source voltage $\mathbf{v}_{Sf}$ and load current $\mathbf{i}_{Lf}$, respectively; while $\mathbf{v}_{Sh} = \mathbf{v}^p_{Sh} + \mathbf{v}^n_{Sh}$ and $\mathbf{i}_{Lh} = \mathbf{i}^p_{Lh} + \mathbf{i}^n_{Lh}$ represent the harmonic components of the source voltage $\mathbf{v}_S$ and $\mathbf{i}_L$ load current, respectively; $k \in \mathcal{H} = \{5, 7, 11, 13...\}$ is a set of harmonic indices. Terms $\mathbf{e}^{\boldsymbol{J}\omega_0 t}$ and $\mathbf{e}^{\boldsymbol{J}k\omega_0 t}$ are rotation matrixes of the form

$$\begin{aligned}
\mathbf{e}^{\boldsymbol{J}\omega_0 t} &= \begin{bmatrix} \cos(\omega_0 t) & -\sin(\omega_0 t) \\ \sin(\omega_0 t) & \cos(\omega_0 t) \end{bmatrix} \qquad (5.25) \\
\mathbf{e}^{\boldsymbol{J}k\omega_0 t} &= \begin{bmatrix} \cos(k\omega_0 t) & -\sin(k\omega_0 t) \\ \sin(k\omega_0 t) & \cos(k\omega_0 t) \end{bmatrix} \qquad (5.26) \\
\mathbf{e}^{-\boldsymbol{J}\omega_0 t} &= \left(\mathbf{e}^{\boldsymbol{J}\omega_0 t}\right)^\top \qquad (5.27) \\
\mathbf{e}^{-\boldsymbol{J}\omega_0 t} &= \left(\mathbf{e}^{\boldsymbol{J}k\omega_0 t}\right)^\top \qquad (5.28) \\
\boldsymbol{J} &= \begin{bmatrix} 0 & -1 \\ 1 & 0 \end{bmatrix} \qquad (5.29)
\end{aligned}$$

and vectors $\mathbf{V}^p_{S,f}$, $\mathbf{V}^n_{S,f}$, $\mathbf{V}^p_{S,k}$, $\mathbf{V}^n_{S,k} \in \Re^2$ are the fundamental and k-th harmonic coefficients for the positive and negative sequence of the source voltage, while $\mathbf{I}^p_{L,1}$, $\mathbf{I}^n_{L,1}$, $\mathbf{I}^p_{L,k}$, $\mathbf{I}^n_{L,k} \in \Re^2$ for the load current.

A6. All coefficients are assumed to be unknown constants, or slowly varying signals.

6. PROPOSED CONTROLLER

The control design is divided in two stages. First, a *regulation stage* considering the fundamental component of the system dynamics, which forces the fundamental component of the active filter current to extract active power from the source to regulate the DC-link capacitor voltage towards a constant reference. The compensation of the reactive current is left to the LC passive filter. This stage is composed by a *fundamental current loop* and the *voltage regulation loop*. Second, a harmonic compensation stage considering the harmonic component of the system dynamics, which forces the injection of a current to the electric grid to compensate the harmonic distortion in the line due to the distorting load.

6.1 Regulation stage: fundamental current loop

In this stage, the active filter is operating as a rectifier disregarding the load current. For control design purposes, the fundamental component of the system dynamics (5.17)-(5.22) is extracted, and referred as the fundamental dynamics. To distinguish the states of the fundamental dynamics with respect to the original ones, a subscript f is included on each variable.

$$L_A \frac{d}{dt}\mathbf{i}_{Af} = \mathbf{v}_{Sf} - \boldsymbol{\vartheta}_f - \mathbf{v}_{CPf} \tag{6.1}$$

$$L_P \frac{d}{dt}\mathbf{i}_{Pf} = \mathbf{v}_{Sf} - \mathbf{v}_{CPf} \tag{6.2}$$

$$C_P \frac{d}{dt}\mathbf{v}_{CPf} = \mathbf{i}_{Af} + \mathbf{i}_{Pf} \tag{6.3}$$

The system dynamics in terms of the increments is described as follows

$$L_A\dot{\tilde{\mathbf{i}}}_{Af} = \mathbf{v}_{Sf} - \tilde{\mathbf{v}}_{CPf} - \mathbf{v}^*_{CPf} - \boldsymbol{\vartheta}_f - L_A\frac{d}{dt}\mathbf{i}^*_{Af} \tag{6.4}$$

$$L_P\dot{\tilde{\mathbf{i}}}_{Pf} = -\tilde{\mathbf{v}}_{CPf} \tag{6.5}$$

$$C_P\dot{\tilde{\mathbf{v}}}_{CPf} = \tilde{\mathbf{i}}_{Af} + \tilde{\mathbf{i}}_{Pf} \tag{6.6}$$

where the error variables are defined as $\tilde{\mathbf{i}}_{Af} \triangleq (\mathbf{i}_{Af} - \mathbf{i}^*_{Af})$, $\tilde{\mathbf{i}}_{Pf} \triangleq (\mathbf{i}_{Pf} - \mathbf{i}^*_{Pf})$ and $\tilde{\mathbf{v}}_{CPf} \triangleq (\mathbf{v}_{CPf} - \mathbf{v}^*_{CPf})$, with $\mathbf{i}^*_{Af}$, $\mathbf{i}^*_{Pf}$ and $\mathbf{v}^*_{CPf}$ the references of $\mathbf{i}_{Af}$, $\mathbf{i}_{Pf}$ and $\mathbf{v}_{CPf}$ respectively; and the time derivatives can be computed as follows

$$L_P\dot{\tilde{\mathbf{i}}}^*_{Pf} = \mathbf{v}_{Sf} - \mathbf{v}^*_{CPf} \tag{6.7}$$

$$C_P\dot{\tilde{\mathbf{v}}}^*_{CPf} = \mathbf{i}^*_{Af} + \mathbf{i}^*_{Pf} \tag{6.8}$$

As it will be shown later, the following controller guarantees asymptotic stable tracking, i.e., $\tilde{\mathbf{i}}_{Af} \to 0$.

$$\boldsymbol{\vartheta}_f = k_f\tilde{\mathbf{i}}_{Af} + \hat{\boldsymbol{\phi}}_f \tag{6.9}$$

where k_f is a positive design parameter to add the required damping and $\hat{\boldsymbol{\phi}}_f$ is a term to reject the disturbances, which will be determined later.

Controller (6.9) in closed loop with subsystem (6.1)-(6.3) yields the following error model

$$L_A\dot{\tilde{\mathbf{i}}}_{Af} = -k_f\tilde{\mathbf{i}}_{Af} - \tilde{\mathbf{v}}_{CPf} + \left(\boldsymbol{\phi}_f - \hat{\boldsymbol{\phi}}_f\right) \tag{6.10}$$

$$L_P\dot{\tilde{\mathbf{i}}}_{Pf} = -\tilde{\mathbf{v}}_{CPf} \tag{6.11}$$

$$C_P\dot{\tilde{\mathbf{v}}}_{CPf} = \tilde{\mathbf{i}}_{Af} + \tilde{\mathbf{i}}_{Pf} \tag{6.12}$$

where $\boldsymbol{\phi}_f = \mathbf{v}_{Sf} - \mathbf{v}^*_{CPf} - L_A\frac{d}{dt}\mathbf{i}_{Af}$ is the term that concentrates all periodic disturbances. This system, referred as the *error dynamics*, is a LTI system perturbed by a periodic disturbance $(\hat{\boldsymbol{\phi}}_f - \boldsymbol{\phi}_f)$.

The equilibrium point of the unperturbed system, given by [$\bar{\tilde{\mathbf{i}}}_{Af}$, $\bar{\tilde{\mathbf{i}}}_{Pf}$, $\bar{\tilde{\boldsymbol{v}}}_{CPf}$] = [0, 0, 0], is stable provided

$$L_P > 0$$

by means of Hurwitz stability analysis.

The system (6.10)-(6.12) satisfies the so called *matching condition*, therefore the perturbation $\boldsymbol{\phi}_f$ can be cancelled by means of the actual control $\hat{\boldsymbol{\phi}}_f$ (see [59] for more details).

6.1.1 The unknown parameters case

According to (5.23)-(5.24) the periodical disturbance ϕ_f and the control signal $\hat{\phi}_f$, at the fundamental frequency, can be rewritten as

$$\phi_f \triangleq \phi_f^p + \phi_f^n = \mathbf{e}^{\boldsymbol{J}\omega_0 t}\boldsymbol{\Phi}_f^p + \mathbf{e}^{-\boldsymbol{J}\omega_0 t}\boldsymbol{\Phi}_f^n \tag{6.13}$$

$$\hat{\phi}_f \triangleq \hat{\phi}_f^p + \hat{\phi}_f^n = \mathbf{e}^{\boldsymbol{J}\omega_0 t}\hat{\boldsymbol{\Phi}}_f^p + \mathbf{e}^{-\boldsymbol{J}\omega_0 t}\hat{\boldsymbol{\Phi}}_f^n \tag{6.14}$$

where vectors $\boldsymbol{\Phi}_f^p$, $\boldsymbol{\Phi}_f^n \in \mathbb{R}^2$ represents the k-th harmonic coefficients for the positive and negative sequence of the disturbance ϕ_f, and $\hat{\boldsymbol{\Phi}}_k^{\,p}$, $\hat{\boldsymbol{\Phi}}_k^{\,n}$ their corresponding estimates.

As a result, the error signal $\tilde{\phi}_f = (\hat{\phi}_f - \phi_f)$ can be expressed as

$$\tilde{\phi}_f \triangleq \tilde{\phi}_f^p + \tilde{\phi}_f^n = \mathbf{e}^{\boldsymbol{J}\omega_0 t}\tilde{\boldsymbol{\Phi}}_f^p + \mathbf{e}^{-\boldsymbol{J}\omega_0 t}\tilde{\boldsymbol{\Phi}}_f^n \tag{6.15}$$

where the errors $\tilde{\boldsymbol{\Phi}}_f^p \triangleq (\hat{\boldsymbol{\Phi}}_f^p - \boldsymbol{\Phi}_f^p)$ and $\tilde{\boldsymbol{\Phi}}_f^n \triangleq (\hat{\boldsymbol{\Phi}}_f^n - \boldsymbol{\Phi}_f^n)$ have been defined.

Thus, the following controller, which considers the estimate for the fundamental coefficient of the periodical disturbance, is proposed

$$\boldsymbol{\vartheta}_f = k_f\tilde{\mathbf{i}}_{Af} + \left(\mathbf{e}^{\boldsymbol{J}\omega_0 t}\hat{\boldsymbol{\Phi}}_f^p + \mathbf{e}^{-\boldsymbol{J}\omega_0 t}\hat{\boldsymbol{\Phi}}_f^n\right) \tag{6.16}$$

The closed loop system (6.10)-(6.12) can be expressed as follows

$$L_A\dot{\tilde{\mathbf{i}}}_{Af} = -k_f\tilde{\mathbf{i}}_{Af} - \tilde{\mathbf{v}}_{CPf} - \left(\mathbf{e}^{\boldsymbol{J}\omega_0 t}\tilde{\boldsymbol{\Phi}}_f^p + \mathbf{e}^{-\boldsymbol{J}\omega_0 t}\tilde{\boldsymbol{\Phi}}_f^n\right) \tag{6.17}$$

$$L_P\dot{\tilde{\mathbf{i}}}_{Pf} = -\tilde{\mathbf{v}}_{CPf} \tag{6.18}$$

$$C_P\dot{\tilde{\mathbf{v}}}_{CPf} = \tilde{\mathbf{i}}_{Af} + \tilde{\mathbf{i}}_{Pf} \tag{6.19}$$

The adaptive laws are obtained by the following a Lyapunov approach, where the energy function is

$$V = \frac{L_A}{2}\tilde{\mathbf{i}}_{Af}^{\top}\tilde{\mathbf{i}}_{Af} + \frac{L_P}{2}\tilde{\mathbf{i}}_{Pf}^{\top}\tilde{\mathbf{i}}_{Pf} + \frac{C_P}{2}\tilde{\mathbf{v}}_{CPf}^{\top}\tilde{\mathbf{v}}_{CPf} + \frac{1}{2\gamma_f}\left[|\tilde{\boldsymbol{\Phi}}_f^p|^2 + |\tilde{\boldsymbol{\Phi}}_f^n|^2\right] \tag{6.20}$$

where γ_f is a positive design constant. Notice that, if the norm of the state variables tends to infinity, then V tends to infinity, therefore, the selected V function is radially unbounded. Its time derivative along the trajectories of the error model (6.17)-(6.19) is

$$\dot{V} = -k_f\tilde{\mathbf{i}}_{Af}^{\top}\tilde{\mathbf{i}}_{Af} - \tilde{\mathbf{i}}_{Af}^{\top}\left[\mathbf{e}^{\boldsymbol{J}\omega_0 t}\tilde{\boldsymbol{\Phi}}_f^p + \mathbf{e}^{-\boldsymbol{J}\omega_0 t}\tilde{\boldsymbol{\Phi}}_f^n\right] + \frac{1}{\gamma_f}\left[(\tilde{\boldsymbol{\Phi}}_f^p)^{\top}\dot{\tilde{\boldsymbol{\Phi}}}_f^p + (\tilde{\boldsymbol{\Phi}}_f^n)^{\top}\dot{\tilde{\boldsymbol{\Phi}}}_f^n\right] \tag{6.21}$$

The following adaptation laws are proposed to make $\dot{V}$ negative semidefinite.

$$\dot{\hat{\mathbf{\Phi}}}_f^p = \gamma_f \mathbf{e}^{-\boldsymbol{J}\omega_0 t}\tilde{\mathbf{i}}_{Af} \tag{6.22}$$

$$\dot{\hat{\mathbf{\Phi}}}_f^n = \gamma_f \mathbf{e}^{\boldsymbol{J}\omega_0 t}\tilde{\mathbf{i}}_{Af} \tag{6.23}$$

where $\dot{\hat{\mathbf{\Phi}}}_f^p = \dot{\tilde{\mathbf{\Phi}}}_f^p$ and $\dot{\hat{\mathbf{\Phi}}}_f^n = \dot{\tilde{\mathbf{\Phi}}}_f^n$ since $\mathbf{\Phi}_f^p$ and $\mathbf{\Phi}_f^p$ are assumed constants .

The time derivative is finally given by

$$\dot{V}(\tilde{\mathbf{i}}_{Af}) = -k_f \tilde{\mathbf{i}}_{Af}^{\top}\tilde{\mathbf{i}}_{Af} \tag{6.24}$$

Since V is radially unbounded, and $\dot{V} < 0$ for $\tilde{\mathbf{i}}_{Af} \neq 0$ and $\dot{V} = 0$ for $\tilde{\mathbf{i}}_{Af} = 0$, it can be stated that $\tilde{\mathbf{i}}_{Af} \in \mathcal{L}_2 \bigcap \mathcal{L}_\infty$, $\tilde{\mathbf{\Phi}}_f^p \in \mathcal{L}_\infty$ and $\tilde{\mathbf{\Phi}}_f^n \in \mathcal{L}_\infty$. Besides, as $\tilde{\mathbf{i}}_{Af}$ and its time derivative signal $\dot{\tilde{\mathbf{i}}}_{Af}$ are periodical signals, consequently $\dot{\tilde{\mathbf{i}}}_{Af} \in \mathcal{L}_\infty$ (see [55] for details on $\mathcal{L}_2$ and $\mathcal{L}_\infty$ spaces). Therefore, by direct application of the Corollary 1.2.2 of the Barbalat's Lemma 1.2.1 on [56], it can stated that since $\tilde{\mathbf{i}}_{Af} \in \mathcal{L}_\infty$ and $\dot{\tilde{\mathbf{i}}}_{Af} \in \mathcal{L}_\infty$ then $\tilde{\mathbf{i}}_{Af}$ is uniformly continuous, which together with the fact that $\tilde{\mathbf{i}}_{Af} \in \mathcal{L}_2$ imply that $\tilde{\mathbf{i}}_{Af} \to 0$ asymptotically as $t \to \infty$, which implies in its turn, from the adaptive laws (6.22) and (6.23), that $\tilde{\mathbf{\Phi}}_f^p$ and $\tilde{\mathbf{\Phi}}_f^n$ are bounded constant vectors. Now, define the vector $\tilde{\boldsymbol{\varphi}}_f \triangleq \left(\mathbf{e}^{\boldsymbol{J}\omega_0 t}\tilde{\mathbf{\Phi}}_f^p + \mathbf{e}^{-\boldsymbol{J}\omega_0 t}\tilde{\mathbf{\Phi}}_f^n\right)$ which rotates at a frequency ω_0. According to (6.18)-(6.19) the rotating vector $\tilde{\boldsymbol{\varphi}}_f$ should fulfill the following relationship $L_P C_P \ddot{\tilde{\boldsymbol{\varphi}}}_f = -\tilde{\boldsymbol{\varphi}}$ which holds for $\tilde{\boldsymbol{\varphi}} = 0$ only, as $L_P C_P \omega_0^2 \neq 1$. Out of this, $\tilde{\boldsymbol{v}}_{CPf} = 0$ as well as $\tilde{\mathbf{i}}_{Pf} = 0$ in the equilibrium, and thus guaranteeing convergence of the estimates toward their true values.

6.1.2 Controller simplification

To facilitate the implementation of these estimations, the following rotations (transformations) are proposed

$$\hat{\boldsymbol{\varphi}}_f^p = \mathbf{e}^{\boldsymbol{J}\omega_0 t}\hat{\mathbf{\Phi}}_f^p \tag{6.25}$$

$$\hat{\boldsymbol{\varphi}}_f^n = \mathbf{e}^{-\boldsymbol{J}\omega_0 t}\hat{\mathbf{\Phi}}_f^n \tag{6.26}$$

Out of these transformations, the fundamental current loop controller can be rewritten as

$$\boldsymbol{\vartheta}_f = k_f \tilde{\mathbf{i}}_{Af} + \left(\hat{\boldsymbol{\varphi}}_f^p + \hat{\boldsymbol{\varphi}}_f^n\right) \tag{6.27}$$

with adaptive laws (6.22)-(6.23) transformed to

$$\dot{\hat{\boldsymbol{\varphi}}}_f^p = \gamma_f \tilde{\mathbf{i}}_{Af} + \boldsymbol{J}\omega_0 \hat{\boldsymbol{\varphi}}_f^p \tag{6.28}$$

$$\dot{\hat{\boldsymbol{\varphi}}}_f^n = \gamma_f \tilde{\mathbf{i}}_{Af} - \boldsymbol{J}\omega_0 \hat{\boldsymbol{\varphi}}_f^n. \tag{6.29}$$

The transfer function expressions of the adaptation laws are given by

$$\hat{\boldsymbol{\varphi}}_f^p = \frac{\gamma_f(s + \boldsymbol{J}w_0)}{s^2 + w_0^2}\tilde{\mathbf{i}}_{Af} \tag{6.30}$$

$$\hat{\boldsymbol{\varphi}}_f^n = \frac{\gamma_f(s - \boldsymbol{J}w_0)}{s^2 + w_0^2}\tilde{\mathbf{i}}_{Af} \tag{6.31}$$

where s is the complex variable.

Therefore the adaptations are reduced to

$$\hat{\boldsymbol{\varphi}}_f = \hat{\boldsymbol{\varphi}}_f^p + \hat{\boldsymbol{\varphi}}_k^n = \frac{2\gamma_f s}{s^2 + k^2 w_0^2}\tilde{\mathbf{i}}_{Af} \tag{6.32}$$

thus, the proposed controller is

$$\boldsymbol{\vartheta}_f = k_f \tilde{\mathbf{i}}_{Af} + \frac{2\gamma_f s}{s^2 + \omega_0^2}\tilde{\mathbf{i}}_{Af} \quad , \quad \boldsymbol{u}_f = \frac{2\boldsymbol{\vartheta}_f}{v_C} \tag{6.33}$$

where $\tilde{\mathbf{i}}_{Af} \triangleq (\mathbf{i}_{Af} - \mathbf{i}_{Af}^*)$ and $k_f > 0$ and $\gamma_f > 0$ are the damping and the resonant filter gains, respectively. This controller includes a damping term to reinforce the stability, and a resonant filter tuned at the fundamental frequency to achieve perfect tracking.

6.2 Regulation stage: voltage regulation loop

The main objective of this *voltage regulation loop* consists in regulating the capacitor voltage v_C towards a constant reference V_d. In others words, this control loop reconstructs the scalar G, used in $\mathbf{i}_{Af}^*$ in the *fundamental current loop*. For the solution of this loop, the fundamental component of the dynamics (5.21) is considered and transform according to $z = v_C^2/2$, which yields a first order system perturbed mainly by an unknown constant as follows

$$C\dot{z} = (\mathbf{i}_{Af})^\top \boldsymbol{\vartheta}_f - \frac{2}{R}z \tag{6.34}$$

According to the decoupling assumption, which establishes that the current dynamics is much faster than the voltage dynamics. It can be assumed that, after a relative short time, the source current is practically tracking its reference, that is, $\mathbf{i}_{Af} \cong \mathbf{i}^*_{Af}$ and $\hat{\boldsymbol{\phi}}_f \cong \boldsymbol{\phi}_f = \mathbf{v}_{Sf} - \mathbf{v}^*_{CPf} - L_A \frac{d}{dt}\mathbf{i}_{Af}$. Under these assumptions, making a direct substitution of the control (6.9) in (6.34), yields the following expression for the capacitor voltage dynamics

$$C\dot{z} = g\mathbf{v}_{Sf}^{\top}\left(\mathbf{v}_{Sf} - \mathbf{v}^*_{CPf}\right) - \frac{2}{R}z \tag{6.35}$$

where the property $\mathbf{i}_{Af}^{\top}\boldsymbol{J}\mathbf{i}_{Af} = 0$ has been used. Solving (6.7)-(6.8), the capacitor voltage dynamics (6.35) can be expressed as

$$C\dot{z} = -C_P L_P w_0 \mathbf{v}_{Sf}^{\top}\mathbf{v}_{Sf} g - \frac{2}{R}z \tag{6.36}$$

where $C_P L_P w_0 << 1$ has been considered. This system can be considered in terms of the increments as follows

$$C\dot{\tilde{z}} = -C_P L_P w_0 v^2_{Sf,RMS} g + \frac{V_d^2}{R} - \frac{2}{R}\tilde{z} \tag{6.37}$$

$$= -a_1 g + a_2 - \frac{2}{R}\tilde{z} \tag{6.38}$$

This dynamics is a linear time invariant (LTI) system, having as output the state $\tilde{z}$ and as control input the signal g, perturbed by an unknown constant signal a_2. Notice that control input is affected by the negative constant a_1. The control design of this stage should include: a damping term to reinforce the asymptotic stability for the close loop system, and a term that incorporates robustness to reject parametric uncertainties of this stage. Thus, it is clear that a simple PI controller, operating on the error signal $\tilde{z}$, would solve the problem since the perturbation is simply an unknown constant. The proposed dynamical controller takes the following form

$$G = k_p\tilde{z} + k_i\zeta \tag{6.39}$$

$$\dot{\zeta} = \tilde{z} \tag{6.40}$$

$$g = \frac{G}{v^2_{Sf,RMS}} \tag{6.41}$$

where $\tilde{z} \triangleq (z - V_d^2/2)$, $z \triangleq v_C^2/2$, and k_p and k_i are the proportional and integral gains, respectively. The scale factor $1/v^2_{S,RMS}$ in (6.41) is introduced to avoid numerical errors in the computation of g. By means of Hurwitz stability analysis, the equilibrium point of the LTI system, given by $\left[\bar{\tilde{z}}, \bar{\zeta}\right] = \left[0, \frac{a_2 C \mathbf{v}^2_{Sf,RMS}}{a_1 k_i}\right]$, is stable provided k_p and k_i are chosen positive.

6.3 Harmonic compensation stage

In this stage, the system (5.17)-(5.22) is expressed in terms of the source currents $\mathbf{i}_S$ and the harmonic part of these system dynamics is extracted, and referred as the harmonics dynamics. To distinguish the states of the harmonic dynamics with respect to the original ones, a subscript h is included on each variable.

$$L_V \frac{d}{dt}\mathbf{i}_{Sh} = \mathbf{v}_{Sh} - \sigma_h \boldsymbol{\vartheta}_h - \mathbf{v}_{CPh} + L_V \frac{d}{dt}\mathbf{i}_{Lh} \tag{6.42}$$

$$C_P \frac{d}{dt}\mathbf{v}_{CPh} = \mathbf{i}_{Sh} - \mathbf{i}_{Lh} \tag{6.43}$$

where $\sigma_h = \frac{L_P}{L_A+L_P}$ and $L_V = \sigma_h L_A$. Notice that, this is a controllable second order system perturbed by a harmonic distortion ($\mathbf{i}_{Lh}$) appearing in both dynamics (6.42) and (6.43)

In the known parameters case, the following controller, formed by a damping term of the form $k_h\mathbf{i}_{Sh}$ and a term $\hat{\boldsymbol{\phi}}_h$ related with the rejection of harmonic distortion, guarantees asymptotic stable tracking, i.e., $\mathbf{i}_{Sh} \to 0$ and $\boldsymbol{v}_{CPh} \to 0$

$$\sigma_h \boldsymbol{\vartheta}_h = k_h \mathbf{i}_{Sh} + \hat{\boldsymbol{\phi}}_h \tag{6.44}$$

Controller (6.44) in closed-loop with subsystem (6.42)-(6.43) yields

$$L_V \frac{d}{dt}\mathbf{i}_{Sh} = -k_h\mathbf{i}_{Sh} - \mathbf{v}_{CPh} + \mathbf{v}_{Sh} + L_V \frac{d}{dt}\mathbf{i}_{Lh} - \hat{\boldsymbol{\phi}}_h \tag{6.45}$$

$$C_P \frac{d}{dt}\mathbf{v}_{CPh} = \mathbf{i}_{Sh} - \mathbf{i}_{Lh} \tag{6.46}$$

the equilibrium point of the unperturbed system given by [$\bar{\mathbf{i}}_{Sh}$, $\bar{\mathbf{v}}_{CPh}$] = [0, 0], studied following standard Hurwitz stability analysis, is stable providing $k_h > 0$. Thus, the problem is now reduced to compute $\hat{\boldsymbol{\phi}}_h$ to reject the disturbances affecting this system. However, notice that, the system does not fulfill the *matching condition* [59], as the disturbances appear in both rows (6.45) and (6.46), while the control input only appears in the first row. Hence, the controller cannot bring to zero the states $\mathbf{i}_{Sh}$ and $\mathbf{v}_{CPh}$, and thus priority is given to bring $\mathbf{i}_{Sh}$ towards zero while a small harmonic distortion is allowed in $\mathbf{v}_{CPh}$. To facilitate the design of the control signal $\hat{\boldsymbol{\phi}}_h$, it is convenient to define the following transformation

$$\tilde{\mathbf{v}}_{CPh} = \mathbf{v}_{CPh} + \boldsymbol{\psi} \tag{6.47}$$

where $\boldsymbol{\psi}$ is a periodic bounded signal constructed by the following stable filter

$$C_P \dot{\boldsymbol{\psi}} = \mathbf{i}_{Lh} \tag{6.48}$$

This yields the following system

$$L_V \frac{d}{dt}\mathbf{i}_{Sh} = -k_h \mathbf{i}_{Sh} - \tilde{\mathbf{v}}_{CPh} + \left(\boldsymbol{\phi}_h - \hat{\boldsymbol{\phi}}_h\right) \tag{6.49}$$

$$C_P \frac{d}{dt}\tilde{\mathbf{v}}_{CPh} = \mathbf{i}_{Sh} \tag{6.50}$$

where all periodic disturbances can be concentrated in $\boldsymbol{\phi}_h = \mathbf{v}_{Sh} + \boldsymbol{\psi} + L_V \frac{d}{dt}\mathbf{i}_{Lh}$. Notice that, after the transformation, the disturbance term appears only in the first row, and has the same harmonic contents as i_{Lh}. Compensation of this type of disturbances has been addressed using different schemes, where the most appealed are based on the use of the *internal model principle* [6][1]. Based in this, it is necessary to know the form of the periodical perturbation $\boldsymbol{\phi}_h$. Thus, appealing the assumption A_4, which considers that, the harmonic component $\mathbf{i}_{Lh}$ extracted of the $\mathbf{i}_L$, is a periodical signal containing higher harmonics of the fundamental frequency w_0. The time derivative of $\mathbf{i}_{Lh}$ and $\boldsymbol{\psi}$ can be explicitly represented as

$$\begin{aligned} L_V \frac{d}{dt}\mathbf{i}_{Lh} &= \frac{d}{dt}\left(\mathbf{i}^p_{Lh} + \mathbf{i}^n_{Lh}\right) = L_V \frac{d}{dt}\left(\sum_{k\in\mathcal{H}} \mathbf{e}^{\boldsymbol{J}k\omega_0 t}\mathbf{I}^p_{L,k} + \sum_{k\in\mathcal{H}} \mathbf{e}^{-\boldsymbol{J}k\omega_0 t}\mathbf{I}^n_{L,k}\right) \\ &= \boldsymbol{J}\omega_0 L_V \sum_{k\in\mathcal{H}} k\left(\mathbf{e}^{\boldsymbol{J}k\omega_0 t}\mathbf{I}^p_{L,k} - \mathbf{e}^{-\boldsymbol{J}k\omega_0 t}\mathbf{I}^n_{L,k}\right) \end{aligned} \tag{6.51}$$

and

$$\boldsymbol{\psi} = -\frac{\boldsymbol{J}}{C_P k\omega_0}\sum_{k\in\mathcal{H}}\left(\mathbf{e}^{\boldsymbol{J}k\omega_0 t}\mathbf{I}^p_{L,k} - \mathbf{e}^{-\boldsymbol{J}k\omega_0 t}\mathbf{I}^n_{L,k}\right) \tag{6.52}$$

therefore, the overall disturbance ϕ_h can be expressed as

$$\boldsymbol{\phi}_h = \sum_{k\in\mathcal{H}}\left(\mathbf{e}^{\boldsymbol{J}k\omega_0 t}\boldsymbol{\Psi}^p_h + \mathbf{e}^{-\boldsymbol{J}k\omega_0 t}\boldsymbol{\Psi}^n_h\right) \tag{6.53}$$

where

$$\boldsymbol{\Psi}^p_h = \left(\mathbf{V}^p_{S,k} - \boldsymbol{J}(C_P k\omega_0)^{-1}\mathbf{I}^p_{L,k} + \boldsymbol{J}k\omega_0\mathbf{I}^p_{L,k}\right) \tag{6.54}$$

$$\boldsymbol{\Psi}^n_h = \left(\mathbf{V}^n_{S,k} + \boldsymbol{J}(C_P k\omega_0)^{-1}\mathbf{I}^n_{L,k} - \boldsymbol{J}k\omega_0\mathbf{I}^n_{L,k}\right) \tag{6.55}$$

Thus, consider that the controller (6.44) has the following form

$$\sigma_h\boldsymbol{\vartheta}_h = k_h\mathbf{i}_{Sh} + \sum_{k\in\mathcal{H}}\left(\mathbf{e}^{\boldsymbol{J}k\omega_0 t}\hat{\boldsymbol{\Psi}}^p_k + \mathbf{e}^{-\boldsymbol{J}k\omega_0 t}\hat{\boldsymbol{\Psi}}^n_k\right) \tag{6.56}$$

[1] The *internal model principle* states that the controller output can reject (track) a class of disturbance (reference commands) without a steady error if the generator (or the model) of the disturbance is included in the stable closed loop system

where $\hat{\mathbf{\Psi}}_k^p$ and $\hat{\mathbf{\Psi}}_k^n$ represent the estimates of $\mathbf{\Psi}_k^p$ and $\mathbf{\Psi}_k^n$, respectively.

Closing the loop between system (6.49)-(6.50) and the above controller yields the following error dynamics

$$L_V \frac{d}{dt}\mathbf{i}_{Sh} = -k_h \mathbf{i}_{Sh} - \tilde{\mathbf{v}}_{CPh} + \sum_{k\in\mathcal{H}} \left(\mathbf{e}^{\boldsymbol{J}k\omega_0 t} \tilde{\mathbf{\Psi}}_k^p + \mathbf{e}^{-\boldsymbol{J}k\omega_0 t} \tilde{\mathbf{\Psi}}_k^n \right) \tag{6.57}$$

$$C_P \frac{d}{dt}\tilde{\mathbf{v}}_{CPh} = \mathbf{i}_{Sh} \tag{6.58}$$

where it has been defined $\tilde{\mathbf{\Psi}}_k^p = \hat{\mathbf{\Psi}}_k^p - \mathbf{\Psi}_k^p$ and $\tilde{\mathbf{\Psi}}_k^n = \hat{\mathbf{\Psi}}_k^n - \mathbf{\Psi}_k^n$.

In what follows a Lyapunov approach is followed to derive the adaptive laws necessary to reconstruct the vector parameters $\mathbf{\Psi}_k^p$ and $\mathbf{\Psi}_k^n$, and thus force $\tilde{\mathbf{\Psi}}_k^p \to 0$ and $\tilde{\mathbf{\Psi}}_k^n \to 0$. For this purpose, the following storage energy function is defined

$$V = \frac{L_V}{2}|\mathbf{i}_{Sh}|^2 + \frac{1}{2}|\tilde{\mathbf{v}}_{CPh}|^2 + \sum_{k\in\mathcal{H}} \frac{1}{2\gamma_k}\left[|\tilde{\mathbf{\Psi}}_k^p|^2 + |\tilde{\mathbf{\Psi}}_k^n|^2 \right] \tag{6.59}$$

where γ_k $(k \in \mathcal{H})$ are positive design constants.

The time derivative of this energy storage function along the trajectories of the error model (6.57)-(6.58) is given by

$$\begin{aligned} \dot{V} &= -k_h|\mathbf{i}_{Sh}|^2 + \mathbf{i}_{Sh}^\top \sum_{k\in\mathcal{H}} \left[\mathbf{e}^{\boldsymbol{J}\omega_0 t} \tilde{\mathbf{\Psi}}_f^p + \mathbf{e}^{-\boldsymbol{J}\omega_0 t} \tilde{\mathbf{\Psi}}_k^n \right] \\ &+ \sum_{k\in\mathcal{H}} \frac{1}{\gamma_k}\left[(\tilde{\mathbf{\Psi}}_k^p)^\top \dot{\tilde{\mathbf{\Psi}}}_k^p + (\tilde{\mathbf{\Psi}}_k^n)^\top \dot{\tilde{\mathbf{\Psi}}}_k^n \right] \end{aligned} \tag{6.60}$$

which is made negative semidefinite by proposing the following adaptive laws

$$\dot{\hat{\mathbf{\Psi}}}_k^p = -\gamma_k \mathbf{e}^{-\boldsymbol{J}\omega_0 t} \mathbf{i}_{Sh} \tag{6.61}$$

$$\dot{\hat{\mathbf{\Psi}}}_k^n = -\gamma_k \mathbf{e}^{\boldsymbol{J}\omega_0 t} \mathbf{i}_{Sh} \tag{6.62}$$

where $\dot{\hat{\mathbf{\Psi}}}_k^p = \dot{\tilde{\mathbf{\Psi}}}_k^p$ and $\dot{\hat{\mathbf{\Psi}}}_k^n = \dot{\tilde{\mathbf{\Psi}}}_k^n$ since $\mathbf{\Psi}_f^p$ and $\mathbf{\Psi}_f^p$ are assumed constants. This yields

$$\dot{V} = -k_h|\mathbf{i}_{Sh}|^2 \tag{6.63}$$

Since V is radially unbounded, and $\dot{V} < 0$ for $\mathbf{i}_{Sh} \neq 0$ and $\dot{V} = 0$ for $\mathbf{i}_{Sh}$, it can be stated that $\mathbf{i}_{Sh} \in \mathcal{L}_2 \bigcap \mathcal{L}_\infty$, $\tilde{\mathbf{\Psi}}_f^p \in \mathcal{L}_\infty$ and $\tilde{\mathbf{\Psi}}_f^n \in \mathcal{L}_\infty$. Besides, as $\tilde{\mathbf{i}}_{Sh}$ and its time derivative signal $\dot{\tilde{\mathbf{i}}}_{Sh}$ are periodical signals, consequently $\dot{\tilde{\mathbf{i}}}_{Sh} \in \mathcal{L}_\infty$. Therefore, by direct application of

the Corollary 1.2.2 of the Barbalat's Lemma 1.2.1 on [56], it can stated that since $\mathbf{i}_{Sh} \in \mathcal{L}_\infty$ and $\frac{d}{dt}\mathbf{i}_{Sh} \in \mathcal{L}_\infty$ then $\mathbf{i}_{Sh}$ is uniformly continuous, which together with the fact that $\mathbf{i}_{Sh} \in \mathcal{L}_2$ imply that $\mathbf{i}_{Sh} \to 0$ asymptotically as $t \to \infty$, which implies in its turn that $\tilde{\mathbf{\Psi}}_f^p$ and $\tilde{\mathbf{\Psi}}_f^n$ as well as $\tilde{\mathbf{v}}_{CPh}$ converge towards constants. However, from (6.57) it can be easily seen that the only possible solution for for the rotating vector $\sum_{k\in\mathcal{H}}\left(\mathbf{e}^{\boldsymbol{J}k\omega_0 t}\tilde{\mathbf{\Psi}}_k^p + \mathbf{e}^{-\boldsymbol{J}k\omega_0 t}\tilde{\mathbf{\Psi}}_k^n\right)$ to be a constant is that $\tilde{\mathbf{v}}_{CPh}$, $\tilde{\mathbf{\Psi}}_f^p$ and $\tilde{\mathbf{\Psi}}_f^n$ are all zero, and thus guaranteeing convergence of the estimates towards their true values. Notice that $\tilde{\mathbf{v}}_{CPh}$ going to zero implies that capacitors C_P allow a certain bounded ripple, as given by (6.47).

6.3.1 Controller simplification

To avoid the cumbersome rotations, the following transformations are proposed

$$\hat{\boldsymbol{\phi}}_k^p = -\mathbf{e}^{\boldsymbol{J}\omega_0 t}\hat{\mathbf{\Psi}}_k^p \tag{6.64}$$

$$\hat{\boldsymbol{\phi}}_k^n = -\mathbf{e}^{-\boldsymbol{J}\omega_0 t}\hat{\mathbf{\Psi}}_k^n \tag{6.65}$$

Out of these transformations, the adaptation laws can be rewritten as

$$\dot{\hat{\boldsymbol{\phi}}}_k^p = \gamma_f \mathbf{i}_{Sh} + \boldsymbol{J}\omega_0\hat{\boldsymbol{\phi}}_k^p \tag{6.66}$$

$$\dot{\hat{\boldsymbol{\phi}}}_k^n = \gamma_f \mathbf{i}_{Sh} - \boldsymbol{J}\omega_0\hat{\boldsymbol{\phi}}_k^n. \tag{6.67}$$

which can be rewritten in the form of transfer function as

$$\hat{\boldsymbol{\phi}}_k = \hat{\boldsymbol{\phi}}_k^p + \hat{\boldsymbol{\phi}}_k^n = \frac{2\gamma_k s}{s^2 + k^2 w_0^2}\mathbf{i}_{Sh} \quad , \quad k \in \mathcal{H} \tag{6.68}$$

and thus

$$\hat{\boldsymbol{\phi}}_h = \sum_{k\in\mathcal{H}} \frac{2\gamma_k s}{s^2 + k^2 w_0^2}\mathbf{i}_{Sh} \tag{6.69}$$

Finally, the proposed controller for the harmonic compensation stage is given by

$$\sigma_h \boldsymbol{\vartheta}_h = k_h \mathbf{i}_{Sh} + \sum_{k\in\mathcal{H}} \frac{2\gamma_k s}{s^2 + k^2\omega_0^2}\mathbf{i}_{Sh} \quad , \quad \boldsymbol{u}_h = \frac{2\boldsymbol{\vartheta}_h}{v_C} \tag{6.70}$$

where k_h and γ_k ($k \in \{3, 5, ...\}$) are referred as the damping gain and the gain of the k-th resonant filter, respectively. Notice that the controller includes a dissipative term associated to $\mathbf{i}_{Sh}$ and bank of resonant filters tuned at the harmonics under compensation, i.e., 3rd, 5th, and so on.

6.4 Estimation of fundamental and harmonics components

The implementation of the proposed controller requires the knowledge of the fundamental and the harmonic components of some state variables and signals, in particular $\mathbf{i}_{Af}$, $\mathbf{v}_{Sf}$, $\mathbf{v}_{Sh}$, $\mathbf{i}_{Sh}$.

Considering only the fundamental component of the unbalance periodical signals (5.23) and (5.24), the following relationships hold

$$\mathbf{x}_f = \mathbf{x}_f^p + \mathbf{x}_f^n = \mathbf{e}^{\boldsymbol{J}\omega_0 t}\mathbf{X}_f^p + \mathbf{e}^{-\boldsymbol{J}\omega_0 t}\mathbf{X}_f^n \tag{6.71}$$

where $\mathbf{x}_f$ represents the fundamental component of state variables, and $\mathbf{x}_f^p$ and $\mathbf{x}_f^n$ represent positive and negative sequences of the fundamental component, respectively. Vectors $\mathbf{X}_f^p$ and $\mathbf{X}_f^n$ are the fundamental harmonic coefficients for the positive and negative sequence representation of the fundamental component $\mathbf{x}_f$, which are assumed to be unknown constants.

Based on description (6.71), the following relationship is obtained

$$\dot{\mathbf{x}}_f = \omega_0 \boldsymbol{J}\mathbf{e}^{\boldsymbol{J}\omega_0 t}\mathbf{X}_f^p - \omega_0 \boldsymbol{J}\mathbf{e}^{-\boldsymbol{J}\omega_0 t}\mathbf{X}_f^n \tag{6.72}$$

$$= \omega_0 \boldsymbol{J}\left(\mathbf{x}_f^p - \mathbf{x}_f^n\right) = \omega_0 \boldsymbol{J}\boldsymbol{\chi}_f \tag{6.73}$$

where it has been defined as auxiliary variable $\boldsymbol{\chi}_f \stackrel{\triangle}{=} \mathbf{x}_f^p - \mathbf{x}_f^n$ to allow a complete description of the unbalance signals. Therefore, a complete model that describes the state variables and signals in the unbalanced case is given by

$$\dot{\mathbf{x}}_f = \omega_0 \boldsymbol{J}\boldsymbol{\chi}_f \tag{6.74}$$

$$\dot{\boldsymbol{\chi}}_f = \omega_0 \boldsymbol{J}\mathbf{x}_f \tag{6.75}$$

In fact, the following relationship can be established

$$\begin{bmatrix} \mathbf{x}_f \\ \boldsymbol{\chi}_f \end{bmatrix} = \begin{bmatrix} 1 & 1 \\ 1 & -1 \end{bmatrix} \begin{bmatrix} \mathbf{x}_f^p \\ \mathbf{x}_f^n \end{bmatrix} \tag{6.76}$$

It is important to notice the need of the auxiliary variable $\boldsymbol{\chi}_f$ to allow a complete description of the unbalance voltage signal.

Remark 6.4.1 Notice that, in the balanced case the description (6.74)-(6.75) is reduced to $\dot{\mathbf{x}}_f = \mathbf{J}\omega_0\mathbf{x}_f$, as in this case $\mathbf{x}_f = \boldsymbol{\chi}_f$. □

Based on the structure (6.76), the objective consists in designing an estimator to reconstruct such signals for the unbalanced case. The proposed estimator consist of a copy of the system model (6.74)-(6.75) to which a damping term is added, that is,

$$\dot{\hat{\mathbf{x}}}_f = \omega_0 \boldsymbol{J} \hat{\boldsymbol{\chi}}_f + \lambda \hat{\mathbf{x}}_h \quad , \quad \hat{\mathbf{x}}_h = \mathbf{x} - \hat{\mathbf{x}}_f \tag{6.77}$$

$$\dot{\hat{\boldsymbol{\chi}}}_f = \omega_0 \boldsymbol{J} \hat{\mathbf{x}}_f \tag{6.78}$$

where $\lambda > 0$ is the estimation gain, $\hat{\mathbf{x}}_f$ and $\hat{\mathbf{x}}_h$ represent the estimates of the fundamental and the harmonics components of vector $\mathbf{x}$, respectively and $\hat{\boldsymbol{\chi}}_f$ is the estimate of the auxiliary variable $\boldsymbol{\chi}_f$.

The estimation error dynamics is given by

$$\dot{\tilde{\mathbf{x}}}_f = \omega_0 \boldsymbol{J} \tilde{\boldsymbol{\chi}}_f - \lambda \tilde{\mathbf{x}}_h \tag{6.79}$$

$$\dot{\tilde{\boldsymbol{\chi}}}_f = \omega_0 \boldsymbol{J} \tilde{\mathbf{x}}_f \tag{6.80}$$

where $\tilde{\boldsymbol{\chi}}_f = \boldsymbol{\chi}_f - \hat{\boldsymbol{\chi}}_f$ represents an estimation error.

Convergence of the proposed estimator is proved following the Lyapunov approach where the following quadratic function of the estimation errors is used

$$H = \frac{1}{2}|\tilde{\mathbf{x}}_f|^2 + \frac{1}{2}|\tilde{\boldsymbol{\chi}}_f|^2$$

Its time derivative along the trajectories of the error model (6.79)-(6.80) yields the following negative semidefinite function

$$\dot{H} = -\lambda \tilde{\mathbf{x}}_h^\top \tilde{\mathbf{x}}_h$$

Since H is radially unbounded and $\dot{H}$ is negative semidefinite then $\tilde{\mathbf{x}}_f \in \mathcal{L}_2 \bigcap \mathcal{L}_\infty$ and $\tilde{\boldsymbol{\chi}}_f \in \mathcal{L}_2 \bigcap \mathcal{L}_\infty$. From (6.79)-(6.80), $\dot{\tilde{\mathbf{x}}}_f \in \mathcal{L}_\infty$ and $\tilde{\boldsymbol{\chi}}_f \in \mathcal{L}_\infty$ then $\tilde{\mathbf{x}}_h$ and $\tilde{\boldsymbol{\chi}}_f$ are uniformly continuous, which together with the fact that $\tilde{\mathbf{x}}_f \in \mathcal{L}_2$ and $\tilde{\boldsymbol{\chi}}_f \in \mathcal{L}_2$ imply that $\tilde{\mathbf{x}}_f \to 0$ and $\tilde{\boldsymbol{\chi}}_f \to 0$, asymptotically. Now, from (6.77), the harmonic estimator can be rewritten as

$$\begin{aligned} \hat{\mathbf{x}}_h &= \mathbf{x}_f - \hat{\mathbf{x}}_f + \mathbf{x}_h \\ &= \tilde{\mathbf{x}}_f + \mathbf{x}_h \end{aligned}$$

therefore, as $\tilde{\mathbf{x}}_f \to 0$ then $\hat{\mathbf{x}}_h = \mathbf{x}_h$ and $\tilde{\mathbf{x}}_h \to 0$. Notice that estimator (6.78) reconstructs both vectors $\mathbf{x}_f$, and $\mathbf{x}_h$, which can then be used to implement the proposed controller. However, the estimator requires the knowledge of the fundamental frequency ω_0, which is practically possible.

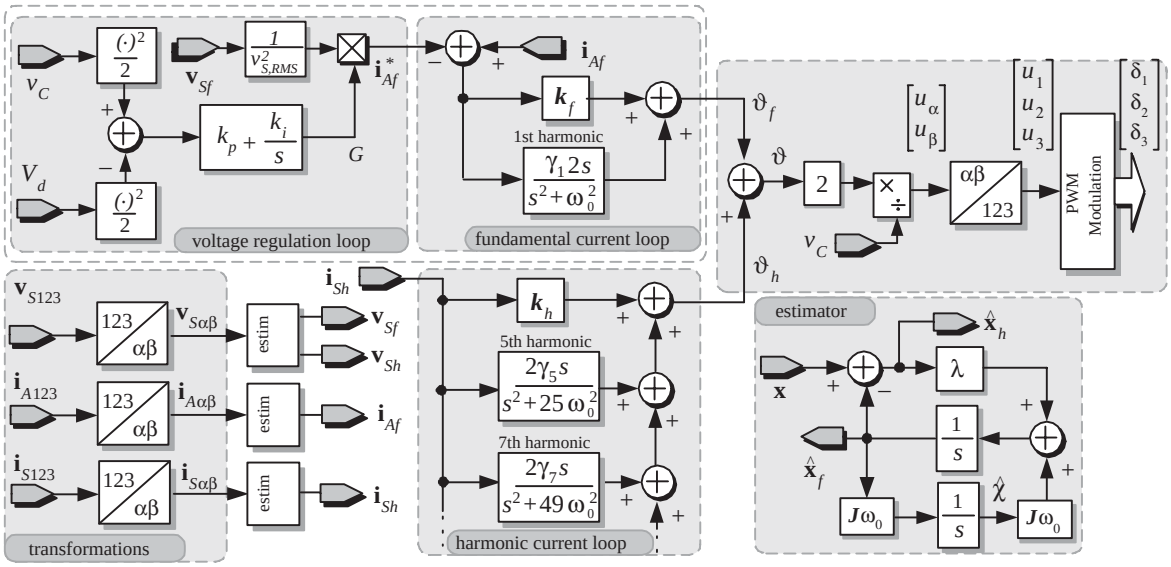

Fig. 6.1: Block diagram of the overall proposed controller.

Summarizing, the final expressions for the overall proposed controller, including *regulation stage*, the *harmonic compensation stage* and the *estimation* of fundamental and harmonics components are given by

$$
\begin{aligned}
\boldsymbol{\vartheta}_f &= k_f \tilde{\mathbf{i}}_{Af} + \frac{2\gamma_f s}{s^2+\omega_0^2}\tilde{\mathbf{i}}_{Af} \\
\boldsymbol{\vartheta}_h &= k_h \mathbf{i}_{Sh} + \sum_{k\in\mathcal{H}} \frac{2\gamma_k s}{s^2+k^2\omega_0^2}\mathbf{i}_{Sh} \\
\boldsymbol{\vartheta} &= \boldsymbol{\vartheta}_f + \boldsymbol{\vartheta}_h \\
\boldsymbol{u} &= \frac{2\boldsymbol{\vartheta}}{v_C} \\
G &= k_p \tilde{z} + k_i \zeta \\
\dot{\zeta} &= \tilde{z} \\
\dot{\hat{\mathbf{x}}}_f &= \omega_0 \boldsymbol{J}\hat{\boldsymbol{\chi}}_f + \lambda \hat{\mathbf{x}}_h \quad , \quad \hat{\mathbf{x}}_h = \mathbf{x} - \hat{\mathbf{x}}_f \\
\dot{\hat{\boldsymbol{\chi}}}_f &= \omega_0 \boldsymbol{J}\hat{\mathbf{x}}_f
\end{aligned}
\tag{6.81}
$$

Notice that the total control signal is computed as the sum of the fundamental component of the control (6.33) and the harmonic component of the control (6.70). A block diagram of the overall proposed controller is shown in Fig. 6.1.

7. EXPERIMENTAL RESULTS

The controller developed in Chapter 6 was experimentally tested in a 1.5 KVA HPF three-phase prototype. The overall prototype was built using the instrumentation described in Appendix B, and includes the three following stages. The *power stage* which includes the active and passive filters, the maneuvering switches and the nonlinear load. The *instrumentation stage* which is composed by the current and voltage sensors and the control interface. The *digital stage* which is conformed by a control board based on digital signal processor (DSP) ACE1103 made by dSPACE, and the software development using Simulink/MATLAB. Each of these stages is described in detail in the Appendix B. The overall implemented scheme of the HPF is shown in Fig. 7.1. Notice that, the sensed signals are the source currents i_{S123}, the passive filter currents i_{A123}, the source voltages v_{S123} and the capacitor voltage v_C.

Different tests were carried out to exhibit the performance of this solution, and to show the correct fulfillment of the main objectives. As it was mentioned before, the implementation of the proposed controller requires the knowledge of the fundamental and the harmonic components of some state variables and signals. Therefore, the experimental results shown in the following sections include, on the one hand, steady state responses of the estimation of fundamental and harmonics components, and on the other hand, steady state and transient responses of the HPF.

7.1 Discussion of the implementation

The passive filter was designed for mitigation of the 5^{th} harmonic using the following parameters: $L_P = 5$ mH, $C_P = 56\,\mu$F. The active filter parameters are the following $L_A = 4$ mH,

$C = 2200\,\mu$F, $R = 2200\,\Omega$, and the reference voltage $V_d = 90$ V$_{DC}$. An unbalanced source voltage of around 127 V_{RMS} at $f_0 = 60$ Hz ($\omega_0 = 377$ r/s) is considered as the line voltage. As pointed out before, the proposed controller is implemented in the dSPACE card model ACE1103 with a sampling frequency $f_s = 14.28$ kHz and a switching frequency $f_{sw} = 10$ kHz. The distorted unbalanced load is composed of a three-phase diode rectifier with an associated load resistance R_L on the DC side, which takes values of $100\,\Omega$ or $50\,\Omega$. A resistor $R_U = 100\ \Omega$ is connected between two phases to create the unbalance condition.

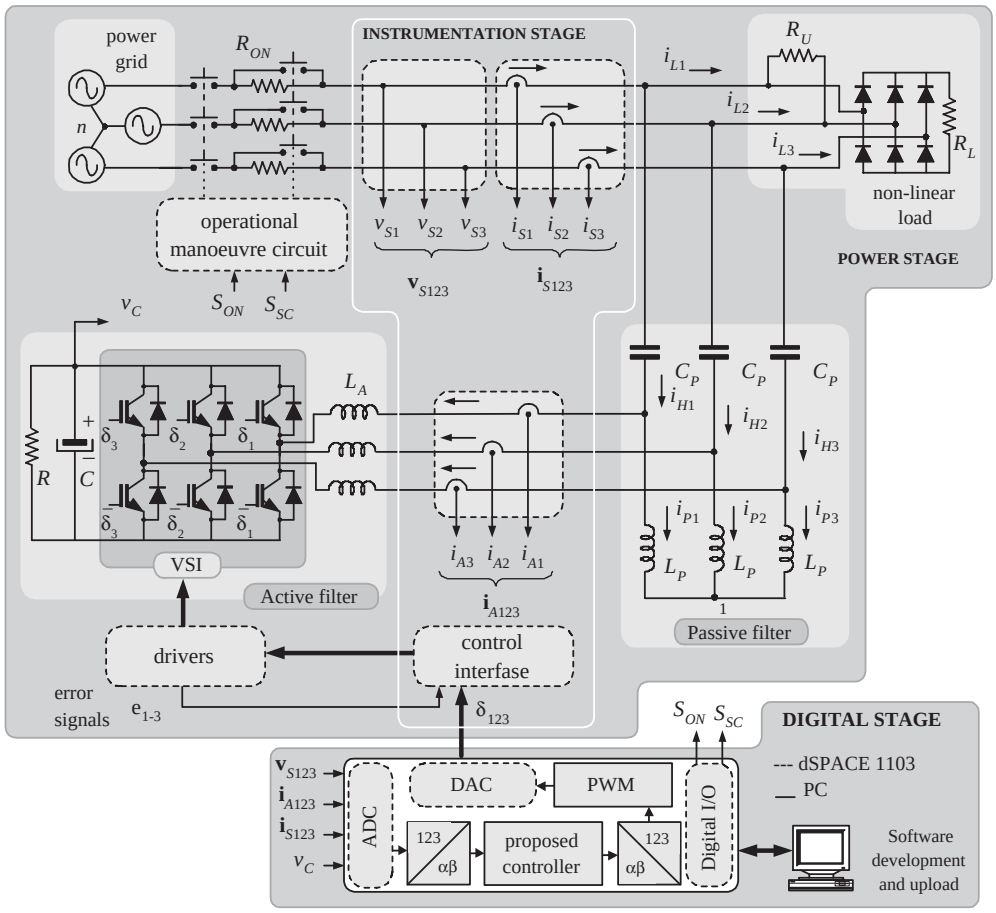

Fig. 7.1: General scheme of the experimental setup for testing the proposed control of the hybrid power filter.

On other hand, an important issue is that the control objectives must be fulfilled in a specific order. That is, first, in the *regulation stage*, the fundamental component of the active filter current must be forced to extract active power from the source in order to regulate the

DC-link capacitor voltage towards a constant reference. Then, in the *harmonic compensation stage*, the necessary current must be injected to the main to cancel the harmonic distortion produced by the load. In general, the design process for the control parameters is based on the time responses requirements. The criteria for the tuning of the control parameters of the *regulation* and the *harmonic compensation stages* is described in the following subsections.

7.1.1 Tuning of the regulation stage parameters

In the *fundamental current loop*, the tuning of k_f is performed following the next approximations. First, notice that the fundamental current closed-loop dynamics, compounded by (6.10)-(6.12), is faster than the voltage closed-loop dynamics (6.37). This current dynamics can be expressed as

$$\begin{bmatrix} L_A s + k_f + \frac{L_P s}{L_P C_P s^2+1} & 0 \\ 0 & L_A s + k_f + \frac{L_P s}{L_P C_P s^2+1} \end{bmatrix} \begin{bmatrix} \tilde{i}_{Af\alpha} \\ \tilde{i}_{Af\beta} \end{bmatrix} = \begin{bmatrix} \tilde{\phi}_{f\alpha} \\ \tilde{\phi}_{f\beta} \end{bmatrix} \tag{7.1}$$

where $\tilde{\boldsymbol{\phi}}_f = [\tilde{\phi}_{f\alpha}, \tilde{\phi}_{f\beta}]^\top$ represents the disturbance rejection error. In this case, the term $L_P s/(L_P C_P s^2 + 1)$ in the nonzero entries of the matrix denotes the resonant passive filter dynamics, which was tuned for mitigation of the 5^{th} harmonic. Since this filter is a notch to an specific frequency in the closed-loop current dynamics, it does not influence the bandwidth of the fundamental current dynamics, and its effect can be neglected from (7.1). Thus, the characteristic polynomial can be reduced to $L_A s + k_f = 0,$ and the bandwidth of the fundamental current dynamics may be determined by k_f/L_A. Following the procedure in [2], the bandwidth of this current dynamics must be at most $1/10$ of the sampling frequency. Therefore, the gain k_f must satisfy $k_f < \pi f_s L_A/5$ which, according to the prototype parameters, yields $k_f < 35.8$ In the present thesis $k_f = 3$ to fulfill the criteria with a enough margin.

On other hand, the infinite gain, provided by the fundamental resonant filter used in this loop, represents a potential source of instability. To assure a safer operation, in the implemented controller, the resonant filter has been replaced by a BPF of the form

$$\frac{(\omega_0 A_f/Q_f)s}{s^2 + (\omega_0/Q_f)s + \omega_0^2}$$

where $A_f > 0$ and $Q_f > 0$ are the desired gain and the quality factor of the k-th bandpass

filters, respectively. The design parameters of the proposed controller are $A_k = 30$ and $Q_k = 40$.

In the *voltage loop* case, the capacitor dynamics (6.37) in closed-loop with the controller (6.39)-(6.41) is given by the following second order system

$$C\dot{\tilde{z}} = -C_P L_P w_0 \left(k_p \tilde{z} + k_i \zeta\right) + a_2 - \frac{2}{R}\tilde{z} \tag{7.2}$$

$$\dot{\zeta} = \tilde{z} \tag{7.3}$$

where a_2 is a constant disturbance. The characteristic polynomial of the previous system is given by

$$s^2 + \frac{RC_P L_P w_0 k_p + 2}{RC} s + \frac{C_P L_P w_0 k_i}{C} = 0 \tag{7.4}$$

Notice that, the system dynamics must fulfill the *decoupling assumption*, which establishes that the current dynamics is much faster than the voltage dynamics. Thus, the fundamental voltage loop was designed to be at least ten times slower than the fundamental current loop (see [9]). The selected parameters were $k_p = 0.25$, $k_i = 1$, which fulfill this assumption.

7.1.2 Tuning of the harmonic compensation parameters

In the *harmonic current loop* BPFs were used instead of resonant filters to assure a safer operation in the implemented controller. The form of these filters is the following.

$$\frac{(k\omega_0 A_k/Q_k)s}{s^2 + (k\omega_0/Q_k)s + k^2\omega_0^2} \quad , \quad \forall\, k = \{3, 5, ..., 13\},$$

where $A_k > 0$ and $Q_k > 0$ are the desired gain and the quality factor of the k-th bandpass filters, respectively. In this case, the damping term introduced in the denominator of the BPFs, limits the gains. The group of the harmonics to be compensated, is composed by 5th, 7th, 11th, and 13th harmonic components, that is, the bank of BPFs includes filters tuned at these harmonics of the fundamental frequency f_0. Thus, the bank of the BPFs and the damping term k_h of the controller (6.70) can be expressed as:

$$\begin{aligned} \boldsymbol{\vartheta}_h &= \sum_{k=\{3,5,11,13\}} \frac{(k\omega_0 A_k/Q_k)s}{s^2 + (k\omega_0/Q_k)s + k^2\omega_0^2}\mathbf{i}_{Sh} + k_h \mathbf{i}_{Sh} \\ &= \sum_{k=\{3,5,11,13\}} \frac{k_h\left(s^2 + \frac{k\omega_0}{Q_k}\left(\frac{k_h + A_k}{k_h}\right)s + k^2\omega_0^2\right)}{s^2 + (k\omega_0/Q_k)s + k^2\omega_0^2}\mathbf{i}_{Sh} \end{aligned} \tag{7.5}$$

Note that the gain k_h in the above expression, allows one to have control over the gain produced in the notches, and on the quality factor of each band pass filter. So, an appropriate gain k_h that incorporates a harmonic selective compensation may be selected by means of an appropriate frequency response. Figure 7.2 shows the Bode plots of the control (7.5) for different values of the damping term k_h.

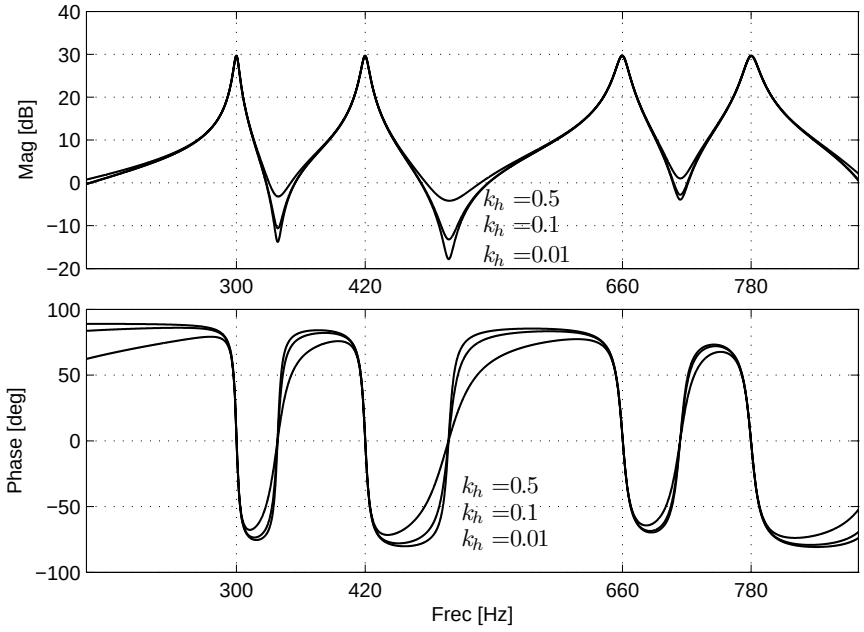

Fig. 7.2: Bode plots of the controller ϑ_h for different values of the damping term k_h.

As it is expected the Bode plot consists in a set of peaks centered at the harmonic frequencies. Moreover, thanks to the presence of the zeros in (7.5), notches appear in the middle points between two consecutive peaks. Based on the Bode plots, a gain $k_h = 0.01$ was selected. This produces positive peaks with a limited amplitude and a zero phase to the harmonics to be compensated (5th, 7th, 11th and 13th). Thus, the proposed scheme incorporates a harmonic selective compensation as in the schemes proposed in [60].

7.2 Steady state responses: estimation of fundamental and harmonics components

Figure 7.3 shows (only for one phase) the load current i_L, the estimation of its fundamental component i_{Lf}, and the estimation of its harmonic component i_{Lh}. Notice that the estimate of the fundamental component i_{Lf} is purely a sinusoidal signal, whereas the estimate of the harmonic components i_{Lh} maintains the remains of the load current i_L. The responses of the other two phases are very similar and are omitted here. Figure 7.4 shows (from top to bottom) the frequency spectrum of the load current i_L, the corresponding fundamental component i_{Lf} and the corresponding harmonic component i_{Lh}. In this case, the load current spectrum is composed mainly by 1st, 5th, 7th, 11th and so on harmonic components of the fundamental frequency. Notice that, the frequency spectrum of i_{Lf} contains only the fundamental component, while the frequency spectrum of i_{Lh} contains the hight harmonic components. The latter can be used in the harmonic compensation stage of the proposed controller.

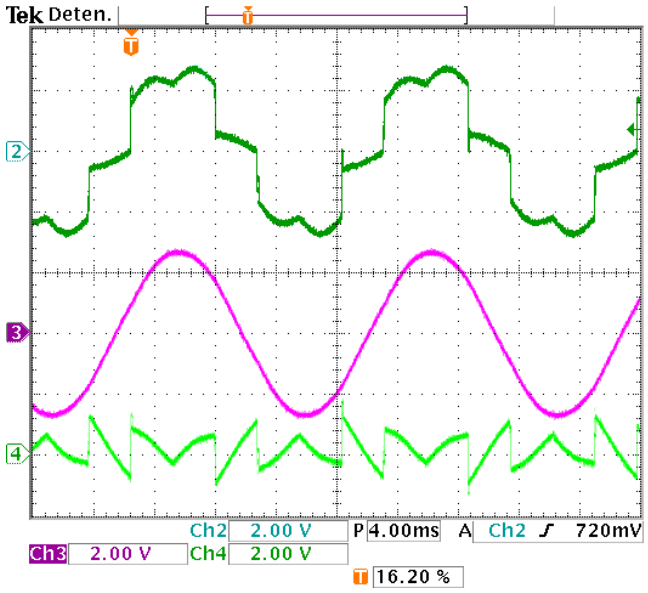

Fig. 7.3: Steady state responses of **(from top to bottom)** load current i_L, the estimation of its fundamental component i_{Lf}, and the estimation of its harmonic component i_{Lh} (x-axis 4 ms/div, y-axis 2 A/div).

Figure 7.5 shows, under the proposed compensator, the source current i_S, the estimation

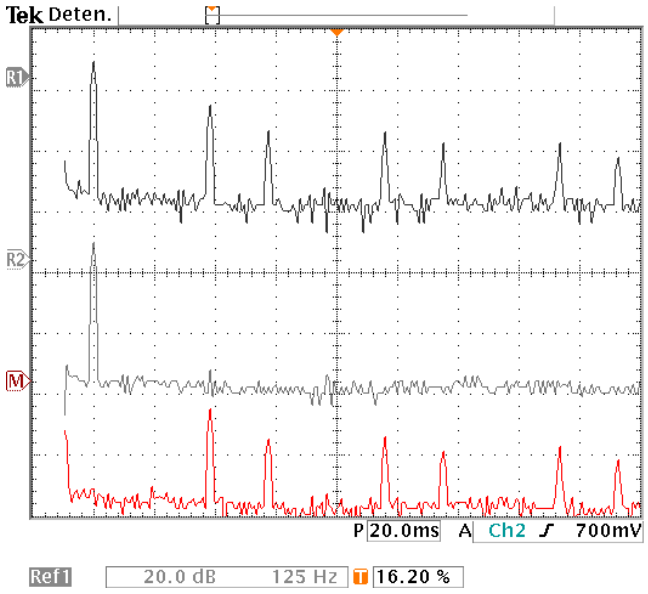

Fig. 7.4: Frequency spectrum of (**from top to bottom)** the load current i_L, fundamental component i_{Lf}, and harmonic component i_{Lh}. (x-axis 125Hz/div, y-axis 20 A/div).

of its fundamental component i_{Sf}, and the estimation of its harmonic component i_{Sh}. Notice that the estimator reconstructs the fundamental component i_{Sf} as a purely a sinusoidal signal, whereas the estimate of the harmonic components i_{Sh} contains the rest of the load current i_S. The responses of the other two phases are very similar and are omitted here. Figure 7.6 shows (from top to bottom) the frequency spectrum of i_S, i_{Sf} and i_{Sh}. Notice that the compensated source current is composed by the fundamental f_0 plus a small 5th harmonic component. In this case, the estimator recovers the fundamental component i_{Sf} of the source current, which can be used in the fundamental current loop of the proposed controller.

7.3 Steady state responses: Hybrid power Responses

Figure 7.7 shows (from top to bottom) the source voltage v_S, the uncompensated source current i_S, the load current i_L, and the injected current i_{Af} under the proposed solution considering only the *regulation stage*. As it was stated in Chapters 4.2 and 5.1, each fundamental injected current i_{Af} is forced to follow a reference signal proportional and in phase with the source fundamental voltage v_{Sf}, which forces the active power from the source to regulate the DC-link capacitor voltage towards a constant reference.

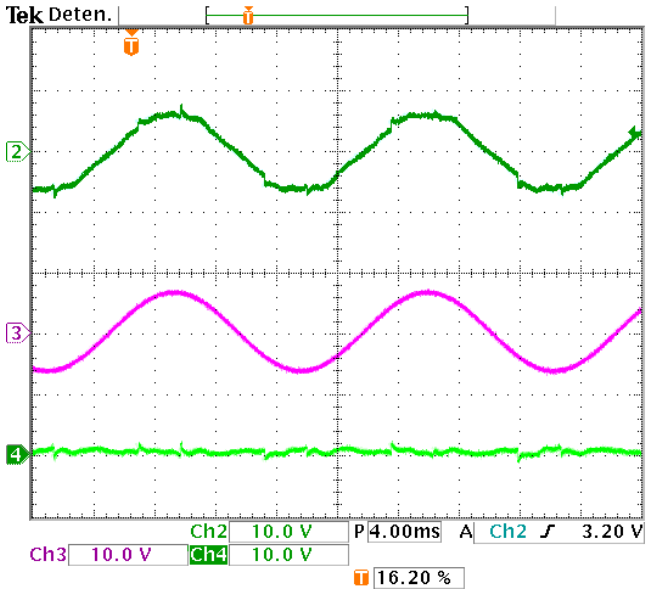

Fig. 7.5: Steady state responses of (**from top to bottom)** source current i_S, the estimation of its fundamental component i_{Sf}, and the estimation of its harmonic component i_{Sh} (x-axis 4 ms/div, y-axis 2 A/div).

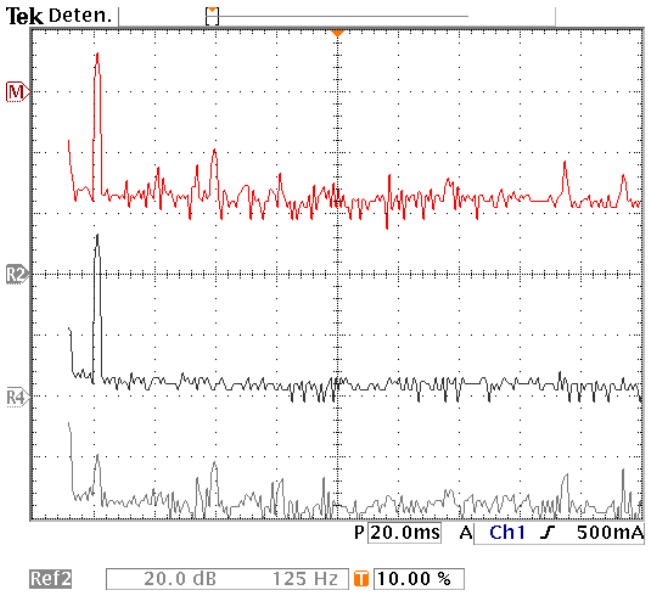

Fig. 7.6: Frequency spectrum of (**from top to bottom)** the source current i_S, fundamental component i_{Sf}, and harmonic component i_{Sh} (x-axis 125Hz/div, y-axis 20 A/div).

It can be observed in this Figure that, the fundamental component of the active filter current i_{Af} is forced to stay in phase with the source voltage v_S. Therefore, active power can be extracted from the source to regulate the DC-link capacitor voltage. However, notice that, the uncompensated source current i_S is a non sinusoidal signal yet.

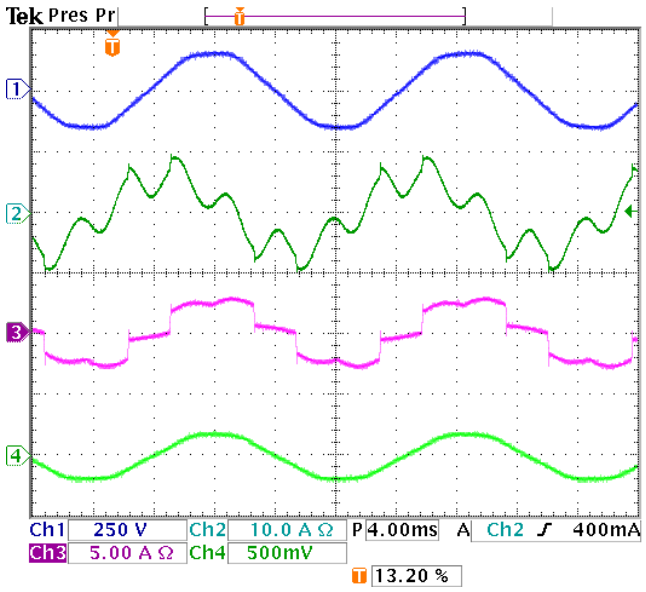

Fig. 7.7: Measured waveforms of the hybrid power filter with only the passive filter connected for mitigation of the harmonic current (**from top to bottom)** line voltage v_S, line current i_S, load current i_L, and injected current i_A.

Figure 7.8 shows (from top to bottom) the source voltage v_S, the compensated source current i_S, the load current i_L, and injected current i_A under the overall proposed solution, that is, when the harmonic current control is enabled. It can be observed that the compensated source current i_S is an almost sinusoidal signal despite the highly distorted load current i_L.

The total injected current i_A is presented in the bottom plot. Figure 7.9 shows the frequency spectrum of the load current i_L (top plot) and the corresponding source current i_S (bottom plot) under the overall control scheme. Notice that when the proposed controller is used, the 5th, 7th, 11th, 13th, and so on, harmonic components are considerably reduced due to the *harmonic compensation stage*. As is shown in Table 7.1, the total harmonic distortion (THD) of i_L is 28%, while that of i_S, obtained under the proposed control scheme, is reduced to 3.19%. The following expression was used to compute the THDs of these currents. Notice that, the computed THD of i_L is in agreement with the THD of three-phase nonlinear loads

(see [50], [51]).

$$\%THD = 100 \times \frac{\left(\sum_{h=5}^{19} I_h^2\right)^{1/2}}{I_f}$$

where I_f is the fundamental-component RMS value of the currents and I_h is the RMS magnitude at the harmonic of order h.

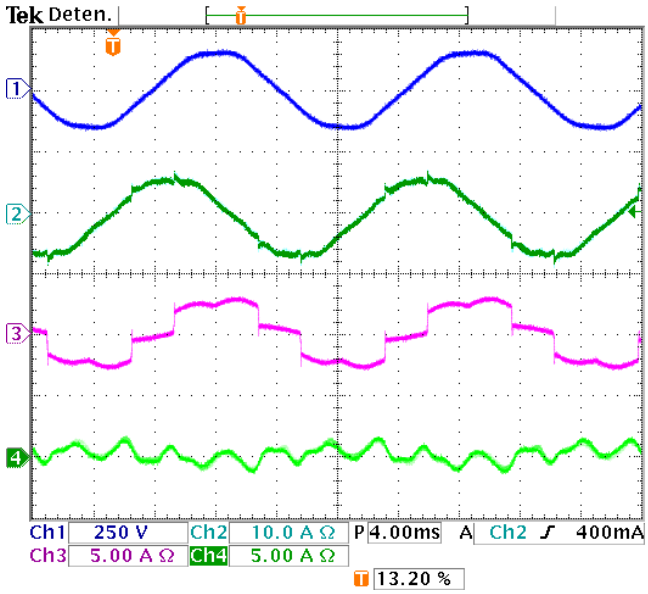

Fig. 7.8: Hybrid power filter behavior with the proposed solution (only one phase) **(from top to bottom)** line voltage v_S, line current i_S, load current i_L, and injected current i_A.

7.4 Transient responses: Hybrid power Responses

Figure 7.10 shows that, after a relatively small transient due to step changes in the load resistance from $R_L = 100\,\Omega$ to $R_L = 50\,\Omega$ and back, the capacitor voltage v_C (top) is maintained close to the reference $V_d = 90$ V$_{DC}$, while the approximate dissipated power G (bottom) converges towards a constant value proportional to the dissipated power in the load resistor. As is shown in Table 7.1, the percentage overshoot (M_P) is 6.6% and the settling times (T_S) are 2 and 3 s for 5% and 2% of final value of the capacitor voltage, respectively. 7.1.

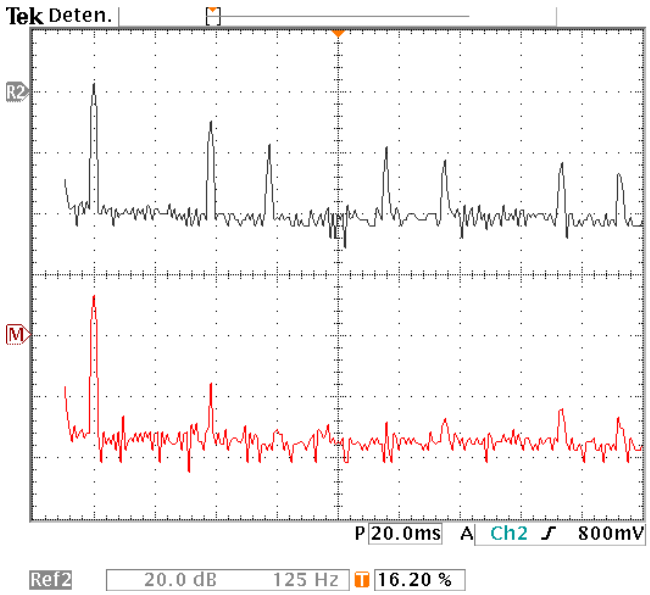

Fig. 7.9: Frequency spectrum of the load current i_L **(top plot)** and the corresponding source current i_S **(bottom plot)** with the proposed solution. (x-axis 125 Hz/div, y-axis 20 dB/div).

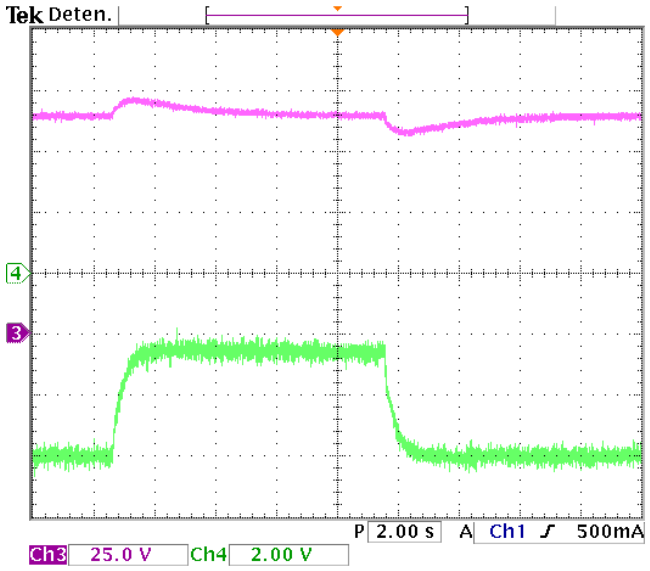

Fig. 7.10: Transient responses under the proposed compensator of **(top)** the capacitor voltage v_C, and **(bottom)** approximate dissipated power G during load step changes from $R_L = 100\,\Omega$ to $R_L = 50\,\Omega$ and back.

	THD [load]	THD [source]	M_P	T_S [2 %]	T_S [5 %]
Performance measurements	28 %	3.19 %	6.6 %	3 s	2 s

Table 7.1: Performance measurements of the closed-loop system.

Figure 7.11 shows the transient response of the load current i_L, the corresponding compensated source current i_S, and the corresponding injected current i_A under the overall proposed controller during a load step change. In this case the resistor R_L of the DC-link of the nonlinear unbalanced load is switched (a) from $R_L = 100\,\Omega$ to $R_L = 50\,\Omega$, and (b) from $R_L = 50\,\Omega$ to $R_L = 100\,\Omega$. Notice that, after a relatively small transient, the source current i_S keeps the desired sinusoidal shape and amplitude.

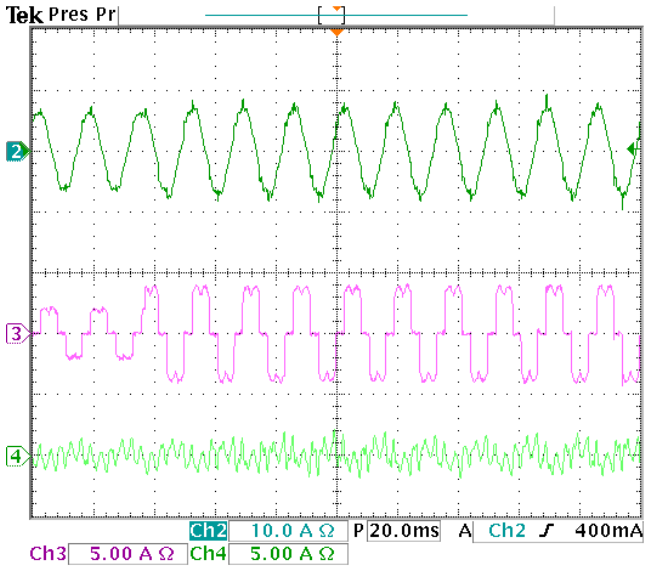

(a)

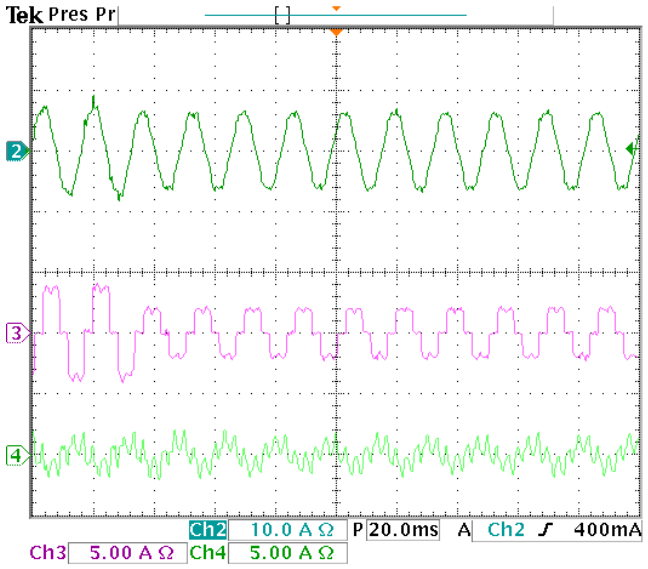

(b)

Fig. 7.11: Transient responses during a load step change (**from top to bottom)** load current i_L, compensated source current i_S, and injected current i_A. **(a)** from $R_L = 100\,\Omega$ to $R_L = 50\,\Omega$, and **(b)** from $R_L = 50\,\Omega$ to $R_L = 100\,\Omega$.

CONCLUSION OF PART II

In this thesis part, a model-based controller for a hybrid power filter to reduce the current harmonic distortion in a three-phase power system in the general case of unbalanced and distorted source voltages and load currents was proposed. The hybrid power filter topology considered is composed of an active filter connected to the grid by means of an LC passive filter. The aim of this topology is to reduce the current rating handled by the active filter. The controller design was split in two stages, a regulation stage considering the fundamental component of the system dynamics, and a harmonics compensation stage considering the harmonic component of the system dynamics. In the regulation stage a current control was established to force the active filter current to extract only active power from the source, which was used to maintain the dc-link capacitor charged to a certain level. Therefore, the load reactive current compensation was mainly left to the passive filter. The harmonic compensation stage forces the injection of current to the mains to compensate the harmonic distortion appearing in the line due to the distorting load. Experimental results are provided to illustrate the benefits of proposed solution.

The proposed control scheme, in contrast with the latter solution proposed in [34], offers the following benefits:

- ◇ The proposed approach is based and justified on the mathematical model of the system.
- ◇ It reduces the current harmonic distortion in a three-phase power system in the general case of unbalanced and distorted source voltages and load currents.
- ◇ The *harmonic compensation stage* includes a damping term to reinforce the stability of the close-loop system. It is shown that, a necessary and sufficient condition to ensure

stability, is to include this damping term positive.

- ◇ The proposed controller maintain a proportional-resonant (PR) structure, which offers a selective harmonic compensation.
- ◇ An estimator, based on a complete description of the unbalance signals, is proposed to reconstruct the fundamental and harmonic components of such signals. Convergence of the proposed estimator is proved following a Lyapunov approach and the Barbalatś lemma.
- ◇ Experimental results are shown to assess the performance of the proposed estimator, which include the estimation of fundamental and harmonic components and the frequency spectrum of the corresponding signals.

Notice that, the solution proposed in [34] is stable due to the damping added by the parasitic resistance of the inductors.

The disadvantages of the proposed controller are the following:

- ◇ The final expression of the proposed controller includes resonant filters that offer a selective harmonic compensation. However, their digital implementation requires a high-computational cost.
- ◇ The control objectives must be fulfilled in an specific order. That is, first, the fundamental and the harmonic components must be estimated. Then, in the *regulation stage*, the fundamental component of the active filter current must be forced to extract active power from the source in order to regulate the DC-link capacitor voltage towards a constant reference. Finally, in the *harmonic compensation stage*, the necessary current must be injected to the main to cancel the harmonic distortion produced by the load.

Part III

AN ADAPTIVE DIRECT-POWER CONTROL (DPC) FOR THE THREE-PHASE PWM RECTIFIER IN UNBALANCED OPERATION

INTRODUCTION

MANY traditional rectifier applications involve the use of diode bridge circuits with a bulk storage capacitor on the dc side. The preference for this topology is based mainly on its low cost, reliability and robustness. However, this type of non controlled rectifiers suffers from the following well known drawbacks: unidirectional power flow, low PF, and generation of a considerable amount of harmonic distortion in the line current [7]. To overcome such issues, new rectifier topologies have emerged. Among the different topologies, it is perhaps the PWM regenerative rectifier the one that has received the most attention because of its viable advantages: bidirectional power flow, low harmonic distortion in the line current, power factor close to unity and regulation of the dc link voltage, among others [11].

As expected, the proliferation of this new converter topology has been accompanied by the development of new controllers that follow different design approaches to exploit the advantages of PWM rectifiers. Among the different controllers for active PWM rectifiers two families can be identified, those controlling the instantaneous line current [10], [11], [37], [38] and those controlling the instantaneous active and reactive powers [39]-[48]. The latter are specially interesting whenever it is necessary to guarantee direct and effective regulation of both instantaneous powers towards presumably constant references, which motivates the name of direct power control (DPC).

DPC is a fairly simple and efficient control strategy that achieves good dynamical performance and a power factor close to unity [40]. The idea behind DPC consists in expressing the model in terms of the instantaneous (active and reactive) powers, instead of currents, and then realize the inner control loop based on these new variables [16]. As in most controllers

for PWM rectifiers, DPC also requires an outer loop with the purpose of computing the reference for the inner loop, in this case the active power. This reference is usually obtained by means of a PI that guarantees regulation of the dc link capacitor voltage. Based on the way in which the switching sequence is obtained, the inner loop in DPC can be performed according to the following two approaches: (i) using a look up table [39], [40], [42]; and (ii) using a PWM to generate the switching sequence [44], [45]. However, most controllers following the DPC approach assume that the source voltage is balanced, which is not common in practice.

In this part theses is proposed an adaptive DPC controller for a PWM rectifier under unbalanced operation, that is, the proposed scheme directly controls the instantaneous (active and reactive) powers for a PWM rectifier subject to an unbalanced source voltage. Instrumental for the proposed approach is the representation of unbalanced signals in a more appropriate form, that is, in terms of both sequences, positive and negative. An adaptive algorithm is included to guarantee robustness of the proposed controller against system uncertainties. Moreover, it is shown that the balanced case is a special case of the proposed scheme, and thus, it can be recovered by simply neglecting the source voltage negative sequence. Simulation and experimental results show the benefits of the proposed scheme. Experimental tests have been carried out in a 1.5 kVA three-phase PWM rectifier prototype to illustrate the merits of the proposed solution.

8. PROBLEM FORMULATION

8.1 System description

In the proposed approach the design of the continuous control signal in based on the averaged version of the system model. In this case the switching sequence vector $[\delta_1,\, \delta_2,\, \delta_3]^\top$ can be replaced, in the model equations, by the corresponding duty ratios vector $[u_1,\, u_2,\, u_3]^\top$ based on the assumption that the carrier signal is of sufficiently high frequency. Thus, the average model of system in Fig. 8.1 in terms of the (fixed frame) $\alpha\beta$-coordinates, using the normalized Clarke's transformation (see Appendix A and [19])

$$\mathbf{x}_{\alpha\beta} = \begin{bmatrix} x_\alpha \\ x_\beta \end{bmatrix} = \sqrt{\frac{2}{3}} \begin{bmatrix} 1 & -\frac{1}{2} & -\frac{1}{2} \\ 0 & \frac{\sqrt{3}}{2} & -\frac{\sqrt{3}}{2} \end{bmatrix} \begin{bmatrix} x_1 \\ x_2 \\ x_3 \end{bmatrix},$$

is described by

$$L\frac{d}{dt}\mathbf{i}_{\alpha\beta} = -\boldsymbol{\vartheta}_{\alpha\beta} + \mathbf{v}_{S\alpha\beta} \tag{8.1}$$

$$C\frac{d}{dt}\left(\frac{v_C^2}{2}\right) = \boldsymbol{\vartheta}_{\alpha\beta}^\top \mathbf{i}_{\alpha\beta} - \left(\frac{v_C^2}{R_L}\right) \tag{8.2}$$

$$\boldsymbol{\vartheta}_{\alpha\beta} \triangleq \frac{v_C \mathbf{u}_{\alpha\beta}}{2} \tag{8.3}$$

where $\mathbf{i}_{\alpha\beta} = [i_\alpha,\, i_\beta]^\top$, $\mathbf{v}_{S\alpha\beta} = [v_{S\alpha},\, v_{S\beta}]^\top$ and $\mathbf{u}_{\alpha\beta} = [u_\alpha,\, u_\beta]^\top$ are the line currents, source voltages and duty ratios, respectively; $\boldsymbol{\vartheta}_{\alpha\beta}$ is the injected voltages vector representing the new control input; v_C is the capacitor voltage; L, C and R_L are the filter inductance, output capacitance and load resistance, respectively.

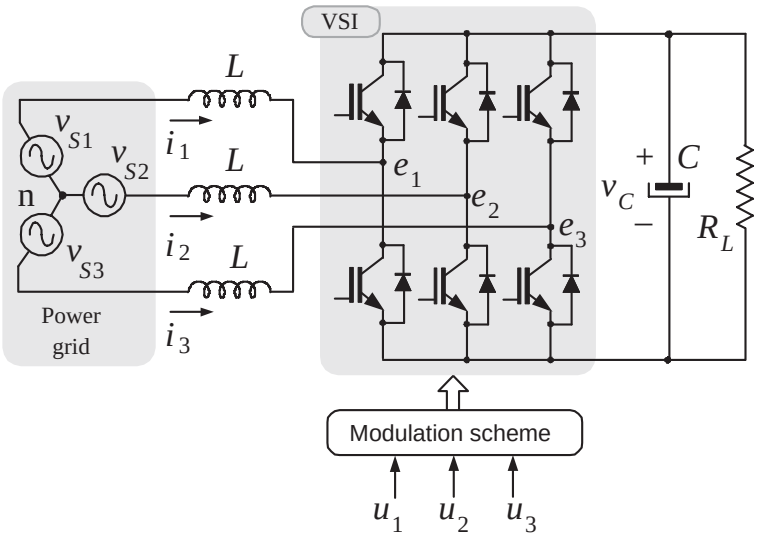

Fig. 8.1: Scheme of the three-phase three-wire rectifier.

8.2 Voltage source description in the unbalanced case

Most controllers following the DPC approach assume that the source voltage is balanced. However, in real operation due to unavoidable faults, phases in the grid voltage may register unequal amplitude drops, unequal phase shifts between them causing the arise of a negative sequence component. To consider this issue in the controller design the proposed approach considers the following more complete description of the voltage source which includes both positive and negative sequences of the fundamental component

$$\mathbf{v}_{S\alpha\beta} = \mathbf{e}^{\mathbf{J}\omega_0 t}\mathbf{V}_S^p + \mathbf{e}^{-\mathbf{J}\omega_0 t}\mathbf{V}_S^n = \mathbf{v}_{S\alpha\beta,p} + \mathbf{v}_{S\alpha\beta,n} \tag{8.4}$$

where $\mathbf{v}_{S\alpha\beta,p}$ and $\mathbf{v}_{S\alpha\beta,n}$ represent the positive and negative sequence components of the source voltage and ω_0 is the fundamental frequency. The term $\mathbf{e}^{\mathbf{J}\omega_0 t}$ is a rotation matrix of the form

$$\mathbf{e}^{\mathbf{J}\omega_0 t} = \begin{bmatrix} \cos(\omega_0 t) & -\sin(\omega_0 t) \\ \sin(\omega_0 t) & \cos(\omega_0 t) \end{bmatrix}$$

$$\mathbf{e}^{-\mathbf{J}\omega_0 t} = \left(\mathbf{e}^{\mathbf{J}\omega_0 t}\right)^\top \ , \ \mathbf{J} = \begin{bmatrix} 0 & -1 \\ 1 & 0 \end{bmatrix}$$

and vectors $\mathbf{V}_S^p, \mathbf{V}_S^n \in \Re^2$ are the fundamental harmonic coefficients for the positive and negative sequence representation of the source voltage, which are assumed to be unknown

constants.

Based on definition (8.4), the complete description of the voltage source in the unbalanced case is

$$\dot{\mathbf{v}}_{S\alpha\beta} = \mathbf{J}\omega_0\boldsymbol{\phi}_{\alpha\beta} \tag{8.5}$$

$$\dot{\boldsymbol{\phi}}_{\alpha\beta} = \mathbf{J}\omega_0\mathbf{v}_{S\alpha\beta} \tag{8.6}$$

where $\boldsymbol{\phi}_{\alpha\beta} \stackrel{\triangle}{=} \mathbf{v}_{S\alpha\beta,p} - \mathbf{v}_{S\alpha\beta,n}$. In fact, the following relationship can be established

$$\begin{bmatrix} \mathbf{v}_{S\alpha\beta} \\ \boldsymbol{\phi}_{\alpha\beta} \end{bmatrix} = \begin{bmatrix} 1 & 1 \\ 1 & -1 \end{bmatrix} \begin{bmatrix} \mathbf{v}_{S\alpha\beta,p} \\ \mathbf{v}_{S\alpha\beta,n} \end{bmatrix} \tag{8.7}$$

It is important to notice the need of the auxiliary variable $\boldsymbol{\phi}_{\alpha\beta}$ to allow a complete description of the unbalance voltage signal.

Remark 8.2.1 Notice that, in the balanced case, the description (8.5)-(8.6) is reduced to $\dot{\mathbf{v}}_{S\alpha\beta} = \mathbf{J}\omega_0\mathbf{v}_{S\alpha\beta}$, as in this case $\mathbf{v}_{S\alpha\beta} = \boldsymbol{\phi}_{\alpha\beta}$. □

8.3 Transformation to instantaneous powers

Consider now the following transformation to the instantaneous active and reactive powers [16]

$$\begin{bmatrix} p \\ q \end{bmatrix} = \begin{bmatrix} v_{S\alpha} & v_{S\beta} \\ -v_{S\beta} & v_{S\alpha} \end{bmatrix} \begin{bmatrix} i_\alpha \\ i_\beta \end{bmatrix} = \mathbf{R}\mathbf{i}_{\alpha\beta} \tag{8.8}$$

whose inverse is given by

$$\begin{aligned} \mathbf{i}_{\alpha\beta} &= \frac{1}{|\mathbf{v}_{S\alpha\beta}|^2} \begin{bmatrix} v_{S\alpha} & -v_{S\beta} \\ v_{S\beta} & v_{S\alpha} \end{bmatrix} \begin{bmatrix} p \\ q \end{bmatrix} = \\ &= \mathbf{R}^{-1} \begin{bmatrix} p \\ q \end{bmatrix} \end{aligned} \tag{8.9}$$

The subsystem (8.1) in terms of these new variables is

$$\begin{bmatrix} L\dot{p} \\ L\dot{q} \end{bmatrix} = \mathbf{R}(-\boldsymbol{\vartheta}_{\alpha\beta} + \mathbf{v}_{S\alpha\beta}) - \sigma\mathbf{J} \begin{bmatrix} \xi \\ \psi \end{bmatrix} \tag{8.10}$$

where $\sigma \triangleq \omega_0 L$, and ξ, ψ are auxiliary variables defined as

$$\begin{bmatrix} \xi \\ \psi \end{bmatrix} = \begin{bmatrix} \phi_\alpha & \phi_\beta \\ -\phi_\beta & \phi_\alpha \end{bmatrix} \begin{bmatrix} i_\alpha \\ i_\beta \end{bmatrix} = \mathbf{Si}_{\alpha\beta} \tag{8.11}$$

According to (8.9) the last is equivalent to

$$\begin{bmatrix} \xi \\ \psi \end{bmatrix} = \mathbf{SR}^{-1} \begin{bmatrix} p \\ q \end{bmatrix}$$

$$= \frac{1}{|\mathbf{v}_{S\alpha\beta}|^2} \begin{bmatrix} \boldsymbol{\phi}_{\alpha\beta}^\top \mathbf{v}_{S\alpha\beta} & \boldsymbol{\phi}_{\alpha\beta}^\top \mathbf{J}\mathbf{v}_{S\alpha\beta} \\ -\boldsymbol{\phi}_{\alpha\beta}^\top \mathbf{J}\mathbf{v}_{S\alpha\beta} & \boldsymbol{\phi}_{\alpha\beta}^\top \mathbf{v}_{S\alpha\beta} \end{bmatrix} \begin{bmatrix} p \\ q \end{bmatrix} \tag{8.12}$$

8.4 Control objectives

The *control objective* consists in designing a controller to guarantee regulation of both active and reactive power towards constant references p_* and q_*, respectively, that is, $p \to p_*$ and $q \to q_*$ as $t \to \infty$. In addition, the controller should guarantee regulation of the capacitor voltage v_C towards a constant reference V_d, that is, $v_C \to V_d$. Notice that, in the case that a power factor close to the unity is required, then $q_* = 0$. Reference p_* is computed in the outer voltage loop as will be shown later.

Remark 8.4.1 Notice that, the usual current tracking problem has been transformed into a regulation problem. In current control the currents are forced to follow a current reference, which usually is a signal proportional to the source voltage [61]. Thus, based on (8.9), the regulation of p and q towards constant references can also be obtained following the current control approach if the current reference is selected as follows

$$\begin{aligned} \begin{bmatrix} i_\alpha^* \\ i_\beta^* \end{bmatrix} &= \mathbf{R}^{-1} \begin{bmatrix} p_* \\ q_* \end{bmatrix} \\ &= p_* \frac{\mathbf{v}_{S\alpha\beta}}{|\mathbf{v}_{S\alpha\beta}|^2} + q_* \frac{\mathbf{J}\mathbf{v}_{S\alpha\beta}}{|\mathbf{v}_{S\alpha\beta}|^2} \end{aligned} \tag{8.13}$$

□

9. CONTROLLER DESIGN

For the controller design, the system dynamics considered include (8.10) and (8.2). To facilitate the design process, it is common in practice to assume that the power (inner) dynamics (8.10) responds much faster than the dynamics involving the capacitor (8.2), and thus, they can be decoupled from one another invoking time scale separation. This assumption allows to split the control design in two loops, namely, power inner loop and voltage outer loop, and thus, it is also referred as decoupling assumption.

9.1 Power (inner) loop

The controller design follows the energy-shaping plus damping injection (ESDI) technique of the passivity-based control (PBC) approach [21], that exploits the structure of the system description. The procedure consists in making a copy of the system which is evaluated at the reference, to which some damping terms are included as follows

$$\begin{bmatrix} L\dot{p}_* \\ L\dot{q}_* \end{bmatrix} = \mathbf{R}(-\boldsymbol{\vartheta}_{\alpha\beta} + \mathbf{v}_{S\alpha\beta}) - \hat{\sigma}\mathbf{J}\begin{bmatrix} \xi \\ \psi \end{bmatrix} + K_1\begin{bmatrix} \tilde{p} \\ \tilde{q} \end{bmatrix} \tag{9.1}$$

where the regulation errors $\tilde{p} \stackrel{\triangle}{=} (p - p_*)$, $\tilde{q} \stackrel{\triangle}{=} (q - q_*)$ have been defined, $K_1 = \text{diag}\{k_{1p},\, k_{1q}\}$ with k_{1p} and k_{1q} two positive design parameters used to introduce damping, and $\hat{\sigma}$ represents an estimate of $\sigma = \omega_0 L$.

Solving from (9.1) for the control vector $\boldsymbol{\vartheta}_{\alpha\beta}$, and considering constant references, i.e.,

$[\dot{p}_*,\ \dot{q}_*] = [0, 0]$, yields

$$\boldsymbol{\vartheta}_{\alpha\beta} = \mathbf{v}_{S\alpha\beta} + \mathbf{R}^{-1}\left\{-\hat{\sigma}\mathbf{J}\begin{bmatrix}\xi\\ \psi\end{bmatrix} + K_1\begin{bmatrix}\tilde{p}\\ \tilde{q}\end{bmatrix}\right\} \tag{9.2}$$

The estimate $\hat{\sigma}$ is reconstructed using an adaptive scheme described next.

System (8.10) in closed loop with controller (9.2) yields the error model

$$\begin{bmatrix}L\dot{\tilde{p}}\\ L\dot{\tilde{q}}\end{bmatrix} = -K_1\begin{bmatrix}\tilde{p}\\ \tilde{q}\end{bmatrix} + \tilde{\sigma}\mathbf{J}\begin{bmatrix}\xi\\ \psi\end{bmatrix} \tag{9.3}$$

where estimation error $\tilde{\sigma} \triangleq (\hat{\sigma} - \sigma)$ has been defined.

The design of the adaptation law follows the Lyapunov approach, for this, the following quadratic function is proposed

$$W = \frac{L}{2}\tilde{p}^2 + \frac{L}{2}\tilde{q}^2 + \frac{1}{2\gamma}\tilde{\sigma}^2 \tag{9.4}$$

Its time derivative along the trajectories of (9.3) is given by

$$\dot{W} = -k_{1p}\tilde{p}^2 - k_{1q}\tilde{q}^2 + \tilde{\sigma}[\tilde{p}\ \ \tilde{q}]\mathbf{J}\begin{bmatrix}\xi\\ \psi\end{bmatrix} + \frac{1}{\gamma}\dot{\tilde{\sigma}}\tilde{\sigma}$$

which is made negative semi-definite by proposing the following adaptive law

$$\dot{\hat{\sigma}} = -\gamma[\tilde{p}\ \ \tilde{q}]\mathbf{J}\begin{bmatrix}\xi\\ \psi\end{bmatrix} = \gamma(\tilde{p}\psi - \tilde{q}\xi) \tag{9.5}$$

where γ is a positive design parameter representing the adaptive gain, and $\dot{\hat{\sigma}} = \dot{\tilde{\sigma}}$ since σ is considered constant. This yields

$$\dot{W} = -k_{1p}\tilde{p}^2 - k_{1q}\tilde{q}^2$$

Since W is radially unbounded and $\dot{W}$ is negative semi-definite then $\tilde{p} \in \mathcal{L}_2 \bigcap \mathcal{L}_\infty$ and $\tilde{q} \in \mathcal{L}_2 \bigcap \mathcal{L}_\infty$ and $\tilde{\sigma} \in \mathcal{L}_\infty$. From (8.12), $\xi \in \mathcal{L}_\infty$ and $\psi \in \mathcal{L}_\infty$. Now, since $\tilde{p} \in \mathcal{L}_\infty$, $\tilde{q} \in \mathcal{L}_\infty$, $\dot{\tilde{p}} \in \mathcal{L}_\infty$ and $\dot{\tilde{q}} \in \mathcal{L}_\infty$ then $\tilde{p}$, $\tilde{q}$ are uniformly continuous, which together with the fact that $\tilde{p} \in \mathcal{L}_2$ and $\tilde{q} \in \mathcal{L}_2$ imply that $\tilde{p} \to 0$ and $\tilde{q} \to 0$, asymptotically. Out of this, and from (9.5), $\tilde{\sigma}$ goes to a constant. Moreover, from (8.12) both $\xi \neq 0$ and $\psi \neq 0$, and thus from (9.3), $\tilde{\sigma} \to 0$ as well.

Remark 9.1.1 In the balanced operation case, the following adaptive controller can be proposed

$$\begin{aligned}\boldsymbol{\vartheta}_{\alpha\beta} &= -\mathbf{v}_{S\alpha\beta} + \mathbf{R}^{-1}\left\{\hat{\sigma}\mathbf{J}\begin{bmatrix} p \\ q \end{bmatrix} - K_1\begin{bmatrix} \tilde{p} \\ \tilde{q} \end{bmatrix}\right\} \\ \dot{\hat{\sigma}} &= -\gamma[\tilde{p}\ \ \tilde{q}]\mathbf{J}\begin{bmatrix} p \\ q \end{bmatrix}\end{aligned}$$

which is very similar to controller (9.2)-(9.5), except that vector $[\xi,\ \psi]$ in the unbalanced case is replaced by vector $[p,\ q]^\top$. In fact, in the balanced case $\boldsymbol{\phi}_{\alpha\beta} = \mathbf{v}_{S\alpha\beta}$, and thus, $[\xi,\ \psi] = [p,\ q]$ from (8.12). Hence, the proposed controller for the unbalanced case is downward compatible with the controller for the balanced case. □

Implementation of the proposed controller (9.2)-(9.5) requires the knowledge of vector $[\xi,\ \psi]^\top$, which in turn implies the knowledge of vector $\boldsymbol{\phi}_{\alpha\beta}$ according to (8.12). However, vector $\boldsymbol{\phi}_{\alpha\beta}$ is not accessible, and thus, an estimator is proposed to reconstruct it as described next.

9.2 Estimation of $\boldsymbol{\phi}_{\alpha\beta}$

Based on the structure of (8.5)-(8.6) the following estimator is proposed

$$\dot{\hat{\mathbf{v}}}_{S\alpha\beta} = \mathbf{J}\omega_0\hat{\boldsymbol{\phi}}_{\alpha\beta} + \lambda\tilde{\mathbf{v}}_{S\alpha\beta} \tag{9.6}$$

$$\dot{\hat{\boldsymbol{\phi}}}_{\alpha\beta} = \mathbf{J}\omega_0\hat{\mathbf{v}}_{S\alpha\beta} \tag{9.7}$$

where $\lambda > 0$ is the estimation gain; $\tilde{\mathbf{v}}_{S\alpha\beta} \triangleq (\mathbf{v}_{S\alpha\beta} - \hat{\mathbf{v}}_{S\alpha\beta})$ is an estimation error; $\hat{\mathbf{v}}_{S\alpha\beta}$ and $\hat{\boldsymbol{\phi}}_{\alpha\beta}$ are the estimates of $\mathbf{v}_{S\alpha\beta}$ and $\boldsymbol{\phi}_{\alpha\beta}$, respectively.

The estimation error dynamics is given by

$$\dot{\tilde{\mathbf{v}}}_{S\alpha\beta} = \mathbf{J}\omega_0\tilde{\boldsymbol{\phi}}_{\alpha\beta} - \lambda\tilde{\mathbf{v}}_{S\alpha\beta} \tag{9.8}$$

$$\dot{\tilde{\boldsymbol{\phi}}}_{\alpha\beta} = \mathbf{J}\omega_0\tilde{\mathbf{v}}_{S\alpha\beta} \tag{9.9}$$

where $\tilde{\boldsymbol{\phi}}_{\alpha\beta} \triangleq (\boldsymbol{\phi}_{\alpha\beta} - \hat{\boldsymbol{\phi}}_{\alpha\beta})$ represents an estimation error.

Convergence of the proposed estimator is proved following the Lyapunov approach where the following quadratic function of the estimation errors is used

$$H = \frac{1}{2}\tilde{\mathbf{v}}_{S\alpha\beta}^2 + \frac{1}{2}\tilde{\boldsymbol{\phi}}_{\alpha\beta}^2$$

Its time derivative along the trajectories of the error model (9.8)-(9.9) yields the following negative semidefinite function

$$\dot{H} = -\lambda\tilde{\mathbf{v}}_{S\alpha\beta}^\top\tilde{\mathbf{v}}_{S\alpha\beta}$$

As before, since H is radially unbounded and $\dot{H}$ is negative semidefinite then $\tilde{\mathbf{v}}_{S\alpha\beta} \in \mathcal{L}_2 \bigcap \mathcal{L}_\infty$ and $\tilde{\boldsymbol{\phi}}_{\alpha\beta} \in \mathcal{L}_2 \bigcap \mathcal{L}_\infty$. Besides, as $\tilde{\mathbf{v}}_{S\alpha\beta}$ and $\tilde{\boldsymbol{\phi}}_{\alpha\beta}$ and its time derivative signals $\dot{\tilde{\mathbf{v}}}_{S\alpha\beta}$ and $\dot{\tilde{\boldsymbol{\phi}}}_{\alpha\beta}$ are periodical signals, consequently $\dot{\tilde{\mathbf{v}}}_{S\alpha\beta}$, $\dot{\tilde{\boldsymbol{\phi}}}_{\alpha\beta} \in \mathcal{L}_\infty$ (see [55] for details on $\mathcal{L}_2$ and $\mathcal{L}_\infty$ spaces). Therefore, by direct application of the Corollary 1.2.2 of the Barbalat's Lemma 1.2.1 on [56], it can stated that since $\dot{\tilde{\boldsymbol{\phi}}}_{\alpha\beta} \in \mathcal{L}_\infty$ and $\dot{\tilde{\mathbf{v}}}_{S\alpha\beta} \in \mathcal{L}_\infty$ then $\tilde{\mathbf{v}}_{S\alpha\beta}$ and $\tilde{\boldsymbol{\phi}}_{\alpha\beta}$ are uniformly continuous, which together with the fact that $\tilde{\mathbf{v}}_{S\alpha\beta} \in \mathcal{L}_2$ and $\tilde{\boldsymbol{\phi}}_{\alpha\beta} \in \mathcal{L}_2$ imply that $\tilde{\mathbf{v}}_{S\alpha\beta} \to 0$ and $\tilde{\boldsymbol{\phi}}_{\alpha\beta} \to 0$, asymptotically as $t \to \infty$. Notice that, in this case similar conclusion can be obtained following the LaSalle's arguments.

Notice that estimator (9.6)-(9.7) reconstructs both vectors $\mathbf{v}_{S\alpha\beta}$ and $\boldsymbol{\phi}_{\alpha\beta}$, which can then be used to implement the proposed controller. However, the estimator requires the knowledge of the fundamental frequency ω_0.

9.3 Voltage loop

As in most controllers for PWM rectifiers, DPC also requires an outer loop with the purpose of computing the reference for the inner loop, in this case p_*. This part of the controller deals with the voltage regulation objective and thus focuses on the voltage dynamics described by subsystem (8.2), which is rewritten here as follows

$$C\dot{z} = \boldsymbol{\vartheta}_{\alpha\beta}^\top\mathbf{i}_{\alpha\beta} - \frac{2z}{R_L} \tag{9.10}$$

where $z \stackrel{\triangle}{=} v_C^2/2$, and thus the regulation objective can be restated as follows $z \to V_d^2/2$.

As stated before, it is assumed that dynamics (9.3) and (9.5) are much faster than dynamics (9.10), thus, appealing time scale separation, it can be assumed that, after a relatively

short time, $p = p_*$ and $q = q_*$, $\hat{\sigma} = \sigma = \omega_0 L$. This allows the simplification of the controller expression (9.2) as follows

$$\overline{\boldsymbol{\vartheta}}_{\alpha\beta} = \mathbf{v}_{S\alpha\beta} - \mathbf{R}^{-1}\omega_0 L\mathbf{J}\left[\begin{array}{c}\overline{\xi}\\ \hline \overline{\psi}\end{array}\right] \tag{9.11}$$

where $\overline{(\cdot)}$ are the values of $(\cdot)$ after the instantaneous powers and the estimates have reached their corresponding reference values.

Using the relationship (8.12) the controller can be further simplified to

$$\overline{\boldsymbol{\vartheta}}_{\alpha\beta} = \mathbf{v}_{S\alpha\beta} + \frac{\omega_0 L}{|\mathbf{v}_{S\alpha\beta}|^2}\left(\mathbf{v}_{S\alpha\beta}^\top\mathbf{J}\boldsymbol{\phi}_{\alpha\beta}\mathbf{I}_2 - \mathbf{v}_{S\alpha\beta}^\top\boldsymbol{\phi}_{\alpha\beta}\mathbf{J}\right)\overline{\mathbf{i}}_{\alpha\beta} \tag{9.12}$$

where $\mathbf{I}_2$ is the 2×2 identity matrix.

The dot product $\boldsymbol{\vartheta}_{\alpha\beta}^\top\mathbf{i}_{\alpha\beta}$ appearing in (9.10) can now be developed as follows

$$\overline{\boldsymbol{\vartheta}}_{\alpha\beta}^\top\overline{\mathbf{i}}_{\alpha\beta} = \mathbf{v}_{S\alpha\beta}^\top\overline{\mathbf{i}}_{\alpha\beta} + \frac{\omega_0 L}{|\mathbf{v}_{S\alpha\beta}|^2}\mathbf{v}_{S\alpha\beta}^\top\mathbf{J}\boldsymbol{\phi}_{\alpha\beta}\overline{\mathbf{i}}_{\alpha\beta}^\top\overline{\mathbf{i}}_{\alpha\beta} \tag{9.13}$$

The products in the second term on the right hand side (RHS) of the previous equation can be rewritten as follows

$$\begin{aligned}\mathbf{v}_{S\alpha\beta}^\top\mathbf{J}\boldsymbol{\phi}_{\alpha\beta} &= (\mathbf{v}_{S\alpha\beta,p} + \mathbf{v}_{S\alpha\beta,n})^\top\mathbf{J}(\mathbf{v}_{S\alpha\beta,p} - \mathbf{v}_{S\alpha\beta,n})\\ &= 2\mathbf{v}_{S\alpha\beta,n}^\top\mathbf{J}\mathbf{v}_{S\alpha\beta,p} \qquad (9.14)\\ \overline{\mathbf{i}}_{\alpha\beta}^\top\overline{\mathbf{i}}_{\alpha\beta} &= [p_*,\, q_*]\left(\mathbf{R}^{-1}\right)^\top\mathbf{R}^{-1}\left[\begin{array}{c}p_*\\ q_*\end{array}\right]\\ &= \frac{1}{|\mathbf{v}_{S\alpha\beta}|^2}(p^{*2} + q^{*2}) \qquad (9.15)\end{aligned}$$

Substitution of expressions (9.13), (9.15) and (9.15) in (9.10), and using the fact that, $p_* = \mathbf{v}_{S\alpha\beta}^\top\overline{\mathbf{i}}_{\alpha\beta}$, yields

$$C\dot{z} = p_* + \frac{2\omega_0 L}{|\mathbf{v}_{S\alpha\beta}|^4}\mathbf{v}_{S\alpha\beta,n}^\top\mathbf{J}\mathbf{v}_{S\alpha\beta,p}(p_*^2 + q_*^2) - \frac{2z}{R_L} \tag{9.16}$$

Notice that the second term on the RHS of (9.16) contributes mainly with a second harmonic component generated by the product $\mathbf{v}_{S\alpha\beta,n}^\top\mathbf{J}\mathbf{v}_{S\alpha\beta,p}$, that is, due to the existence of the negative sequence $\mathbf{v}_{S\alpha\beta,n}$ which is a consequence of the unbalance. Notice also that this harmonic

component grows with the power demand. Moreover, in subsystem (9.16) the reference p_* acts as the control input, which, as stated above, must be constructed to regulate z towards its desired constant reference. Besides, reference q_* is a constant previously fixed to allow reactive power injection. Usually, $q_* = 0$ to guarantee a power factor close to unity. In the best scenario, p_* would reach a constant value in the steady state, and thus, according to (9.16), there must appear an unavoidable disturbance composed mainly of a second order harmonic. Therefore, the regulation objective can only be fulfilled in average, that is, the control design will focus on the regulation of the dc component of the state, disregarding the fluctuations due to the unbalance. Roughly speaking, the controller is designed with a bandwidth short enough to avoid the effects of the second harmonic component introduced by the unbalance, which results in a slow dynamical response.

The usual controller for this part of the system consists of a proportional plus integral controller of the following form

$$p_* = k_p\chi + k_i\zeta \tag{9.17}$$

$$\tau\dot{\chi} = (\tilde{z} - \chi) \tag{9.18}$$

$$\dot{\zeta} = \tilde{z} \tag{9.19}$$

where $\tilde{z} \triangleq (z - V_d^2/2)$, and k_p, k_i are the proportional and integral gains, respectively, and $1/\tau$ is the cutoff frequency of the low pass filter.

Summarizing, the overall controller is composed by (9.2)-(9.5), the estimator (9.6)-(9.7), and the voltage loop represented by (9.17)-(9.19). A block diagram of this controller is presented in Fig. 9.1.

9.4 The balanced case

In the balanced case the source voltage is composed of a positive sequence only, that is,

$$\mathbf{v}_{S\alpha\beta} = \mathbf{e}^{\mathbf{J}\omega_0 t}\mathbf{V}_{S,1}^{p} \tag{9.20}$$

which satisfies the following relationship

$$\dot{\mathbf{v}}_{S\alpha\beta} = \mathbf{J}\omega_0\mathbf{v}_{S\alpha\beta}$$

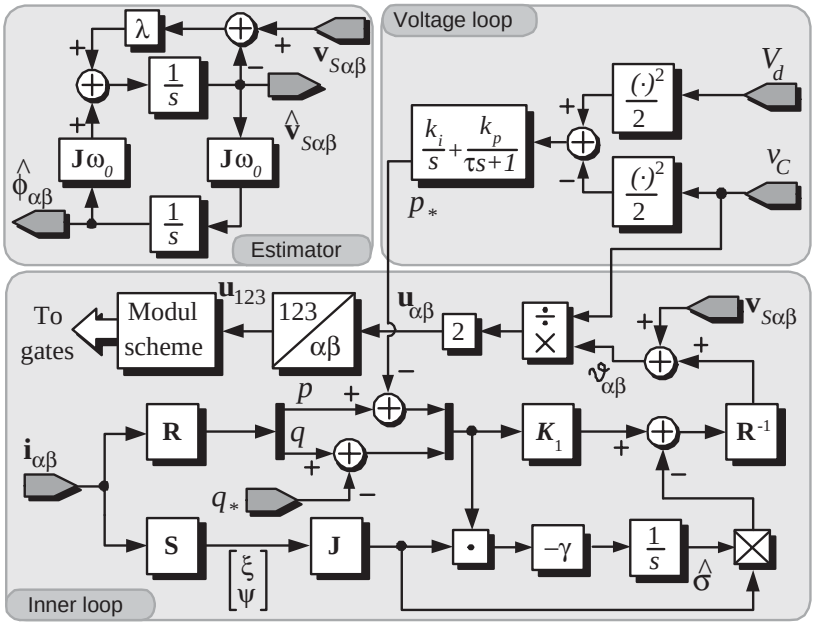

Fig. 9.1: Block diagram of the proposed controller.

where $\mathbf{V}_{S,1}^{p}$ is the fundamental harmonic coefficient of the positive sequence component of the source voltage.

Based on definition (8.8) and (9.20) the system dynamics can be rewritten as

$$\begin{bmatrix} L\dot{p} \\ L\dot{q} \end{bmatrix} = \mathbf{R}(-\boldsymbol{\vartheta}_{\alpha\beta} + \mathbf{v}_{S\alpha\beta}) - \sigma\mathbf{J}\begin{bmatrix} p \\ q \end{bmatrix} \tag{9.21}$$

which is very similar to (8.10), except for the last term on the RHS of (9.21) that uses vector $[p,\, q]^{\top}$, instead of the $[\xi,\, \psi]^{\top}$ used in the unbalanced case (8.10).

Following a similar procedure as in Section 9.1, the following adaptive controller can be proposed

$$\boldsymbol{\vartheta}_{\alpha\beta} = -\mathbf{v}_{S\alpha\beta} + \mathbf{R}^{-1}\left\{\hat{\sigma}\mathbf{J}\begin{bmatrix} p \\ q \end{bmatrix} - K_1\begin{bmatrix} \tilde{p} \\ \tilde{q} \end{bmatrix}\right\} \tag{9.22}$$

$$\dot{\hat{\sigma}} = -\gamma[\tilde{p}\;\; \tilde{q}]\mathbf{J}\begin{bmatrix} p \\ q \end{bmatrix} \tag{9.23}$$

which is very similar to controller (9.2), (9.5), except that vector $[\xi,\, \psi]$ in the unbalanced case is replaced by vector $[p,\, q]^{\top}$. In fact, as in the balanced case $\boldsymbol{\phi}_{\alpha\beta} = \mathbf{v}_{S\alpha\beta}$, then $[\xi,\, \psi] = [p,\, q]$

from (8.12). Hence, under these considerations, the proposed controller (9.2), (9.5) for the unbalanced case is downward compatible with the controller (9.25), (9.25) for the balanced case.

Moreover, notice that, as $\mathbf{v}_{S\alpha\beta,n} = 0$, then the voltage dynamics described by (9.16) is reduced to

$$C\dot{z} = p_* - \frac{2z}{R_L} \tag{9.24}$$

where the harmonic distortion due to the negative sequence has disappeared. Hence, if the same controller (9.17)-(9.19) is applied, the regulation can be guaranteed without fluctuations.

Remark 9.4.1 In the balanced case, following a similar procedure, the system dynamics can be rewritten in terms of the instantaneous powers as follows

$$\begin{bmatrix} L\dot{p} \\ L\dot{q} \end{bmatrix} = \mathbf{R}(-\boldsymbol{\vartheta}_{\alpha\beta} + \mathbf{v}_{S\alpha\beta}) - \sigma\mathbf{J}\begin{bmatrix} p \\ q \end{bmatrix}$$

This expression is very similar to (8.10) except for the last term on the right hand side (RHS) that uses vector $[p,\, q]^\top$ in the balanced case, instead of the $[\xi,\, \psi]^\top$ used in the unbalanced case (8.10).

In the balanced operation case, the following adaptive controller can be proposed

$$\begin{aligned} \boldsymbol{\vartheta}_{\alpha\beta} &= -\mathbf{v}_{S\alpha\beta} + \mathbf{R}^{-1}\left\{\hat{\sigma}\mathbf{J}\begin{bmatrix} p \\ q \end{bmatrix} - K_1\begin{bmatrix} \tilde{p} \\ \tilde{q} \end{bmatrix}\right\} \\ \dot{\hat{\sigma}} &= -\gamma[\tilde{p}\ \ \tilde{q}]\mathbf{J}\begin{bmatrix} p \\ q \end{bmatrix} \end{aligned}$$

which is very similar to controller (9.2)-(9.5), except that vector $[\xi,\, \psi]$ in the unbalanced case is replaced by vector $[p,\, q]^\top$. In fact, in the balanced case $\boldsymbol{\phi}_{\alpha\beta} = \mathbf{v}_{S\alpha\beta}$, and thus, $[\xi,\, \psi] = [p,\, q]$ from (8.12). Hence, the proposed controller for the unbalanced case is downward compatible with the controller for the balanced case. □

10. EXPERIMENTAL RESULTS

The proposed adaptive controller, which is developed in Chapter 9, was tested in a three-phase PWM rectifier prototype. In this case, the overall prototype was built using the following three stages. The *power stage*, including a VSI; the *instrumentation stage*, composed by the current and voltage sensors and the control interface; and the *digital stage*, conformed by a control board based on DSP ACE1103 made by dSPACE, and the software development using Simulink/MATLAB. All of these stages were described in Appendix B. The overall scheme of the three-phase PWM rectifier is shown in Fig. 10.2. in this case, the sensed signals are the line currents i_{123}, the line voltages v_{S123} and the capacitor voltage v_C.

The tests performed consider a phase-to-neutral fault on one phase only to generate the unbalanced operation. This is created by means of the interruptor S_X which short circuits the phase 1 to the neutral wire. The three phase signal coming form the faulted source is then introduced to the delta-wye transformer, which delivers an unbalanced signal to the rectifier. Now, under such an unbalanced operation, the load resistance is changed from 100 Ω to 50 Ω, and back from 50 Ω to 100 Ω to test the performance of the proposed scheme under load changes. Figure 10.1 shows the phasors at the secondary of the transformer, v'_{S123} for the balanced operation, and v_{S123} after the fault.

10.1 Discussion of the implementation

The parameters used for the PWM rectifier are $L = 5$ mH, $C = 2200\,\mu$F, the load resistance R_L takes either 100 Ω or 50 Ω. The source has a voltage amplitude of 100 V at 60 Hz, which is delivered to the rectifier by means of a delta-wye transformer. As pointed out before, the

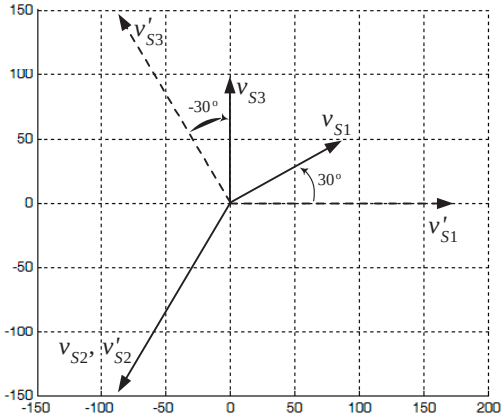

Fig. 10.1: Source voltage phasors before and after the phase-to-ground fault.

proposed controller is implemented in the dSPACE card model ACE1103 with a sampling frequency $f_s = 18$ kHz and a switching frequency $f_{sw} = 10$ kHz.

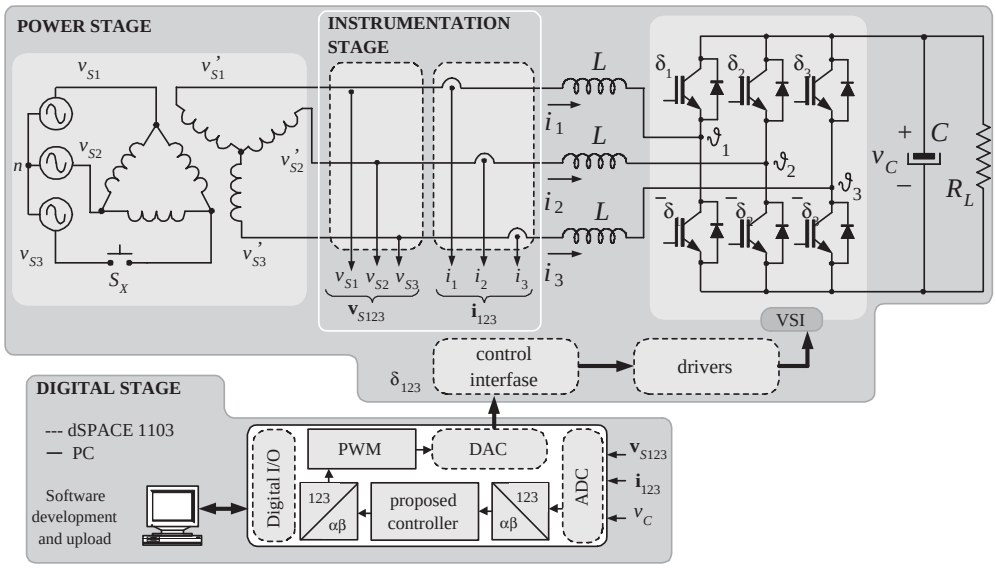

Fig. 10.2: Scheme of the experimental setup to test the proposed adaptive DPC controller for the three-phase rectifier under unbalanced operation.

On other hand, an important issue is that the control objectives must be fulfilled on different time responses. That is, to obtain a power factor close to the unity, first, in the *power*

inner loop, both active and reactive power must track constant references p_* and $q_* = 0$, respectively. Afterwards, in the *voltage loop*, the capacitor voltage v_C is forced to a constant reference V_d. In general, the design process for the power and voltage loops is based on the time responses requirements. The criteria for the tuning of the control parameters of the *power inner* and the *voltage loops* is described in the following section.

10.1.1 Tuning of power inner loop

The tuning of K_1 is performed following the next approximations. First, notice that the fastest power dynamics (9.3) can be expressed as

$$\begin{bmatrix} Ls + K_1 & 0 \\ 0 & Ls + K_1 \end{bmatrix} \begin{bmatrix} \tilde{p} \\ \tilde{q} \end{bmatrix} = \tilde{\sigma}\mathbf{J} \begin{bmatrix} \xi \\ \psi \end{bmatrix} \tag{10.1}$$

where $\tilde{\sigma} \triangleq (\hat{\sigma} - \sigma)$ represents the estimation error. In this case, the bandwidth of (10.1) may be determined by K_1/L. Following the procedure in [2], the bandwidth of this power dynamics must be at most $1/10$ of the sampling frequency $2\pi f_s$. Therefore, the gain K_1 must satisfy $K_1 < \pi f_s L/5$ which, according to the prototype parameters, yields $K_1 < 56.5$ In the present thesis $K_1 = 45$.

10.1.2 Tuning of voltage loop

The control parameters tuning of the *voltage loop* is performed as follows. First, it is considered from (9.16) that $q_* = 0$ and p_* reaches a constant value in the steady state, to guarantee a power factor close to the unity. Hence, according to (9.16), an unavoidable disturbance must arise, which is composed mainly of a second order harmonic. Then, the regulation objective can only be fulfilled in average. The control parameters tuning is focused on the regulation of the dc component of the state, disregarding the fluctuations due to the unbalance. Therefore, the voltage dynamics for the balanced case (9.24) denoted in terms of the increments, may be considered:

$$C\dot{\tilde{z}} = -p_* + \frac{V_d^2}{R} - \frac{2}{R}\tilde{z} \tag{10.2}$$

This dynamics above under the controller (9.17)-(9.19) is given by the following third order system

$$C\dot{\tilde{z}} = -k_p\chi - k_i\zeta - \frac{2}{R}\tilde{z} + \frac{V_d^2}{R} \tag{10.3}$$

$$\tau\dot{\chi} = (\tilde{z} - \chi) \tag{10.4}$$

$$\dot{\zeta} = \tilde{z} \tag{10.5}$$

Then, as in [2], τ is selected such that $\tau < 1/(2\omega_0) = 1$ ms, where ω_0 represents the fundamental of the line voltage. In this case, $\tau = 0.1$ ms has been fixed. Therefore, its effect can be neglected from the previous control expression, and thus, the characteristic polynomial can be reduced to

$$s^2 + \frac{R_L k_p + 2}{R_L C}s + \frac{k_i}{C} = 0 \tag{10.6}$$

Notice that, due to the ripple on the dc voltage at twice the supply frequency during unbalanced operation, the voltage loop bandwidth must be at least ten times slower than 120 Hz, that is, a cutoff frequency of approximately 12 Hz avoids a possible amplification of the above-mentioned second harmonic. In the present work the parameters $k_p = 0.005$ and $k_i = 0.7$ have been selected, which fulfill this assumption.

10.2 Steady state and transient responses

The effect of the phase-to-neutral fault is observed (in the top plot) in Fig. 10.3, where the three-phase source voltages on the secondary of the transformer are shown. The voltage and reactive power references are fixed (all time) to $V_d = 220$ VDC and $q_* = 0$, respectively. In the same figure (three following plots) the three line currents are shown. Notice that they acquire a quite distorted shape due the unbalance operation. As it was mentioned before, this distortion in the current is necessary to maintain the instantaneous powers as constant as possible during the regulation.

Figure 10.4 depicts the transient responses of (from top to bottom) the reference p_*, the instantaneous active power p, and the instantaneous reactive power q when the proposed solution is enabled under the unbalance operation. In this case, the instantaneous active power p is regulated in average towards a constant value near of its reference p_* while the instantaneous reactive power q tends in average to zero.

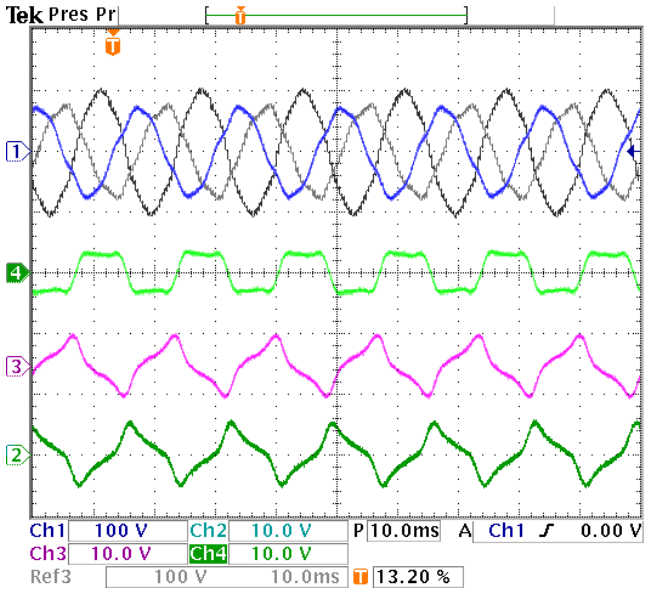

Fig. 10.3: **(top)** Three-phase source voltages after the phase-to-ground fault and **(three next plots)** line currents in the three phases.

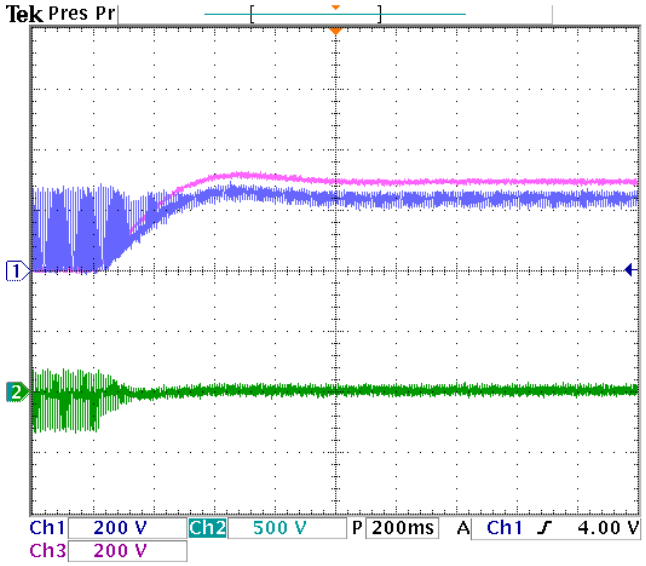

Fig. 10.4: Transient response when the proposed solution is enabled. (**from top to bottom)** Reference for the active power p_*, instantaneous active powers p, and instantaneous reactive power q.

Figure 10.5 shows (top) the capacitor voltage v_C and (bottom) estimated parameter $\hat{\sigma}$ during the unbalance fault. Notice that the capacitor voltage v_C is maintained close to its reference $V_d = 220$ VDC after short transients due to the load changes. As is shown in Table 7.1, the percentage overshoot (M_P) is 12% and the settling times (T_S) are 0.4 and 0.7 s for 5% and 2% of the final value of the capacitor voltage, respectively. Also, notice that the estimated parameter $\hat{\sigma}$ converges in average towards a constant value close to $\omega_0 L = 1.885\,\Omega$.

	M_P	T_S [2 %]	T_S [5 %]
Performance measurements	12 %	0.4 s	0.7 s

Table 10.1: Performance measurements of the closed-loop system.

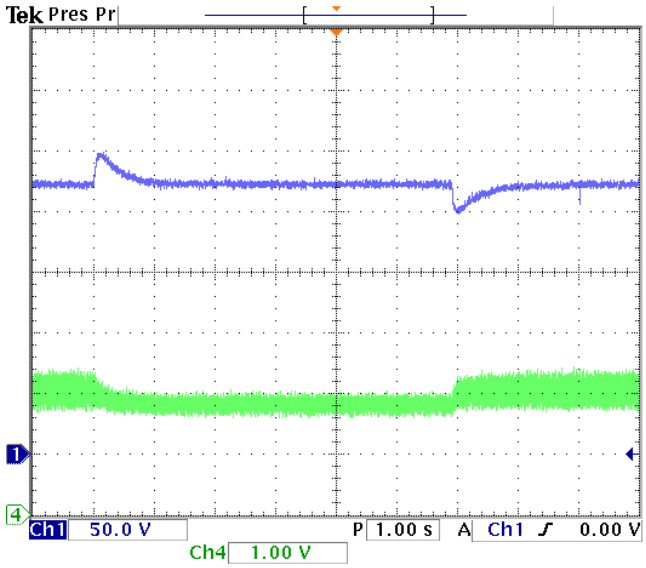

Fig. 10.5: Transient responses during a load change from $R_L = 50\,\Omega$ to $R_L = 100\,\Omega$ and back. **(top)** Capacitor voltage v_C, and **(bottom)** estimated parameter $\hat{\sigma} \to \omega_0 L = 1.885$.

Figure 10.6 shows the transient response of (from top to bottom) the reference p_*, the instantaneous active power p, and the instantaneous reactive power q. In this case the resistor R_L of the DC-link of the nonlinear unbalanced load is switched (a) from $R_L = 100\,\Omega$ to $R_L = 50\,\Omega$, and (b) from $R_L = 50\,\Omega$ to $R_L = 100\,\Omega$. Notice that, after a relatively small transient, the instantaneous active and reactive powers p and q tend in average to a constant value and zero, respectively.

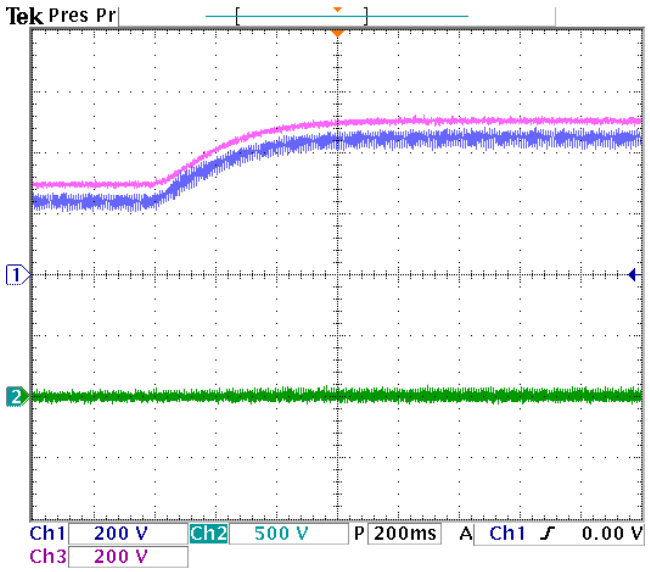

(a)

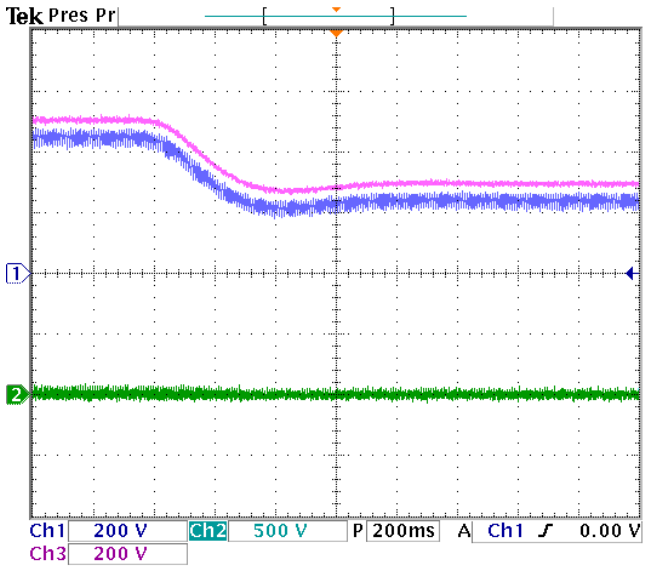

(b)

Fig. 10.6: Transient responses during a load step change. (**from top to bottom)** Reference for the active power p_*, instantaneous active power p, and instantaneous reactive power q. **(a)** from $R_L = 100\,\Omega$ to $R_L = 50\,\Omega$, and **(b)** from $R_L = 50\,\Omega$ to $R_L = 100\,\Omega$.

CONCLUSION OF PART III

In this Part, a DPC for a three-phase rectifier operating is presented in an unbalanced situation. The scheme included an adaptation to cope with system uncertainties. The controller was able to directly control the instantaneous active and reactive powers towards constant references. The controller design was based on a more complete description of the source voltage. That is, the unbalanced case both positive and negative sequence components were considered for the voltage description. It was shown that the balanced case can be recovered by simply neglecting the source voltage negative sequence component, and thus, it is a particular case of the proposed scheme. It was shown that, to achieve regulation of both powers, a deformation of the line current was necessary. Experimental results have been carried out to assess the performance proposed solution

The proposed approach has the following features and advantages in comparison to previous works [42], [46], [47]:

- ◇ The design was based on a more complete mathematical model that considers unbalanced operation of the source voltage (the balanced case is studied in a recent work [47]).
- ◇ In contrast with [42], [46], the switching sequences are generated by a PWM modulator instead of the switching table, therefore the proposed scheme has the following benefits.
  - A constant switching frequency (variable switching frequency is a classical drawback of a lookup-table-based DPC algorithm).
  - A lower sampling frequency for digital implementation (in a lookup-table-based

DPC algorithm, a high sampling frequency is needed for implementation of hysteresis comparators).

- Ease of implementation in a digital signal processor (DSP).

A drawback that increase the cost of the proposed scheme, commonly arising in PWM DPC algorithms, is that line voltage sensors are required.

11. GENERAL CONCLUDING REMARKS, FUTURE WORK AND SCIENTIFIC PRODUCTION

11.1 Concluding remarks

THE present thesis work was aimed to obtain a solution of the harmonic and reactive power compensation for different power electronics systems. The studied systems have been analyzed considering the general case of distorted and unbalance source voltage and load currents. In particular, the following three power electronics systems have been studied:

- ◇ **Part I**. Single-phase shunt active filter connected to a more realistic distribution system.
- ◇ **Part II**. Hybrid power filter with the active filter connected between the passive elements.
- ◇ **Part III**. Three-phase three-wire PWM rectifier.

General concluding remarks of interest for the studied systems are highlighted next:

- ◇ The problem of harmonic compensation was recast as a tracking problem, where the disturbance signal was assumed as a periodical signal. To facilitate the study, the disturbance was expressed as a Fourier series composed by an infinite number of terms, referred to as harmonic components.

- ◇ The methodology for the solution of these problems is based on adaptive techniques to cope with system parameters uncertainties.
- ◇ The proposed controllers are based on the mathematical model in $\alpha\beta$-coordinates. Therefore, in contrast with the original circuits, the control input has a common reference point. A similar equivalent circuit is obtained for either α or β-coordinates.
- ◇ Thanks to suitable transformations, the proposed controllers were reduced to a controller with structure very close to the conventional one plus a bank of resonators, thus facilitating implementation.
- ◇ The proposed solutions may be practically implemented given that either realistic numerical or experimental results have been provided assessing the performance for each studied system in closed-loop.
- ◇ Stability proofs were developed for each control scheme in a quite general closed loop control system.

11.2 Future work

The following issues, divided for each part, may be considered for future works.

- ◇ Part I
  - The proposed solution may be extended to the three-phase case. In this case, the state variables of the mathematical model are vectors and the control inputs of the equivalent circuits of the model must have a common reference point which may make the analysis non trivial.
  - The stability conditions may be analyzed considering different load and line impedances to the studied case. For example, the case when the power-factor correction capacitor, studied in this thesis work, is changed for a shunt passive filter.
  - The obtaining of experimental results considering the shunt active filter connected to a more realistic distribution system in order to validate the proposed solution.

◇ Part II

- An analysis of when the source voltage is not purely a sinusoidal signal. In this case, if the source voltage includes harmonic components (which is commonly found in practice), the shunt passive filter may serve as a current sink at such frequencies. This issue may be alleviated if an appropriate objective control is defined.
- The study of a possible solution based on repetitive control for the harmonic compensation stage. That is, determining if the whole bank of resonant filters can be replaced by a repetitive scheme to reduce the computational cost, while the performance is preserved. In this case, the repetitive scheme must generate harmonic multiples of $6n \pm 1$ (for $n = 1, 2, ...$) of the fundamental frequency, that is, without fundamental component. At the present moment, this modified repetitive scheme has not been addressed in the literature.

◇ Part III

- The experimental results may be improved for the studied PWM rectifier. The studied case considers that the source voltage is a purely sinusoidal signal, however, the experimental results do not totally reflect the studied case because the source voltage included an undesirable fifth harmonic.

11.3 Scientific production

The results, generated from this thesis work, have been recently reported in the following journals and conferences of international arbitration:

◇ [26] A.A. Valdez, G. Escobar and R. Ortega, "An adaptive controller for the shunt active filter considering a dynamic load and the line impedance," *IEEE Trans. On Control Systems Technology*, Vol. 17(2), pp. 458-464, March 2009.

◇ [35] A.A. Valdez, G. Escobar and M.F. Martínez-Montejano, "A Model-based Controller for a Hybrid Power Filter to Compensate Harmonic Distortion in Unbalanced Operation," in *Proc. 39th IEEE Power Electronics Specialists Conference PESC'08*, Rhodes, Greece, June 15-19 2008, pp. 3861-3866.

- [49] G. Escobar, M.F. Martinez-Montejano, R.E. Torres Olguin and A.A.Valdez, “An Adaptive Direct Power Control for Three-Phase PWM Rectifier in the Unbalanced Case,” in *Proc. 39th IEEE Power Electronics Specialists Conference PESC’08*, Rhodes, Greece, June 15-19 2008, pp. 3150-3155.

APPENDIX A. CLARKE'S TRANSFORMATION

THE Clarke's transformation consists in a linear operator mapping from an orthogonal three-phase system to another, in other words, a space vector described in terms of 123-coordinates is described in another reference frame with only two orthogonal axis placed in the plane, and referred as $\alpha\beta$, and a third coordinate referred as γ or "0" component orthogonal to the plane. The 123-coordinates are also known in the literature as abc-coordinates or rts-coordinates. The main benefit of transforming to $\alpha\beta\gamma$-coordinates is that the γ coordinate is usually neglected, most of all in balanced three phase systems and in three-phase three-wire systems, thus reducing the model expressions and, most of all, the controller design work. A usual three-phase VSI is composed of three branches, also referred as legs, each formed with the cascade connection of two switching devices, as shown in Figures 5.1 and 8.1. Both switching devices work in a complementary form, thus, the control of each branch is performed by a single control signal represented by u_i, $i \in \{1, 2, 3\}$, where every u_i takes values from the discrete set $\{0, 1\}$. The different combinations of such control signals can be represented as three dimensional space vectors described in 123-coordinates as can be seen in Fig. A.1(a).

The goal is to describe the vectors, relative to the original coordinate system 123, with respect to the orientation of the new rotated coordinate system $\alpha\beta\gamma$. This transformation is equivalent to perform two rotations given by the Euler's angles as described next. First, the 23-axes are rotated around the α-axis through an angle θ_1 counterclockwise. Second, the 12-axes are rotated around the β-axis through an angle θ_2 clockwise. These rotations are described by (A.1) and (A.2), respectively. They are shown in Fig. A.1(b), which describes how the rotated space $\alpha\beta\gamma$ shown in the Fig. A.1(c) is obtained.

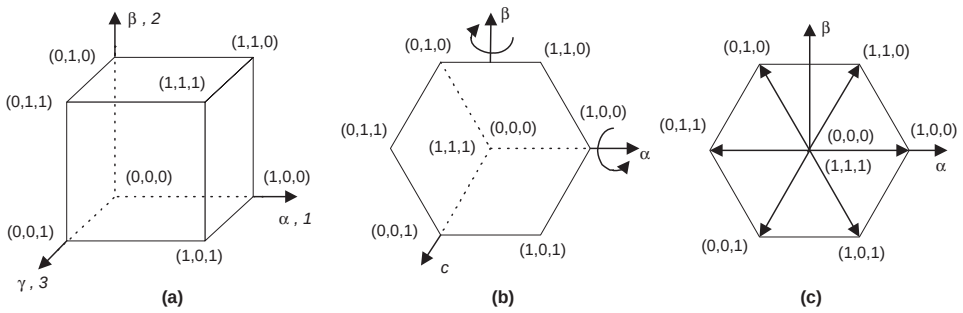

Fig. A.1: **(a)** Space vectors in 123-coordinates, **(b)** rotations to the transformed 123-coordinates into $\alpha\beta\gamma$-coordinates, and **(c)** resulting space vectors in $\alpha\beta\gamma$-coordinates.

$$R_\alpha(\theta_1) = \begin{bmatrix} 1 & 0 & 0 \\ 0 & \cos(\theta_1) & -\sin(\theta_1) \\ 0 & \sin(\theta_1) & -\cos(\theta_1) \end{bmatrix} \tag{A.1}$$

$$R_\beta(\theta_2) = \begin{bmatrix} \cos(\theta_2) & 0 & -\sin(\theta_2) \\ 0 & 1 & 0 \\ \sin(\theta_2) & 0 & \cos(\theta_2) \end{bmatrix}. \tag{A.2}$$

The total rotation is described by the following matrix product

$$R(\theta_1, \theta_2) \;\; = \;\; R_\beta(\theta_2) R_\alpha(\theta_1). \tag{A.3}$$

After multiplication the following matrix is obtained

$$R(\theta_1, \theta_2) = \begin{bmatrix} \cos(\theta_2) & -\sin(\theta_1)\sin(\theta_2) & -\cos(\theta_1)\sin(\theta_2) \\ 0 & \cos(\theta_1) & -\sin(\theta_1) \\ \sin(\theta_2) & \sin(\theta_1)\cos(\theta_2) & \cos(\theta_1)\cos(\theta_2) \end{bmatrix}.$$

The previous matrix can be rewritten also as

$$R(\theta_1, \theta_2) = T = \sqrt{\frac{2}{3}} \begin{bmatrix} 1 & -\frac{1}{2} & -\frac{1}{2} \\ 0 & \frac{\sqrt{3}}{2} & -\frac{\sqrt{3}}{2} \\ \frac{1}{\sqrt{2}} & \frac{1}{\sqrt{2}} & \frac{1}{\sqrt{2}} \end{bmatrix} \tag{A.4}$$

where $\sin(\theta_1) = \cos(\theta_1) = \frac{1}{\sqrt{2}}$, $\sin(\theta_2) = \frac{1}{\sqrt{3}}$ and $\cos(\theta_2) = \sqrt{\frac{2}{3}}$ have been used. They represent the director cosines in terms of the Euler's angles. Moreover, the total rotation $R(\theta_1, \theta_2)$ has been concentrated in the matrix T, for which the following properties hold

$$\begin{aligned} T^{-1} &= T^T \\ T^{-1}T^T &= T^T T^{-1} = I \end{aligned}$$

where T^{-1} is the inverse matrix, T^T is the transposed matrix, and I is the unitary matrix. Therefore, the Clarke's transformation is defined as the transformation from space vectors in 123-coordinates to space vectors in $\alpha\beta\gamma$-coordinates and the opposite. It is applied in the following form.

$$\begin{aligned} x_{123} &= T x_{\alpha\beta\gamma} \\ x_{\alpha\beta\gamma} &= T^T x_{123} \end{aligned}$$

where $x_{123} = [x_1 \ x_2 \ x_3]^T$ and $x_{\alpha\beta\gamma} = [x_\alpha \ x_\beta, \ x_\gamma]^T$.

APPENDIX B. PHYSICAL IMPLEMENTATION

IN this Appendix is described the implementation of each stage used in the instrumentation of the three-phase prototypes, that were used to experimentally prove the control schemes described in Chapters 6 and 9. The overall prototypes are built up of the following three stages: The *power stage* including a voltage source inverter (VSI), switches and the nonlinear load; the *instrumentation stage* composed by the current and voltage sensors and the control interface; and the *digital stage* conformed by a control board based on digital sinal processor (DSP) ACE1103 made by dSPACE, and the software development using Simulink/MATLAB. Each of these stages is described in detail next.

B.1 Digital stage

The proposed controller was implemented in a digital signal processor (DSP) based card ACE1103 made by dSPACE. The controller has been programmed using the environment Simulink/MATLAB, and then compiled and downloaded to the dSPACE card using the Realtime-Workshop tools included in the Simulink package.

The principal steps to generate the switching sequence are described next. First, the dSPACE card performs the analog-to-digital conversion, then, the sensed signals are transformed from 123-coordinates to $\alpha\beta$-coordinates, which are the feedback signals used in the proposed controller. Once the control signal u is computed, it is transformed from $\alpha\beta$-coordinates to 123-coordinates. This control signal is then mapped back to the duty cycle u_{123}, which is then injected in the SPWM to generate the switching sequence δ_{123}.

B.2 Power stage

The *active filter* of the HPF and the PWM rectifier studied in Parts II and III, respectively, are built using a VSI produced by SEMIKRON under the commercial name *"Power Electronics Teaching System"*. This VSI system is formed by three legs of half-bridge modules SKM50-GB123D implemented by two insolated gate bipolar transistor (IGBT), with antiparallel free-wheeling diode, connected in series. Each inverter leg is controlled and protected by a driver SKHI-22A. Each driver protects an inverter leg against short circuit and low power supply voltage by means of an error signal of negative logic (e_1, e_2 and e_3). The drivers are independent from each other, therefore it is necessary to take all the precautions to shut the system off when an error condition is sensed. All these precautions have been considered in the *control interface card* described below. The *passive filter* of the HPF has been designed, for mitigation of the 5^{th} harmonic, using the following parameters: $L_P = 5$ mH and $C_P = 56\,\mu$F.

B.2.1 Maneuvering switches

The *maneuvering switches* are based on three-phase contactors with the purpose of connect and disconnect the hybrid power filter studied in Part II, pre-charge of the DC-link capacitors, and connect and disconnect the load. Each contactor is controlled from the computer by means of an *operational manoeuvre circuit*, which is shown in Fig. B.1. The buffer SN74LS541N reinforces the signals S_{ON} and S_{SC} coming from the dSAPACE card. The resistances R_4 limit the current across the base terminal of transistor Q_1. Diode D_2 deviates the inverse current produced by the coil of the power relay during turn-off. The light emitter diode D_1 indicates the actual state of the power relay. Notice that, if the dSPACE control signal is in the logic ON, then the transistor Q_1 conducts, activating the coil of the power relay, thus allowing the output current to flow. The devices used in the maneuvering switches are collected in Table B.1.

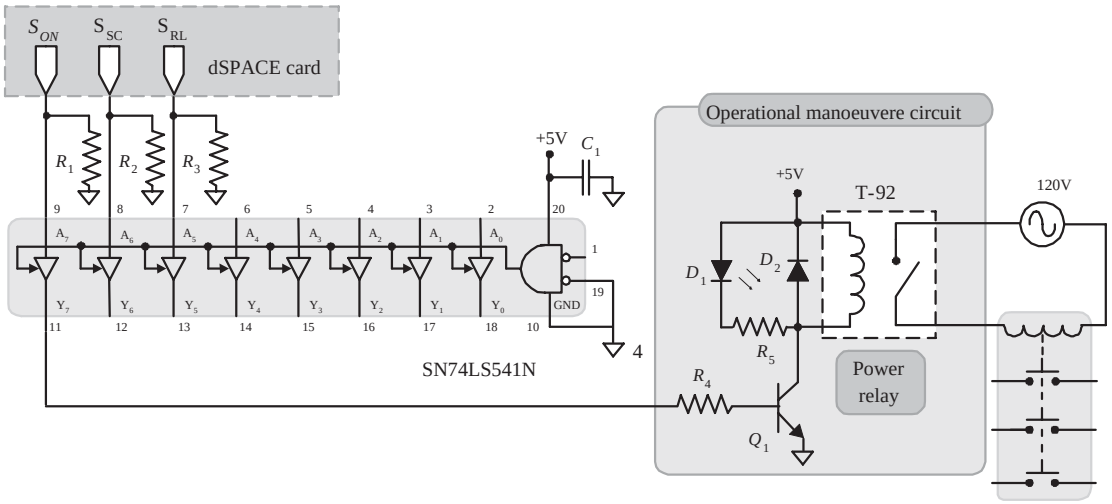

Fig. B.1: Electric circuit of the maneuvering switches.

B.2.2 Unbalance nonlinear load

The *unbalance nonlinear load* is composed of a three-phase diode rectifier PSD-31/12 with and associated load resistance R_L on the DC-side. This resistance takes values of $100\,\Omega$ or $50\,\Omega$ to observe the transient responses during load changes. A resistor $R_U = 100\Omega$ is connected between two phases to create the unbalance condition. Figure B.2 shows the implemented electrical circuit for the unbalanced nonlinear load.

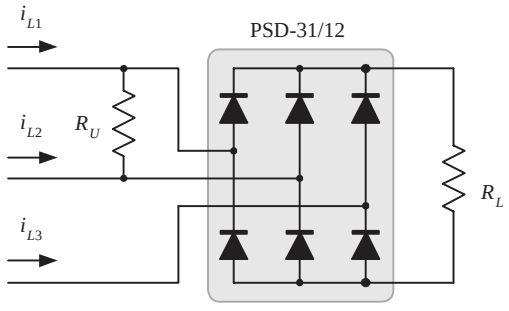

Fig. B.2: Unbalance nonlinear load.

The elements used in the distorted unbalanced load are collected in Table B.1. Figure B.3 shows the time responses for the three measured load currents.

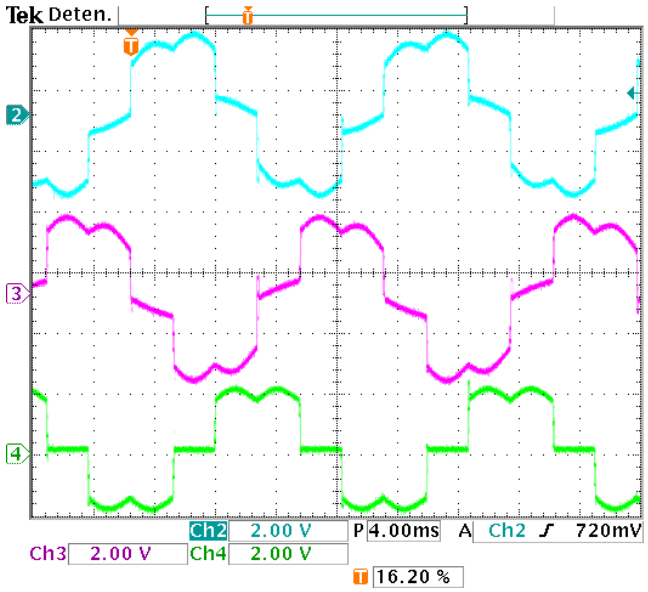

Fig. B.3: Steady state responses of the three load currents (x-axis 4 ms/div, y-axis 2 A/div)s.

B.3 Instrumentation stage

As the proposed controller was implemented using a dSPACE based controller card, it is necessary to provide isolation between the *power stage* and the dSPACE card to protect the acquisition ports of the dSPACE. Moreover, each sensed signal should be in an admissible range ($\pm 10V$) prior to being driven to the analog-digital converters (ADC) of the dSPACE. All these precautions have been considered in the design of sensors described below.

B.3.1 Current sensor

The electric circuit of the implemented *current sensor* is shown in Fig. B.4. The current is sensed with the current sensor CLN-50, which provides electric isolation between the current carrying conductor and the control circuit. The CLN-50 is a closed-loop Hall effect current sensor that accurately measures DC and AC currents. The output voltage v_o is limited to the admissible range by means of the OP295GPZ, which is a dual rail-to-rail operational amplifier guaranteeing a maximum output voltage swing for a power supply of $\pm 8V$. The first operational amplifier of the OP295GPZ is connected as *current-to-voltage converter* to obtain a proportional voltage to the current sensor CLN-50. The second operational amplifier

POWER STAGE					
L	:	4mH	R_4	:	1kΩ
L_P	:	5mH	R_4	:	560Ω
C_P	:	56μF	Q_1	:	BC548
C_1	:	0.1μF	D_2	:	1N4937
C	:	2200μF	Power relay	:	RAS-0510
R	:	2200Ω	IGBTs	:	SKM50-GB123D
R_{ON}	:	100Ω	Rectifier	:	PSD-31/12
R_L	:	50Ω-100Ω	Drivers	:	SKHI-22A
R_{1-3}	:	10kΩ	LED	:	D_1

Table B.1: Devices and parameters of the power stages.

of the OP295GPZ recovers the correct sign of the capacitor voltage. The transfer function of the delivered voltage v_o is given by expression (B.5). The devices and parameters used in the combined current sensor circuit are collected in Table B.2.

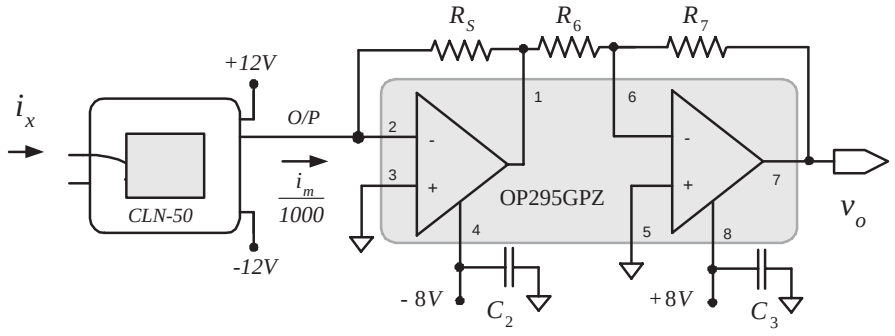

Fig. B.4: Electric circuit of the current sensor.

$$v_o = 1 \times 10^{-3} \frac{R_7}{R_6} R_S \cdot i_x \tag{B.5}$$

B.3.2 Voltage sensor

Figure B.5 shows the implemented electric circuit for the *voltage sensor*. The voltage transducer LV25-P gives galvanic isolation between the sensed voltage and the control stage. The transducer requires an external resistor on the primary side of the circuit transducer, which is connected in series to the sensed voltage. Thus, the transducer delivers a current proportional to the measured voltage on the secondary side. The first operational amplifier of the OP295GPZ is connected as *current-to-voltage converter* to obtain a proportional voltage to the sensor current CLN-50. The second operational amplifier of the OP295GPZ regains the sign of the sensed voltage. The transfer function of the delivered voltage v_o is given by the expression (B.6). The devices and parameters used in the capacitor voltage sensor circuit are given in Table B.2.

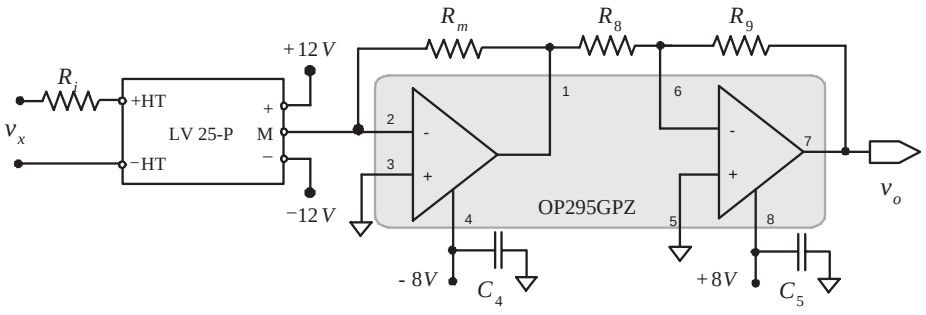

Fig. B.5: Electric circuit of the voltage sensor.

$$v_o = 0.4\frac{R_m}{R_i}\frac{R_9}{R_8} \cdot v_x \tag{B.6}$$

B.3.3 Control interface

The control interface permits the transfer of the PWM switching sequences generated in the dSPACE card to the drivers SKHI-22A, providing galvanic isolation. In addition, this card protects the hybrid power filter system against short circuit and power supply low voltage condition, which is performed by interpreting the error signals of the drivers (e_1, e_2 and e_3) SKHI-22A shown in Fig. 7.1 (left bottom side). Moreover, the control interface is able to interrupt the operation, by software, if conditions of over-voltage or over-current are detected in the power stage. Figure B.6 shows the implemented electrical diagram for this card. The

buffer SN74LS541N reinforces the PWM switching and the chip enable (CE) digital signals coming from the dSPACE card. The buffer stops the input signals if any error condition is detected. The three optocouplers HCPL-2211, in the top side, provide galvanic insolation for the error signals produced in the drivers. The six optocouplers, in the bottom side, provide galvanic insolation for the PWM switching signals produced in the dSPACE control card. As it was mentioned, the drivers SKHI-22A provide a negative logic error signal, i.e., they give a 15V signal when no error has occurred. The NAND logic gate SN74LS40N enables the buffer. Therefore, the conditions for the buffer to allow the transfer of the PWM switching signals, are if no error condition has been detected and if the CE signal is at a logical ON level. The devices and parameters used in the control interface card are given in Table B.2.

INSTRUMENTATION STAGE					
R_S	:	50Ω	Drivers	:	SKHI-22A
R_i	:	40kΩ	Operational amplifier	:	OP295GPZ
R_m	:	82Ω	Current sensor	:	CLN-50
R_6, R_8, R_9	:	10kΩ	Optocouplers	:	HCPL-2211
R_7	:	5kΩ	Buffer	:	SN74LS541N
R_{10-34}	:	2.2kΩ	NAND logic gate	:	SN74LS40N
C_{2-16}	:	0.1μF			

Table B.2: Devices and parameters of the combined current sensor.

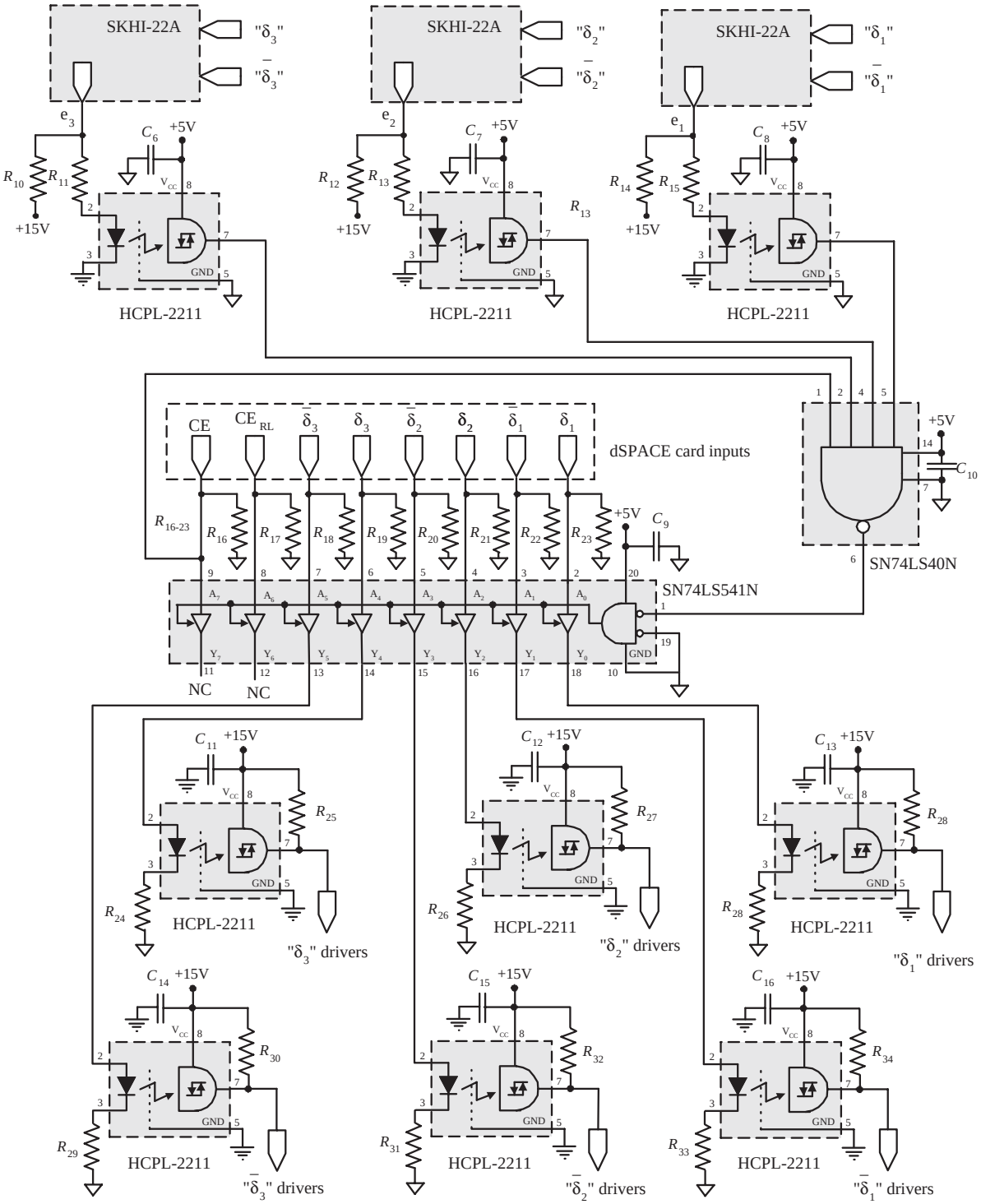

Fig. B.6: Electric circuit of the control interface.

BIBLIOGRAPHY

[1] G. Escobar, A.M. Stanković, P.Mattavelli. Reactive power and unbalance compensation using STATCOM with dissipativity-based control. In *Proc. Ind. Appl. Soc. Annual meeting IAS'2000*, Rome, Italy, October 2000, Vol. 4, pp. 2058-2065.

[2] G. Escobar, A.A. Valdez, R. Torres-Olguin, and M. Martinez-Montejano, "A Model-Based Controller for A Three-Phase Four-Wire Shunt Active Filter With Compensation of the Neutral Line Current" *IEEE Transction on Power Electronics*, Vol. 22, No. 6, pp. 2261-2270, November 2007.

[3] D. N. Zmood, D. G. Holmes and G. Bode, "Frequency domain analysis of three phase liner current regulators," in *Conf. Rec. IEEE-IAS Annual Meeting*, Phoenix, AZ, October 1999, pp. 818-825.

[4] X. Yuan, W. Merk, H. Stemmler and J. Allmeling, "Stationary-frame generalized integrators for current control for active power filters with zero steady-stable error for current harmonics of concern under unbalanced and distorted operating conditions," *IEEE Trans on Industry Applications*, Vol. 38(2), pp. 523-532, March/April 2002.

[5] I. Etxeberria-Otadui, A. Lopez-de-Heredia, H. Gaztaña, S. Bacha and R. Reyero, "A single synchronous frame hybrid (SSFH) multifrequency controller for power active filters," *IEEE Trans on Industry Applications*, Vol. 53(5), pp. 1640-1648, October 2006.

[6] B. Francis and W. Wonham, "The Internal Model Principle for Linear Multivariable Regulators". *Applied Mathematics and Optimization*, Vol. 2, pp. 170-194, 1975.

[7] M. H. J. Bollen, *Understanding power quality problems: Voltage Sags and Interruptions*, Wiley-IEEE Press, 1999.

[8] O. García, J. A. Cobos, R. Prieto, P. Alou and J. Uceda, "Single Phase Power Factor

Correction: A Survey," *IEEE Trans. on Power Electronics*, Vol. 18(3), pp.749-755, May. 2003.

[9] M. H. Rashid, *Handbook of Power Electronics*. New York: Academic, 2001.

[10] J. R. Rodríguez, J. W. Dixon, J. R. Espinoza, J. Pontt, and P. Lezana, "PWM Regenerative Rectifiers: State of the Art," *IEEE Trans. on Ind. Electronics*, Vol. 52(1), pp.5-22, Feb. 2005.

[11] M.P. Kazmierkovski and L. Malesani, "Current control techniques for three-phase voltage-source PWM converters: A survey," *IEEE Trans. on Ind. Electronics*, Vol. 45(5), pp.691-703, Oct. 1998.

[12] J. Shlabbach, D. Blume and T. Stephanblome, "Voltage quality in electrical power systems," *IEE Power series* , No. 36, England, 2001.

[13] G. Escobar, A.M. Stankovic, and P. Mattavelli, "An Adaptive Controller in Stationary Reference Frame for D-Statcom in Unbalance Operation," *IEEE Trans. on Industrial Electronics*, Vol. 51(2), pp. 401-409, April 2004.

[14] H. Akagi, "Trends in Active Power Line Conditioners," *IEEE Trans. on Power Electron.*, Vol. 3(9), pp. 263-268, May 1994.

[15] H. Akagi and A. Nabae, "Control Strategy of Active Power Filters Using Multiple Voltage Source PWM Converters," *IEEE Trans. on Ind. App.*, Vol. IA-22(3), pp. 460-465, May/June 1986.

[16] H. Akagi, Y. Kanazawa, and A. Nabae, " Instantaneous Reactive Power Compensator Comprising Switching Devices Without Energy Storage Components," *IEEE Trans. on Ind. App.*, vol. IA-20(3), pp. 326-630, 1984.

[17] L. Malesani, L. Rossetto and P. Tenti, "Active Filter for Reactive Power and Harmonic Compensation," in *IEEE Power Electronics Specialists Conference PESC*, 1986, pp. 321-330.

[18] V. Cárdenas, N. Vásquez, and C. Hernández, "Sliding Mode Control Applied to a 3ϕ Shunt Active Power Filter Using Compensation with Instantaneous Reactive Power Theory," in *IEEE Power Electronics Specialists Conference PESC*, vol. 1, 1998, pp. 236-241.

[19] H. Akagi, E. Watanabe, and M. Aredes. *Instantaneous Power Theory and Applications to Power Conditioning*. IEEE Press, 2007.

[20] H. Akagi, H. Fujita, and K. Wada, "A shunt active filter based on voltge detection for harmonic termination of a radial power distributions systems," *IEEE Trans. on Ind. App.*, Vol. 35, pp. 638-645, 1999.

[21] R. Ortega, A. Loria, P.J. Nicklasson, and H. Sira-Ramirez, *Passivity–based control of Euler–Lagrange systems*. Springer-Verlag, 1998.

[22] H. Akagi, "Control Strategy and Site Selection of a Shunt Active Filter for Damping of Harmonic Propagation in Power Distribution Systems," *IEEE Trans on Power Delivery*, Vol. 12(1), pp. 354-362, January 1997.

[23] S. Sangwongwanich S. Khositkasame, "Design of harmonic current detector and stability analysis of a hybrid parallel active filter," in *Proc. of Power Conversion Conf.*, Nagaoka, Japan, 1997, pp. 181-186.

[24] L. Malesani, P. Mattavelli, and S. Buso, "On the applications of Active Filters to Generic Load," In *Proc. International Conference on Harmonic and Quality of Power ICHQP8*, 1998, Vol. I, pp. 310-319.

[25] C. Tuttas, "Compensation of capacitive loads by a voltage-source active filter," in *ETEP*, Vol. 2(1), pp. 15-19, Jan./Feb. 1992.

[26] A.A. Valdez, G. Escobar and R. Ortega, "An adaptive controller for the shunt active filter considering a dynamic load and the line impedance," in *IEEE Trans. On Control Systems Technology*, Vol. 17(2), pp. 458-464, March 2009.

[27] F. Z. Peng, H. Akagi and A. Nabae, "A New Approach to Harmonic Compensation in Power Systems – A Combined System of Shunt Passive and Series Active Filters," in *Conference Record IEEE-IAS Annual Meeting*, 1988, pp. 874-880. (*IEEE Trans. on Ind. App.*, Vol. 26(6), pp. 983-990, Nov/Dec, 1990.)

[28] S. Bhattacharyaa and D. M. Divan, "Hybrid Solutions for Improving Passive Filter Performance in High Power Applications," in *IEEE Trans. on Ind. App.* Vol. 33(3), pp. 1312-1321, 1997.

[29] H. Fujita and H. Akagi, "A Practical Approach to Harmonic Compensation in Power Systems - Series Connection of Passive and Active Filters," in *IEEE Trans. on Ind. App.* Vol. 27(6), pp. 1020-1025, 1991.

[30] S. Park, J. Sung and K. Nam, "A New Parallel Hybrid Filter Configuration Minimizing Active Filter Size," in *IEEE Power Electronics Specialists Conference PESC*, 1999, Vol. 1, pp. 400-405.

[31] H. Fujita, T. Yamasaki and H. Akagi, "A Hybrid Active Filter for Damping of Harmonic Resonance in Industrial Power Systems," in *IEEE Trans. on Power Electronics*, Vol. 15(2), pp. 215-222, March 2000.

[32] L. Chen, A. von Jouanne, "A Comparison and Assessment of Hybrid Filter Topologies and Control Algorithms," in *IEEE Power Electronics Specialists Conference PESC*, 2001, Vol. 2, pp. 565-570.

[33] F. Z. Peng, H. Akagi and A. Nabae, "Compensation Characteristics of the Combined System of Shunt Passive and Series Active Filters," in *IEEE Trans. on Ind. App.*, Vol. 29(1), pp. 144-152, Jan/Feb, 1993.

[34] L. Asiminoaei, W. Wiechowski, F. Blaabjerg, T. Krzeszowiak and B. Kedra, "A New Control Structure for Hybrid Power Filter to Reduce the Inverter Power Rating," in *IEEE International Symposium on Industrial Electronics ISIE*, 2006, pp. 2712-2717.

[35] A. A. Valdez, G. Escobar and M.F. Martínez-Montejano, "A Model-based Controller for a Hybrid Power Filter to Compensate Harmonic Distortion in Unbalanced Operation," in *Proc. 39th IEEE Power Electronics Specialists Conference PESC'08*, Rhodes, Greece, June 15-19 2008, pp. 3861-3866.

[36] P. Antoniewicz and M.P. Kazmierkowski, "Virtual-Flux-Based Predictive Direct Power Control of AC/DC Converters With Online Inductance Estimation," *IEEE Trans. on Ind. Electronics*, Vol. 55(12), pp. 4381-4390, December 2008.

[37] O. Stihi and B. Ooi, "A Single-phase Controlled-Current PWM Rectifier," *IEEE Trans. on Power Electronics*, Vol. 3(4), pp.453-459, Oct. 1988.

[38] Y. Lo, T. Song, and H. Chiu, "Analysis and Elimination of Voltage Imbalance Between the Split Capacitors in Half-Bridge Boost Rectifier," *IEEE Trans. on Ind. Electronics*, Vol. 49(5), pp.1175-1177, Oct. 2002.

[39] T. Ohnishi, “Three Phase PWM Converter/Inverter by means of Instantaneous Active and Reactive Power Control,” in *Proc. International Conference on Industrial Electronics, Control and Instrumentation IECON’91*, Vol. 1, 1991, pp. 819 -824.

[40] T. Noguchi, H. Tomiki, S. Kondo, and I. Takahashi, “Direct power control of PWM converter without power-source voltage sensors,” *IEEE Trans. on Industry Applications*, Vol. 34(3), pp. 473-479, May-June 1998.

[41] Y. S. Suh, V. Tijeras, and T. A. Lipo, “A Nonlinear Control of the Instantaneous Power in dq Synchronous Frame for PWM AC/DC Converter Under Generalized Unbalanced Operating Conditions,” in *Proc. Ind. Appl. Soc. Annual meeting IAS’2002*, Pittsburgh, PA, 2000, pp. 1189-1196.

[42] M. Malinowski, M.P. Kazmierkowski, S. Hansen, F. Blaabjerg, and G.D. Marques, “Virtual-flux-based direct power control of three-phase PWM rectifiers,” *IEEE Trans. on Industry Applications*, Vol. 37(4), pp. 1019-1027, July-August 2001.

[43] G. Escobar, A.M. Stanković, J.M. Carrasco, E. Galván and R. Ortega, “Analysis and design of direct power control (DPC) for as three phase synchronous rectifier via output regulation subspaces,” *IEEE Trans. on Power Electronics*, Vol. 18(3), pp. 823-830, May 2003.

[44] M. Malinowski and M.P. Kazmierkowski, “Direct power control of three-phase PWM rectifier using space vector modulation - simulation study”, *Proc. IEEE International Symposium on Industrial Electronics ISIE 2002*, Vol. 4, 2002, pp. 1114-1118.

[45] V. Blasko and V. Kaura, “A new mathematical model and control of a three-Phase ac-dc voltage source converter,” *IEEE Trans. Pow. Electronics*, Vol. 12, pp. 116-123, Jan. 1997.

[46] M. Malinowski, M. Jasiński, and M.P. Kazmierkowski, “Simple Direct Power Control of Three-Phase PWM Rectifier Using Space-Vector Modulation (DPC-SVM),” *IEEE Trans. on Ind. Electronics*, Vol. 51(2), pp. 447-454, April 2004.

[47] S. Vazquez, J.A. Sanchez, J.M. Carrasco, J.I. Leon, and E. Galvan, “A Model-Based Direct Power Control for Three-Phase Power Converters,” *IEEE Trans. on Ind. Electronics*, Vol. 55(4), pp. 1647-1657, April 2008.

[48] A. Bouafia, F. Krim, and J.P. Gaubert, "Fuzzy-Logic-Based Switching State Selection for Direct Power Control of Three-Phase PWM Rectifier," *IEEE Trans. on Ind. Electronics*, Vol. 56(6), pp. 1984-1992, June 2009.

[49] G. Escobar, M.F. Martinez-Montejano, R.E. Torres Olguin and A.A.Valdez, "An Adaptive Direct Power Control for Three-Phase PWM Rectifier in the Unbalanced Case," in *Proc. 39th IEEE Power Electronics Specialists Conference PESC'08*, Rhodes, Greece, June 15-19 2008, pp. 3150-3155.

[50] J. Schlabbach, D. Blume and H. Stephanblome, *Voltage Quality in Electrical Power Systems*. The Institution of Electrical Enginners, 2001.

[51] D. Rice, "A Detailed Analysis of Six-Pulse Converter Harmonic Currents," *IEEE Trans on Industry Applications*, Vol. 30(2), pp. 294-304, March 1994.

[52] L. Magoarou and F. Monteil, "Influence of the load on the design process of an active power filter," in *Proc. IEEE Industrial Electronics, Control and Instrumentation IECON*, Vol 1, pp. 416-421, Sept. 1994.

[53] J.G. Kassakian, M.F. Sclecht and G.C. Verghese, *Principles of power electronics*. Addison-Wesley Pub., 1991.

[54] G. Weiss, D. Neuffer, and D.H. Owens, "A simple scheme for internal model based control," in *Proc. UKACC International Conference on Control* (Conf. Publ. No. 455), Sept. 1998, Vol. 1, pp. 630-634.

[55] K. Zhou, *Essential of Robust Control*. Prentice-Hall, New Jersey, USA, 1998.

[56] S. Sastry and M. Bodson, *Adaptive control: stability, convergence and robustness*. Prentice-Hall, New Jersey, USA, 1989.

[57] R. Ortega and T. Yu, "Robustness of Adaptive Controllers: A Survey," *Automatica*, Vol. 25(5), pp. 651-677, Sept. 1989.

[58] B. D. O. Anderson, R. R. Bitmead, C. R. Johnson, Jr, P. V. Kokotovic, R. L. Kosut, I. M. Y. Mareels, L. Praly, and B. D. Riedle, *Stability of Adaptive Systems: Passivity and Averaging Analysis*. The M.I.T. Press, Cambridge, MA and London, 1986.

[59] H.K. Khalil, *Nonlinear systems*. Prentice Hall, 2nd edition, 1996.

[60] P. R. Martínez, *On repetitive control for harmonic compensation in power electronic systems*. Thesis IPICYT, sep. 2007.

[61] A.V. Timbus, P. Rodriguez, R. Teodorescu, M. Liserre and F. Blaabjerg, "Control strategies for distributed power generation systems operating on faulty grid," in *Proc. IEEE International Symposium of Industrial Electronics ISIE*, 2006, Montreal, Canada, pp. 1601-1607.